Experimental Study of Nitrogen-based Pulsating Heat Pipes with Varied Configurations

By

Zhiyi Jiang

A dissertation submitted in partial fulfillment of

the requirements for the degree of

Doctor of Philosophy

(Mechanical Engineering)

at the

UNIVERSITY OF WISCONSIN - MADISON

2024

Date of final oral examination: 07/17/2024

The dissertation is approved by the following members of the Final Oral Committee:

John Pfotenhauer, Professor, Mechanical Engineering
Franklin Miller, Professor, Mechanical Engineering
Gregory Nellis, Professor, Mechanical Engineering
Allison Mahvi, Assistant Professor, Mechanical Engineering
Brian Rebel, Professor, Department of Physics

Abstract

A lot of effort has been made to incorporate the cryogenic pulsating heat pipes (PHPs) into the application for cooling down the low temperature sensors and superconducting magnets [1], [2]. The basic geometric parameters of the cryogenic PHP, the diameter of the capillary tube and the adiabatic length, can be defined directly from the Bond number and the equation of the motion for the liquid slug. However, it is difficult to determine the optimal configuration (number of turns) for the PHP analytically.

The primary goal of this research is to build and run a nitrogen-based PHP experiment test rig with two PHP sub-sections in a parallel configuration that can vary the number of turns to characterize performance as a function of the number of turns in a PHP module, identify desirable performance features, and thereby choose an optimal number of turns for practical application of PHPs. In our study, we found that 1-turn and 7-turn PHPs exhibit amazing heat transfer performance with near or greater than 1000000 W/m-K effective thermal conductivity at certain test conditions. However, 1-turn PHP and 7-turn PHP have their own issues during operation. Although the measured effective thermal conductivity in our 1-turn PHP experiments sometimes exceeds 1000000 W/m-K at the condenser temperature of 77.4 K and the initial fill ratio of 50% and at the condenser temperature of 84.5 K and the initial fill ratio of 63%, the 1-turn PHP experienced dry out multiple times during the sequential heat tests for these two test conditions. A 7-turn PHP also exhibits significantly high effective thermal conductivity around 1000000 W/m-K and 730000 W/m-K at the condenser temperature of 77.4 K with the initial fill ratio of 30% and 38%, but the 7-turn PHP also exhibits undesirable pseudo steady state behavior at certain low and moderate heat load conditions.

The original goal of this research was to find the optimal configuration of the PHP with the best heat transfer performance. Although we found the answer to this question, 1-turn and 7-turn PHPs both can achieve an outstanding value of the effective thermal conductivity. However we realized that optimal performance goes beyond simply searching for the best value of effective thermal conductivity. If we choose a 1-turn PHP or 7-turn PHP in real life applications by virtue of their large values of effective thermal conductivity, other potential problems, even failure may arise. Any unexpected large heat load, for example from the local hot spot of an HTS magnet, could result in the 1-turn PHP drying out causing unacceptable failure of the entire system, even though a 1-turn PHP might show outstanding performance at the designed heat load. Noting that can be difficult to control the temperature of a given device, such as infrared sensors and HTS magnets, the heat transfer performance of a 7-turn PHP at low power settings would be problematic since it fluctuates periodically at low and moderate heat load conditions.

With the data collected from the 1-turn, 3-turn, 5-turn, and 7-turn PHPs in the parallel configuration at two different condenser temperatures (77.4 K and 84.5 K) and different initial fill ratios, we found that the 5-turn configuration has the best stability and repeatability. The 5-turn PHP has very good heat transfer performance over a wide range of fill ratios at both condenser temperatures. The 5-turn PHP also has a very stable value of optimal effective thermal conductivity, ranging from 500000 W/m-K to 600000 W/m-K, between the initial fill ratio of 38% and 56.5% at the condenser temperature of 77.4 K. At the condenser temperature of 84.5 K the 5-turn PHP also produces a very stable optimal effective thermal conductivity, ranging between 550000 W/m-K and 670000 W/m-K for PHP1 between the initial fill ratio of 38% and 63%. The nitrogen PHPs in our study with other number of turns only perform well in a much smaller fill ratio range.

From all the experimental data collected from the 1-turn, 3-turn, 5-turn and 7-turn configurations in this study, the 5-turn PHP is the best configuration because of its decent heat transfer performance over a wide range of operable heat loads, good repeatability and stability. The 5-turn PHP configuration would be the most practical choice for the real-life applications.

Acknowledgment

In this tough and wonderful journal of pursuing my PhD, there are I would like to thank. First, I want to thank Professor John Pfotenhauer and Professor Franklin Miller for their guidance and support. My advisor John Pfotenhauer taught me how to roll indium, how to braze and other hands-on skills, which makes me a hands-on skill orientated person. I enjoyed listening to Franklin explaining the concepts and stories about the low temperature matters and methods. One of the most important reasons I wanted to join the Cryogenic Engineering Lab is I am fascinated by the NASA story told by Franklin when I was his student in ME361. And I want to thank Gregory Nellis for giving me the opportunity to get a TA assistantship at the very beginning. Of course, I need to thank Greg for creating EES which makes my life much easier when solving thermal and heat transfer problems.

There are a lot of folks who provide the help to me here in the Cryogenics Engineering Lab, I want to thank Chris Hummel, Jennifer Detlor, Luis Fonseca, Logan Kossel, Mason Mok, Uzoma Mmeje, and Bryant Muller for sharing their knowledge and experience with me selflessly. I also want to thank Allen Yingling and Gabriel Bernhardt for donating the pipe fittings and parts to me when I am in desperate need. I especially want to thank Gabe again for navigating me through different opportunities out there.

Lastly, I want to thank my parents Jiongcheng Jiang and Qinglan Ma for their unconditional support and love for sending me to pursue my college and graduate education in the United States. And I want to thank my partner Ran Tao and my cat Hoodie Zhiyi for the accompany through all these years

Table of Contents

List of Tables

List of Figures

Nomenclature

PHP	Pulsating Heat Pipe
K_{eff}	Effective Thermal Conductivity
HTS	High Temperature Superconducting
ρ_{vap}	Contribution to the uncertainty of
ρ_{liq}	Data acquisition
MLI	Multi-Layer Insulation
$LN2$	Gas chromatograph
FR	Fill Ratio
PRT	Platinum Temperature Sensor
I	Current
V	Voltage
Q	Heat Load
A_C	Cross-sectional are of the capillary tube
T_e	Temperature of the evaporator
T_c	Temperature of the condenser
N	Number of capillary tubes
T_{left}	Temperature of the left adiabatic section
T_{right}	Temperature of the right adiabatic section
μ	uncertainty
P	Pressure
PID	Proportional integral derivative
Vol_{liq}	Volume of the liquid
Vol_{total}	Total volume of the PHP core
R	Electrical resistance
m	mass
DAQ	NI Data Acquisition Device

1. Background and Motivation

The pulsating heat pipe (PHP), sometimes referred to as the oscillating heat pipe (OHP), is a passive heat transfer device invented by Akachi [3] in the late 90s to serve the heat dissipation of electronic devices. PHPs have gained much attention because of their lightweight feature and high heat transfer coefficient. The PHP, as an innovative heat transfer mechanism, not only can significantly reduce the weight of the thermal transfer component but also can maintain a much smaller temperature gradient between the hot and the cold end when compared with a conventional thermal link such as copper [1]. Unlike conduction heat transfer across a copper busbar, the heat transfer of the PHP is mainly driven by the contraction and expansion of the two-phase working fluid that flows through the condenser and the evaporator. The cryocooler has already played an important role in reducing the consumption of helium and other cryogens by installing them on an MRI or as the key component of mobile refrigeration systems [4]. However, the surface area of the cold finger of the cryocooler is limited and might not be large enough for certain applications, such as condensing the cryogens in a closed volume. A greater cooling surface area could be achieved if a PHP is coupled with a cryocooler. In addition, the PHP has been proven to work as a reliable heat switch for cryogenic applications with no mechanical moving parts [5].

There are extensive research studies of room-temperature pulsating heat pipes since the invention of the PHP. Experimental studies of heat transfer performance, visualization experiments, and numerical modeling are the major investigation methods. In the last decade, the number of studies on cryogenic pulsating heat pipes has surged. The project reported here results from a nitrogen-based PHP experiment assembly that includes two PHP subsections operating in parallel, sharing a single condenser, but having their own separate and identical

evaporator and adiabatic sections. Because of the unique design of the capillary tubes on the condenser section, the configuration of the PHP can be changed into a 1-turn, 3-turn, 5-turn, or 7-turn PHP. With the experimental data collected in these configurations, a clear guideline for the PHP configuration will be achieved with the goal of not only optimizing the heat transfer performance but also targeting the practical use of the PHP in real-world applications. In the past, researchers have been pursuing the optimum performance of the PHP, but a repeatable heat transfer performance and a reliable performance within a range of heat loads are more critical in real applications. A good PHP should not only have a good performance at one specific heat load but also needs to be operable over a wide range based on the engineering design needs. For example, a set of single-turn PHPs might be a good solution to cool the HTS magnets, but a spike of heat load on the PHP from the local hot spot on the HTS magnet will cause the PHP to dry out. This study aims to determine the best configuration of the cryogenic nitrogen PHP from the perspective of effective thermal conductivity, heat transfer per turn, stability, and repeatability.

2. Literature Review

One finds in general that the performance of a PHP depends on three groups of factors: 1) the properties of the contained fluid, 2) operating factors such as the applied heat load, fill ratio, orientation with respect to gravity, etc., and 3) geometry factors such as the number of turns, the lengths of the various sections, etc. Each of these groups of factors has been studied extensively and the following paragraphs summarize findings most closely related to the present work.

2.1 Fluid Properties

Past experimental results suggest that it is an advantage for the latent heat of the working fluid to be relatively low at the operating temperature in order to have rapid nucleation and contraction of the vapor bubbles when the fluid flows through the evaporator and the condenser [6] . It is also important that the slope of the saturation line, $(dP/dT)_{sat}$ is large enough so that the pressure difference between the hot and cold ends will easily drive the liquid slugs from the evaporator toward the condenser. The condenser temperature of our experiment is maintained at either 77.36 K (normal boiling point of the nitrogen) or 84.5 K. The value of $(dP/dT)_{sat}$ for nitrogen at 90 K, which is the level of the evaporator temperature at high heat load, is nearly three times its value at 77.36 K. The effect of $(dP/dT)_{sat}$ will be studied with our experimental results.

Another important property is the surface tension. A dominant surface tension contributes to the formation of separate vapor bubbles and liquid slugs and is crucial to sustainable fluid motion within the PHP. Surface tension also dictates the diameter of the capillary tube, a key design parameter of the PHP. The diameter of the capillary tube of the PHP cannot be greater

than a critical value so that the surface tension is big enough to form a distinct vapor-liquid interface. This critical value is defined by [6]

$$D_{CRITICAL} \leq 2\sqrt{\frac{\sigma}{(\rho_{liq} - \rho_{vap})g}} \quad (1)$$

where ρ_{liq} and ρ_{vap} are the densities of the saturated liquid and vapor, and σ is the surface tension of the fluid. The diameter of the capillary tube needs to be chosen based on the operating temperature and the above properties of the working fluid. For a nitrogen PHP, the critical diameter varies from ~ 2.25 mm just above its triple point at 63.2 K to ~ 0.4 mm at its critical point at 126 K. In this work, the PHP inner diameter is fixed at 0.5 mm. For comparison, the largest temperature produced in this study is 103.8 K on the PHP evaporator.

Besides the pressure drop and the surface tension, other properties of the fluid such as the density and the fluid viscosity also play important roles in the characteristics of the fluid flow. There are attempts to correlate these properties to the heat transfer performance or the fluid velocity by incorporating the dimensionless parameters such as the Reynolds number (viscosity), Karman number (pressure difference and viscosity), Jakob number (sensible heat and latent heat of evaporation), and Bond number (surface tension and gravitational force) [7], [8].

2.2 The Gravitational Effect and the Operating Orientation

The experimental results of a parametric study on water, ethanol, and R-123 working fluids by Khandekar's team [9] show that the number of turns of the PHP must be greater than a fluid-specific critical value in order to operate in a horizontal orientation. Since the gravitational effect is missing in a horizontal mode, the main driving force of the flow is the pressure difference caused by the temperature difference [10]. The possibility of perturbations increases when the number of tubes increases. The experimental results of the 12, 22, and 36-tube nitrogen

PHP in a horizontal orientation conducted by Barba et al. [11] agree with Khandekar's conclusion. The oscillatory motion of the PHP was never achieved with the 12-tube PHP and the optimal performance of the 36-tube PHP is 3.5 times that of the 22-tube PHP [11]. Another one-meter-long horizontal nitrogen pulsating heat pipe experiment conducted by Barba's research group demonstrated an optimal effective thermal conductivity of around 85 kW/m-K and a dry-out limit of around 25 W [12].To our best knowledge, no meter-scale vertical PHP has been tested before. The experimental results from the 5-turn and 7-turn configuration of the vertical nitrogen PHP with a 1-meter adiabatic section in this study will provide a good comparison to the data from Barba to study the gravitational effect.

Khandekar et al. also suggest that the performance of the PHP will be in an optimal range when the tilt angle is greater than 60˚ (zero degrees equals horizontal). A similar result is also observed in a cryogenic helium-based PHP [13] . Here the dry-out limit and the optimal effective thermal conductivities are nearly the same when the inclination angle is 60˚ and 90˚(vertical) at a fill ratio of 94.2% and 66.1%. Further analysis of the visualization results by Khandekar's team suggests that even though the PHP with enough turns can operate at a near-horizontal orientation, the annular flow pattern cannot be achieved [7] . Annular flow pattern is typically observed when the PHP has good performance at high heat load [7].

A visualization experiment with a 1-turn water-based PHP was conducted at various orientations [14]. In our study, the PHP is vertical orientation where gravity plays an important role. This visualization study might help the researchers in the future to predict the performance of the cryogenic nitrogen PHP at other orientations with our experimental results. In this case, the nose of the vapor bubble is observed to be symmetrical along the centerline of the tube when the PHP is vertical, but the bubble nose shifts towards the upper wall of the tube when the

orientation of the PHP approaches horizontal. Combining the effect of the bubble nose shape and the effect of gravity on the rise velocity, a relationship between the bubble velocity and the inclination angle has been plotted as shown in Figure 2-1 [14]. The velocity of the vapor bubble reaches a maximum near the vertical mode, and the liquid slug pushed by the vapor bubble also moves faster. The authors suggest that the heat transfer performance of the PHP is improved because of the increasing sensible heat transfer caused by the movement of the liquid slug. This might explain why the heat transfer performances are comparable when the orientation angle of the PHP is between 60˚ and 90˚ in Khandekar's and Li's experiments.

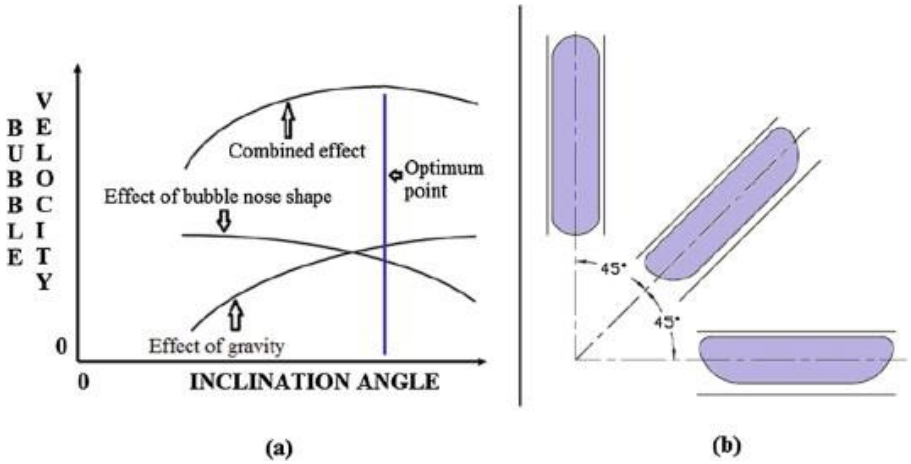

Figure 2-1 (a) The bubble velocity versus the inclination angle plot from the combined influence from the gravitational force and the bubble nose shape and (b) the bubble nose shape from vertical to horizontal from Saha's visualization experimental analysis [14].

2.3 Fill Ratio

The fill ratio of the PHP is defined as:

$$FR = {Vol_{liq}}/{Vol_{total}} \tag{2}$$

where Vol_{liq} is the volume of the saturated liquid within the cold PHP core and Vol_{total} is the total volume of the PHP.

Many experiments show that in order to optimize the thermal performance of a PHP, extremely low and high fill ratios have to be avoided [10], [13], [14]. Continuous annular flow can only be observed between 30% and 70% from the visualization experimental results of a PHP with water as the working fluid [14]. This result agrees with the 25-65% optimal fill ratio range from Khandekar's investigation on the PHP with water, ethanol, and R-123a as the working fluid [10]. Khandekar [10] also suggests the range of the fill ratio in which the PHP can perform well depends on the choice of the working fluid.

The fill ratio of a cryogenic PHP was found to decrease or increase with respect to the working temperature if the initial fill ratio is below or above the fluid-specific critical value [15]. Furthermore, the trend of heat transfer performance along with the heat load is different when the initial fill ratio is below or above the critical filling ratio of the fluid [15]. The critical fill ratio is 38.5 % at the normal boiling point for nitrogen.

A multi-turn helium PHP result suggests that the PHP with a lower FR would reach an optimal heat transfer performance at a low heat load and vice versa [13]. Sagar suggests that an inadequate amount of liquid in a PHP with a low FR will result in a lower dry-out limit than the high fill ratio PHP [16]. The fill ratio of the PHP in the practical application will depend on the required thermal conductivity and magnitude of the heat load significantly. The range of fill ratio in Sagar's cryogenic nitrogen-based PHP experiment ranges from 38% to 95%, and the optimal performance is mostly observed at a fill ratio of 57% [16].With the goal of characterizing the heat transfer performance with the fill ratio, our nitrogen-base PHP is tested at 50%, 63%, and 75% at both condenser temperatures (77.36K and 84.5K).

2.4 Flow Pattern and Heat Load

As a result of extensive PHP visualization experiments conducted in the last two decades [7], [14], [17], [18] a basic relationship between the flow pattern and the heat load is observed. After the heat load is applied to the evaporator, small bubbles are nucleated producing a two-phase condition called bubbly flow. As the heat load increases, the agglomeration of the small bubbles forms stable Talyor bubbles with distinct vapor plugs and liquid slugs observed [19]. At a high heat load, the flow transitions from slug flow to annular flow when the vapor plugs coalesce into long vapor bubble trains with a thin liquid film on the tube wall. Although the general trend of the flow pattern with respect to the heat flux is observed in most PHP visualization experiments, the transition between the flow patterns also depends on the fill ratio significantly [14], [18]. Slug flow is predominant if the fill ratio is high and the proportion of PHP that having the slug flow reduces with the increasing heat load [18]. These observations provide a foundation for interpreting the thermal and pressure dependent measurements of the present work. Since we cannot visualize the flow pattern of our PHP, these experimental visualization results would help us to understand the behavior of the fluid flow of our PHP with our collected temperature and pressure measurements.

2.5 Number of Capillary Tubes

Singh [20] developed a 1-D numerical model of the PHP and validated the model with the results from a 41-turn LN2 PHP experiment by Fonseca [21]. Singh simulated one of the experimental conditions conducted by Fonseca but with a varying number of turns. He shows that the effective thermal conductivity plotted against the number of turns displays a positive trend when the number of turns is below 5 and a negative trend when the number of turns is greater than 5 as presented in Figure 2-2 [20]. He also suggests that the marginal gain of the heat

transfer performance from building a PHP with more than a critical number of turns is small, the optimal number of the LN2 PHP2 with other geometry the same as Fonseca's should be less than 10 [20]. Even though Singh's numerical model agrees with Fonseca's 41-turn nitrogen-based PHP experimental result, this numerical model still has its potential problem because the model is only one-dimensional and the model is only simulating the slug-plug flow. Our experimental results of the 1-turn, 3-turn, 5-turn, and 7-turn PHP will test Singh's numerical model and investigate the conclusion derived from his model.

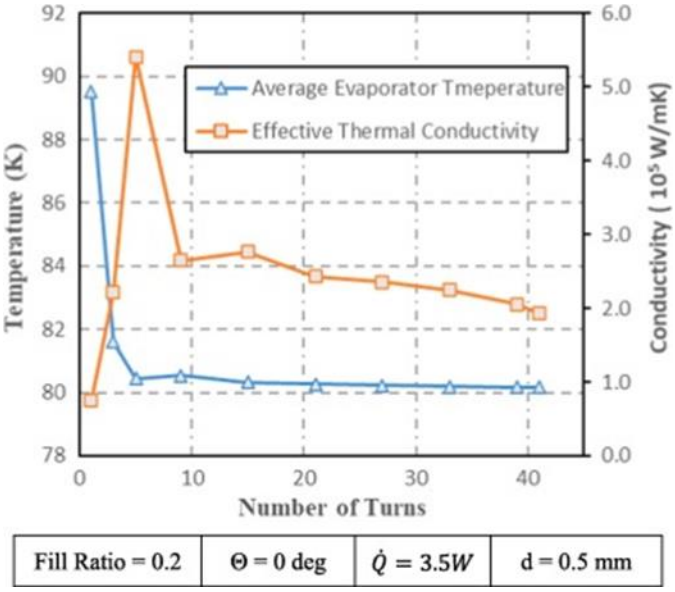

Figure 2-2 The effective thermal conductivity versus the number of turns and the evaporator temperature against the number of turns for LN2 PHP with other conditions constant [18].

The comparison of the 8-turn and the 48-turn helium-based cryogenic PHP by Li et al. [22] show that the PHP with a small number of turns has an advantage in the low heat load range. The PHP with a large number of turns needs a big enough heat load in order to reach a decent heat transfer performance as shown in Figure 2-3. Li et al. [22] proposed an alternative configuration of the PHP that is composed of several PHPs, each with a small number of turns, operated in parallel to produce an optimal heat transfer performance at a high heat load. This

same observation forms the primary motivation for the present study, that is to determine the number of turns that produces the highest heat transfer per turn. Forming a practical PHP for a desired heat load could then be accomplished by operating the requisite number of optimal PHPs in parallel.

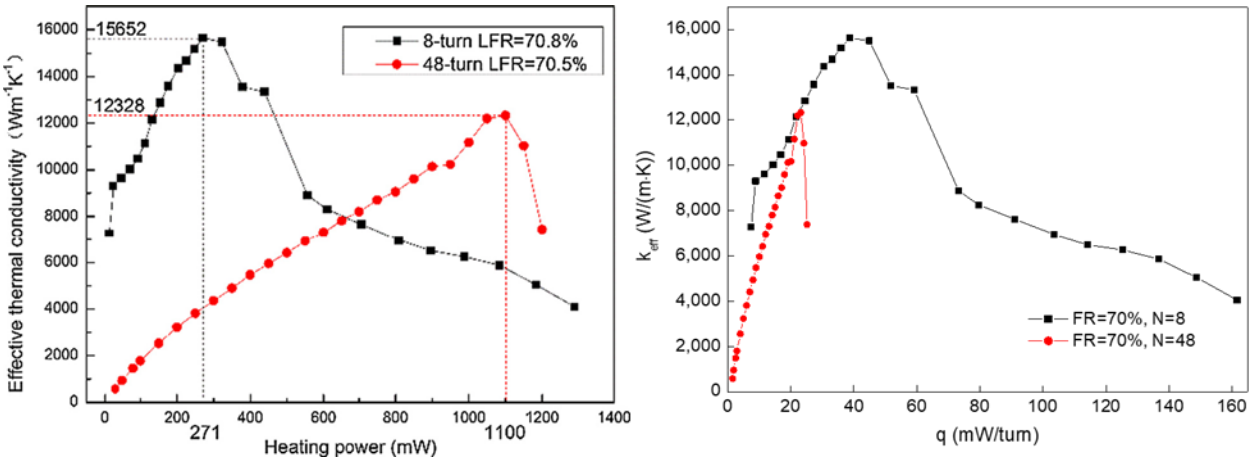

Figure 2-3 Effective thermal conductivity vs heat load plot (left) and the effective thermal conductivity vs heat flux per turn plot(right) for 8-turn and 48-turn helium-based cryogenic PHP by Li et al [22].

3. Experimental Setup and Instrumentations

3.1 Test Rig

Figure 3-1 shows the PHP test rig (without the MLI layers) before installing it into the vacuum Dewar. The vacuum Dewar is made by Precision Cryogenics Inc. with an inner diameter of 0.51 m and a height of 1.65 m. The Dewar end plate is a 1-inch thick aluminum round plate with a 0.605 m diameter. The Dewar end plate has various gas and electrical feedthroughs to accommodate the gas lines and electrical wires into the vacuum system inside the Dewar. The end plate is bolted on the Dewar by twelve M6 socket head cap screws in a circular pattern. The

vacuum seal inside of the Dewar is maintained by the O-ring clamped between the top plate and the Dewar.

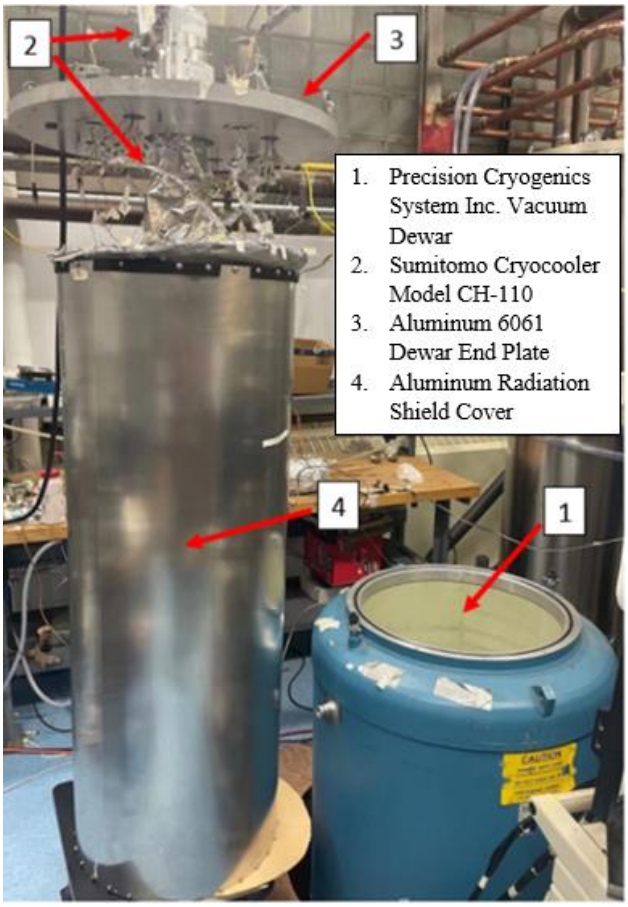

Figure 3-1 The overview of the experiment setup

3.2 Radiation Shield and Cryocooler

As shown in Figure 3-1, a Sumitomo CH-110 cold head is mounted on the aluminum Dewar end plate. This is a single-stage Gifford-McMahon cryocooler paired with a Sumitomo F-50 compressor. The measured cooling capacity of the CH-110 cold head is around 200 W at 75 K with the F-50 compressor.

Figure 3-2 Sumitomo CH-110 Cryocooler (left) and Sumitomo F-50 Compressor (right)

An octagon shape copper adapter plate with a thickness of 22 mm and a side length of 50 mm is mounted on the bottom of the cold finger of the cryocooler. Four 50W model KAL-50 resistive heaters are mounted on the side walls of the adapter plate as part of the temperature control system of the cold head. The four heaters are electrically wired in a schematic presented in Figure 3-3 providing a 50 Ohm heater with a maximum power output of 200 W.

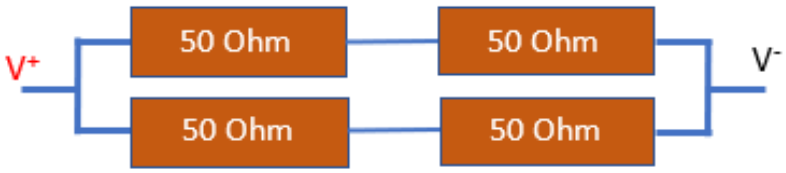

Figure 3-3 Electric schematic of the four KAL-50 resistive heaters

This control heater is powered by an HP 6443B power supply (120 volts, 2.5 amps). The top plate of the radiation shield that covers the PHP core is bolted on the bottom of the copper adapter plate. The radiation shield is highlighted as Item 4 in Figure 3-1. The top and bottom of the radiation shield are 6061 aluminum plates with an 18-inch diameter and a half-inch thickness. The side wall of the radiation shield is bolted on the top and bottom through thirty

screws on each plate. The side wall is comprised of two 6061 aluminum sheet plates with a 1mm thickness. The multilayer insulation (MLI) blanket is wrapped around the aluminum radiation shield to provide a high thermal resistance between the Dewar and the radiation shield. The temperature of the radiation shield bottom is between 94 to 95 K during the PHP operation from the measurement of the PRT temperature sensor mounted on the center of the radiation shield bottom plate.

3.3 PHP Core

Two identical PHP sub-sections are thermally anchored at their common condenser end to the cryocooler through the radiation shield top plate and through the octagonal copper block. Indium foils are sandwiched between the cryocooler cold finger, the copper adapter plate, the radiation shield top plate, and the PHP condenser block to reduce the thermal contact resistance between the PHP condenser and the cryocooler.

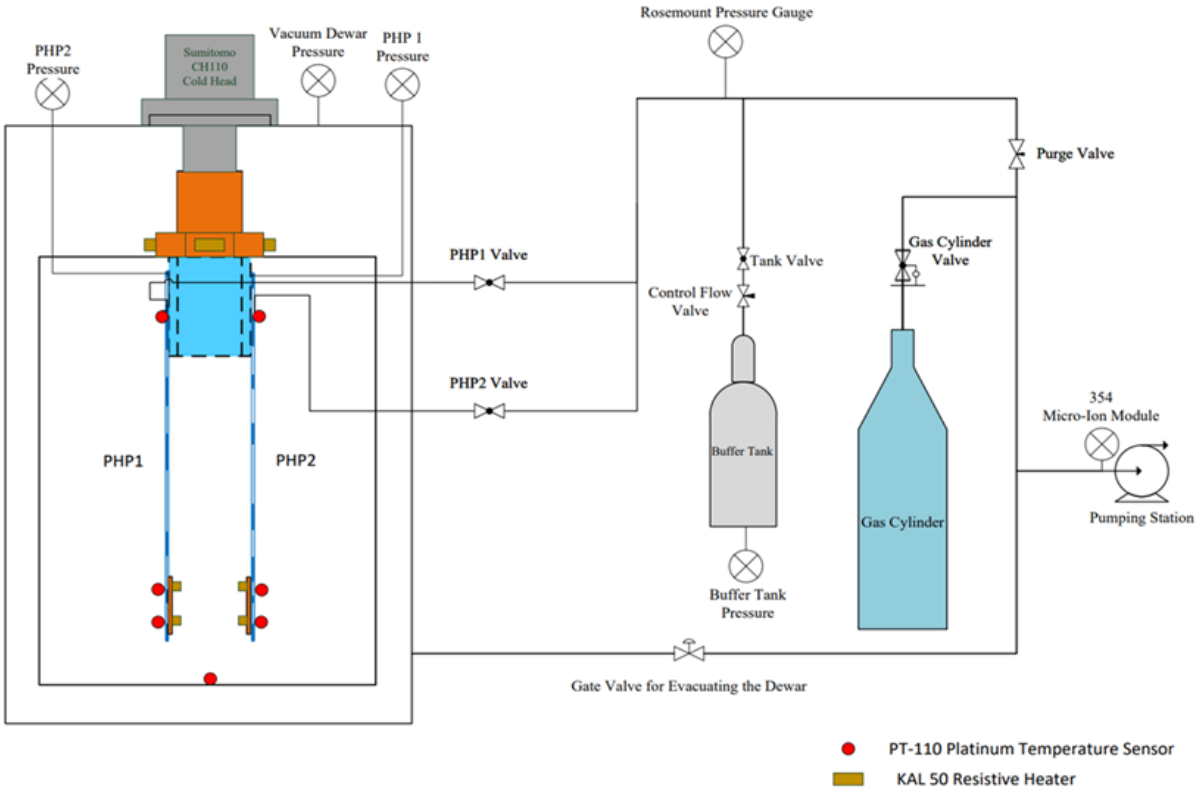

Figure 3-4 Schematic of the PHP Core and the Pipeline

Each PHP sub-section is comprised of the condenser, evaporator, and adiabatic section. The condenser is made of a 4.25 mm-thick copper plate with a height of 90 mm and a width of 70 mm. The evaporator is made from a copper plate with the same thickness as the condenser but with a width of 76.2 mm and a height of 60 mm. A total of 14 parallel grooves spaced 1 mm apart and with a depth of 0.65 mm are machined evenly across the condenser and evaporator plates to fit the capillary tubes. The adiabatic section between the condenser and the evaporator is 1 m long. The capillary tubing extending from the condenser, through the adiabatic section, and to the evaporator is made from 304 stainless steel with an inner diameter of 0.5 mm and an outer diameter of 0.8 mm. The capillary tubes are soldered into the channel of the condenser and evaporator as shown in Figure 3-5 below.

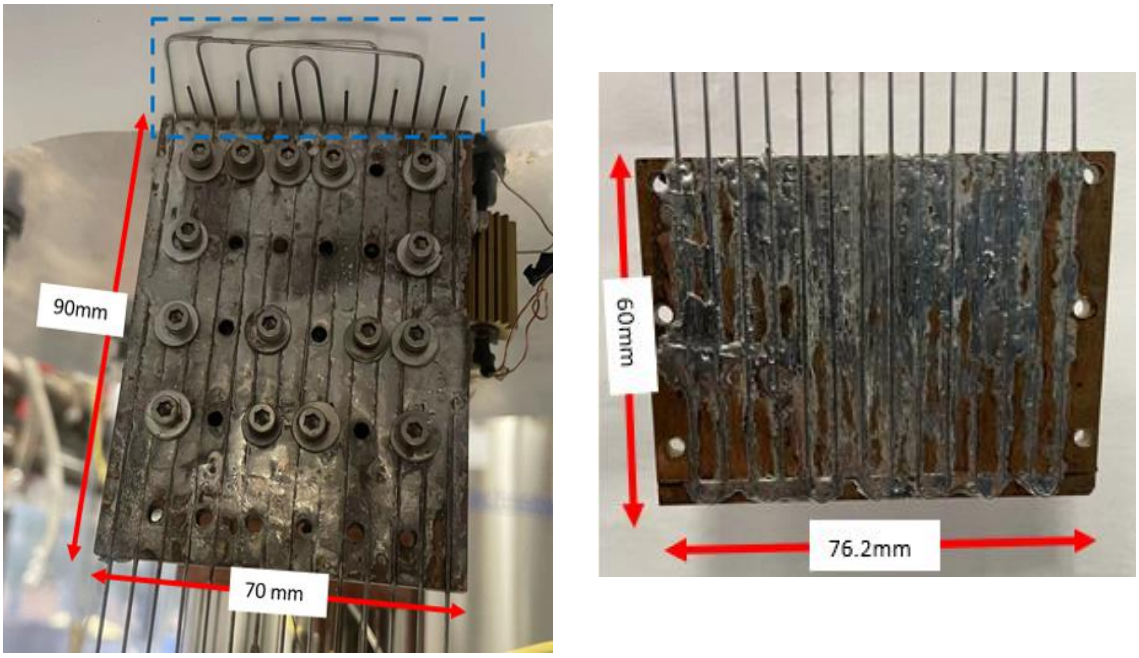

Figure 3-5 Condenser (left) and Evaporator (right) sections

One main reason that the thin wall stainless-steel capillary tubing is used is the thermal conductivity of the stainless steel is very poor in the working temperature range of the LN2 PHP. In one of the extreme PHP operating conditions that we observed, the temperature of the condenser and evaporator for PHP2 are measured at 77.3 K and 103.8 K. The estimated conduction heat transfer of the total 14 stainless steel capillary tubing across the PHP2 is only 4.7 mW, which is only 0.27% of the 1.72 W of heat load applied to the evaporator. Therefore, the heat transfer of the capillary tube itself is insignificant.

The two PHP sub-sections form a parallel configuration. The main reason we built two near-identical PHPs is that we wanted to see how big the influence of fabrication will be on the overall performance. Please keep mind that only one of the PHP (PHP1) has pressure transducers tapped on the condenser and the evaporator as shown in Fig 3-11. Each PHP has its own fill line and PHP valve to enable the fill ratio of both PHPs to be identical. The open ends and the u-bend

of the capillary tubes highlighted in the blue dashed box in Figure 3-4 are designed for changing the number of turns in the future. The 7th and 8th capillary tubes counted from the left side of the condenser form a closed u-turn for the 1-turn PHP. The number of turns of the PHP are determined by the connection of U-bends on the condenser. Because of the unique feature of the capillary tube on the top of each condenser, we can later convert the PHP test rig into a 3-turn, 5-turn, and 7-turn PHP with a parallel configuration as shown in Figure 3-6 below.

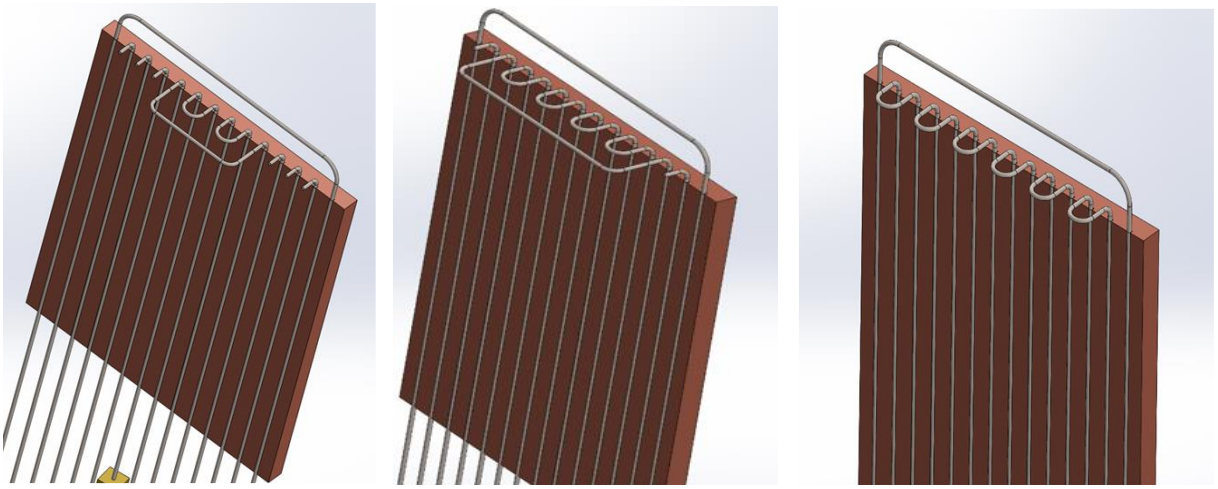

3-turn PHP 5-turn PHP 7-turn PHP

Figure 3-6 The 3-turn, 5-turn and 7-turn PHP setup

Figure 3-7 shows the fabrication process when we convert the 3-turn PHP into 5-turn PHP. We also present the schematic of the 1-turn and 5-turn PHP setup in Fig 3-12.

Figure 3-7 The fabrication of the leftmost U-bend for the 5-turn PHP

Two KAL-50 resistive heaters in a parallel configuration shown in Figure 3-8 are thermally anchored on the back side of the evaporator plate to provide the heat load to each PHP.

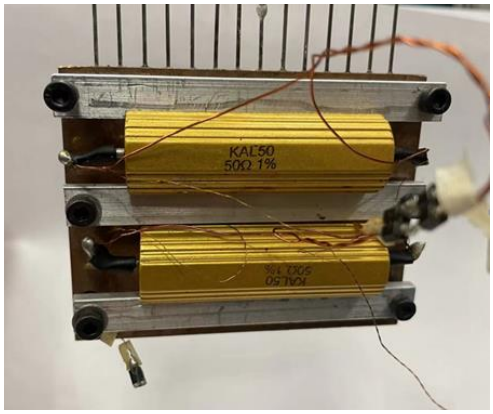

Figure 3-8 Two KAL-50 resistive heaters on the back side of the evaporator

3.4 Gas-Line

A fill line is connected to each PHP through a T-shaped copper block. There are two additional T-shaped copper blocks on the top and bottom of the adiabatic section of the 7th capillary tube on PHP1 each of which connect to an Endevco pressure transducer that is installed on the feedthrough of the Dewar top plate. The two Endevco pressure transducers measure the pressure of the condenser and the evaporator. On the capillary tubing that connects each copper block to the corresponding room temperature component, a VCR connection joint allows the PHP core to be removed from the test rig for configuration modification. All these connections are shown below in Figure 3-9.

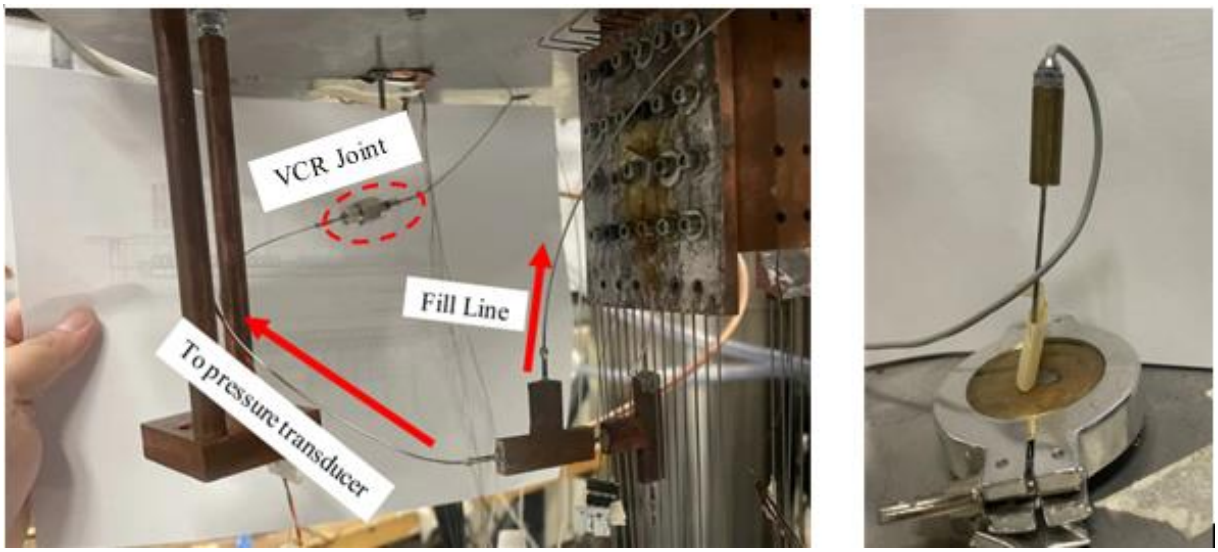

Figure 3-9 The copper fittings that connect to the fill line and the condenser pressure transducer on PHP1(left) and the pressure transducer on the Dewar top plate.

The gas line assembly in the ambient environment is defined as the internal space of the pipeline between the tank valve, PHP1 valve, PHP2 valve, the gas cylinder valve, and the valve to the pump station as presented in Figure 3-10 below. A nitrogen gas cylinder is connected to a buffer tank through ¼ inch copper tubing. The buffer tank supplies the nitrogen gas to each PHP section from a Swagelok Tee section to the PHP valve. An Endevco pressure transducer is installed into the bottom of the buffer tank. The total amount of nitrogen gas charged into the PHP is measured by the pressure drop of the buffer tank. A KF25 vacuum port on the left side of

the pipeline assembly connects to a Leybold turbo and mechanical pumping station. An Endress & Hauser pressure gauge measures the internal pressure of the gas line assembly.

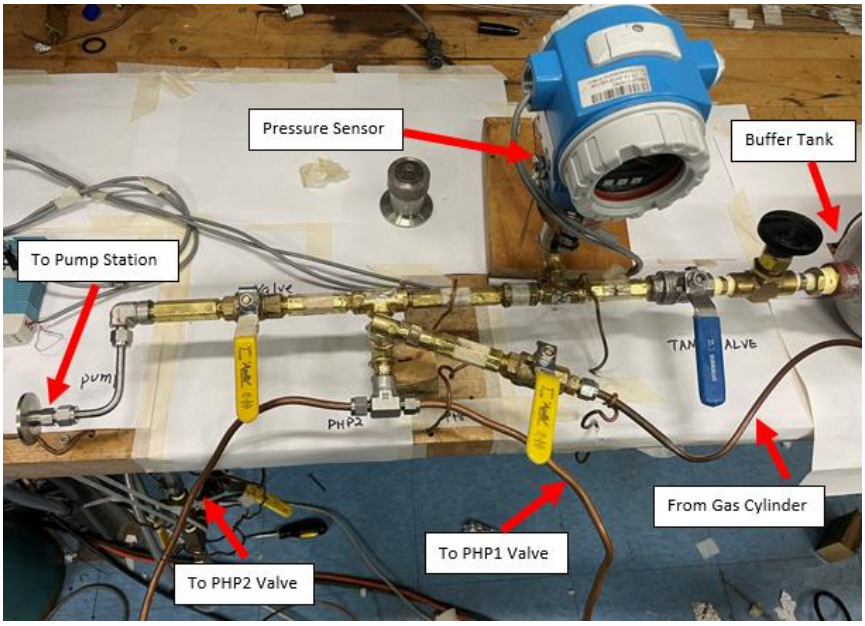

Figure 3-10 The overview of the gas line that is outside of the Dewar

As shown in Figure 3-11, a KF-40 four-way vacuum cross-fitting is installed on one of the gas feedthroughs of the Dewar top plate. The fill lines for PHP1 and PHP2 are fed into the vacuum environment through the KF vacuum flange on the top of the cross-fitting. A pressure relief valve is mounted on the stainless-steel tubing that is behind the PHP valve which goes into the PHP core. An MKS 122A pressure sensor measures the internal pressure (vacuum) of the Dewar and is mounted on the left side of the cross-fitting. A gate valve is installed on the right side of the cross-fitting allowing the pump station to evacuate the air within the Dewar.

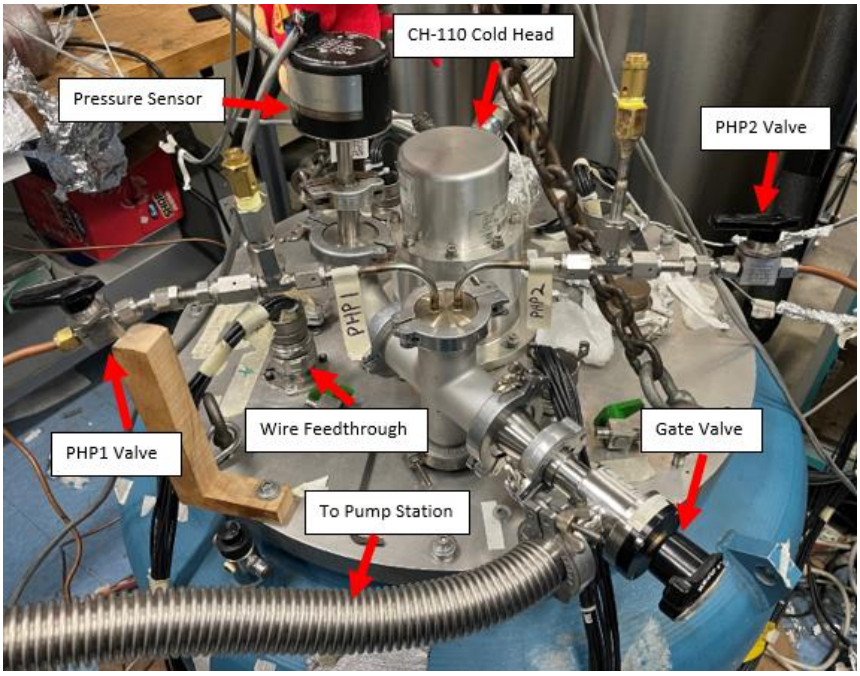

Figure 3-11 Gas feedthroughs and wire feedthroughs on the Dewar top plate

3.5 Instrumentation

A total of six Lakeshore PT-100 series platinum resistance thermometers (PRT) are installed on each PHP subsection. One PRT is thermally anchored on the center of each condenser and evaporator plate with Lakeshore VGE-7031 varnish. Two PRTs are mounted on the center of the adiabatic section and another two PRTs are mounted on the adiabatic section that is 0.25 m away from the evaporator. The locations of the temperature sensors are specified in Figure 3-12 below.

The PRT that measures the temperature of the adiabatic section is installed on the back side of a customized copper plate. The capillary tube is soldered into the machined channel of the thermometer mounting plate. The distance between the capillary tubing and the backside side

of the plate is around 0.75 mm. It will take around 0.476 ms for the thermal wave to travel from the capillary tubing to the PRT temperature sensors at around 80 K.

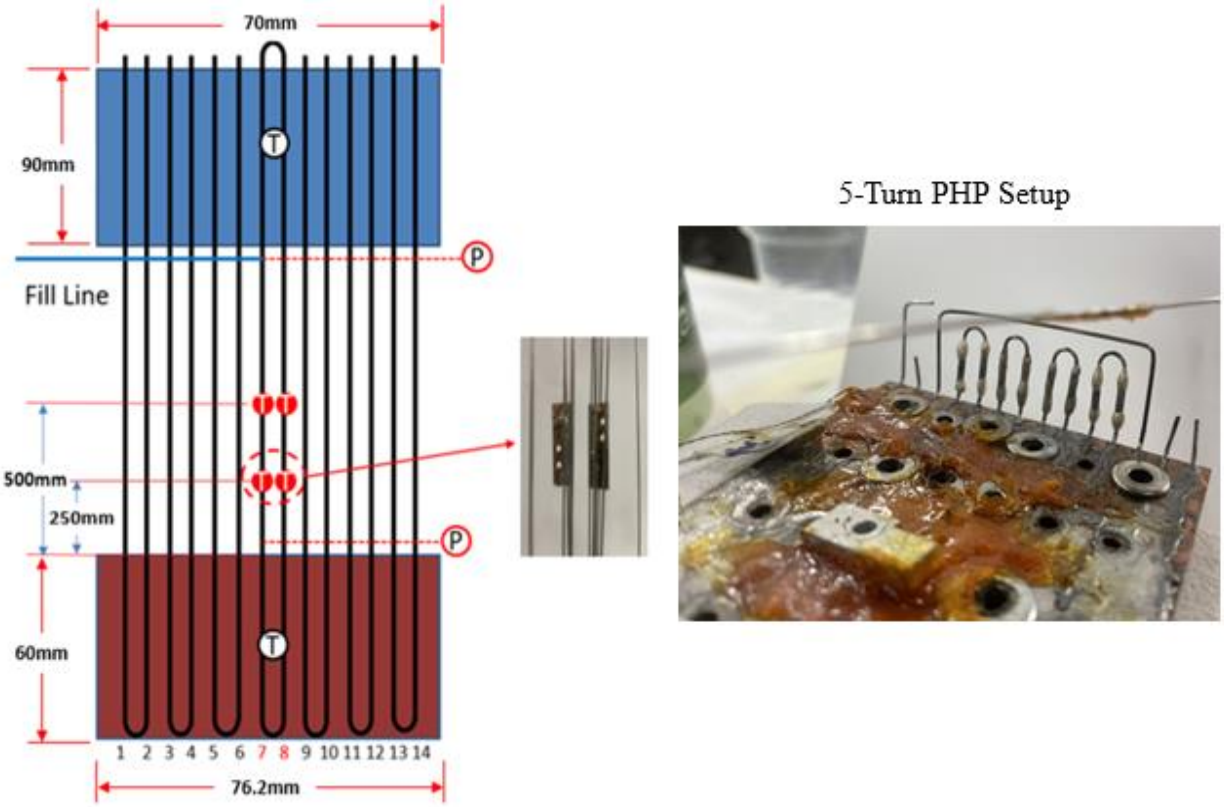

Figure 3-12 The dimension of the 1-turn PHP is presented in the schematic at the left. The adiabatic section is 1m long. The location of the PRT is labeled as 'T' in the schematic. The condenser and evaporator pressure transducers are tapped on the tube number 7 and marked as 'P' on the schematic. The picture at the right shows the U-bend tubing on the condenser for the 5-turn PHP setup.

The four-wire configuration is applied to each PRT temperature sensor. Two wires leads (I+ and I-) are connected to a LakeShore 120 current source and the other pair of leads (V+ and V-) are connected to the channels of a National Instruments 6218 Data Acquisition Device (DAQ). The resistance of the PRT temperature sensor is calculated by Ohm's law.

Figure 3-13 The LakeShore 120 Current Source supplies the current of the PRT temperature sensors (top left). NI USB-6211 and the relay (lower left) will shut down the power supply of the heaters in case of power shortage, water pump failure and other accidents. NI USB-6218 (right) measures the voltage across the temperature sensors and the voltage from the pressure transducers.

The resistive heaters on the backside of the evaporator plate are powered by an Agilent E3620A DC power supply. The voltage across the resistive heater is measured by the HP 34401A digital multimeter.

The Endevco pressure transducers that measure the pressure of the buffer tank and the internal of the PHP are powered by a 10-V constant voltage from an HP 3611A DC power supply. The pressure measurement is calculated by the output voltage generated by the transducer. The output voltage is read by the NI-6218 DAQ.

Figure 3-14 The HP3611A power supply supplies the 10-V constant voltage to the Endevco pressure transducers.

4. Experimental Procedure and the Uncertainty Analysis

4.1 Clogging Test and Leak Test

After the PHP is fabricated, we will go over a clogging test before closing the last joint of the capillary tube at the adiabatic section. One end of the tube opening is connected to a nitrogen buffer tank and the other end is connected to a flowmeter as shown in Figure 4-1 below.

Figure 4-1 The PHP1 is checked for the clogging before closing the last joint of the capillary tube on the adiabatic section.

The charge pressure of the nitrogen buffer tank and the flow rate measurement for the clogging tests on all PHP configurations are listed in Table 4-1 below.

Table 4-1 Charge pressure of the nitrogen buffer tank and the flow rate reading for the clogging test after fabricating the PHP.

	Charge Pressure on PHP1 [psig]	Flow Rate for PHP1 [LPM]	Charge Pressure on PHP2 [psig]	Flow Rate for PHP2 [LPM]
1-turn PHP	20	0.41	20	0.42
3-turn PHP	21.8	0.18	21.8	0.19
5-turn PHP	37	0.24	37	0.25
7-turn PHP	33	0.16	32	0.17

After closing the last opening of the capillary tube, the PHP core will be leak tested before installing the PHP on the adapter of the cryostat as shown in Figure 4-2. The fill line of the PHP is connected to the leak detector and leak rate reading is checked when sparying the helium on the PHP core. The leak rate for the PHP core that is being tested in Figure 4-2 below is $1.9x10^{-9}$ Torr-L/s and the background of the leak detector is about $1.2 x10^{-9}$ Torr-L/s. There is no spike on the leak rate reading while we spray the helium on the PHP core. The PHP core is leak tight.

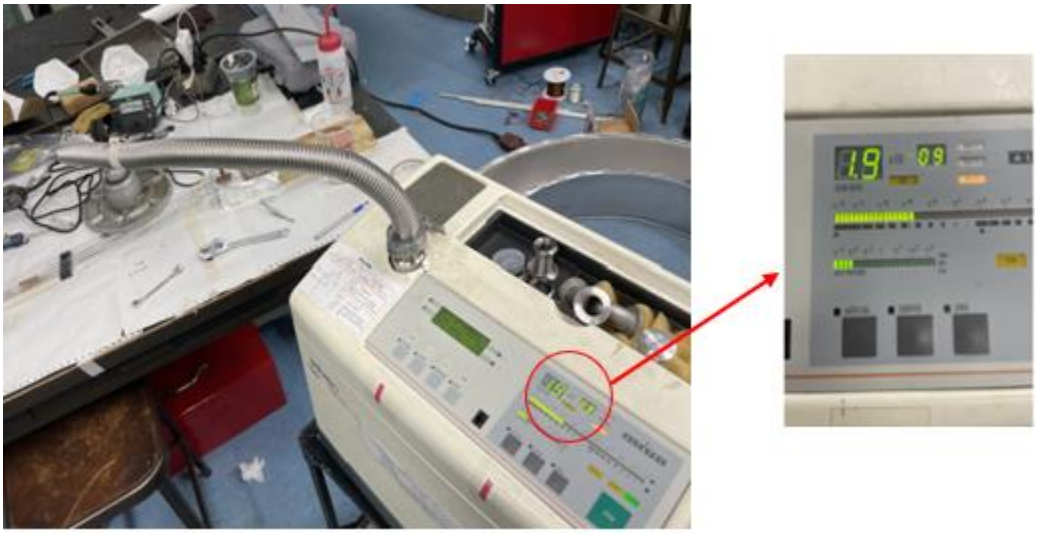

Figure 4-2 The PHP core is being leak tested before the installation process. The leak rate for the PHP core that is being tested is $1.9x10^{-9}$ Torr-L/s, and there is no spike on the leak rate reading while we spray the helium on the PHP core.

After the PHP core is installed on the test rig and the fill lines are connected to the gas line of the entire system. We will perform the leak test one more time to ensure the VCR fittings that connect the PHP to the pressure transducers and to the PHP fill lines are leak tight. Then we will install the radiation, wrap the MLI insulation around the radiation shield and then take the PHP test rig into the vacuum chamber.

After we put the test rig into the vacuum chamber, a leak test of the vacuum chamber will be performed by connecting the leak detector to the gate valve of the vacuum chamber shown in Figure 3-10. If the leak rate is less than $1x10^{-7}$ Torr-L/s and no spike of the leak rate is observed while the helium is spraying around the top flange of the vacuum chamber, the vacuum chamber is leak tight. A leak tight vacuum chamber can be maintained at the level of 10^{-6} Torr when the PHP experiment is running.

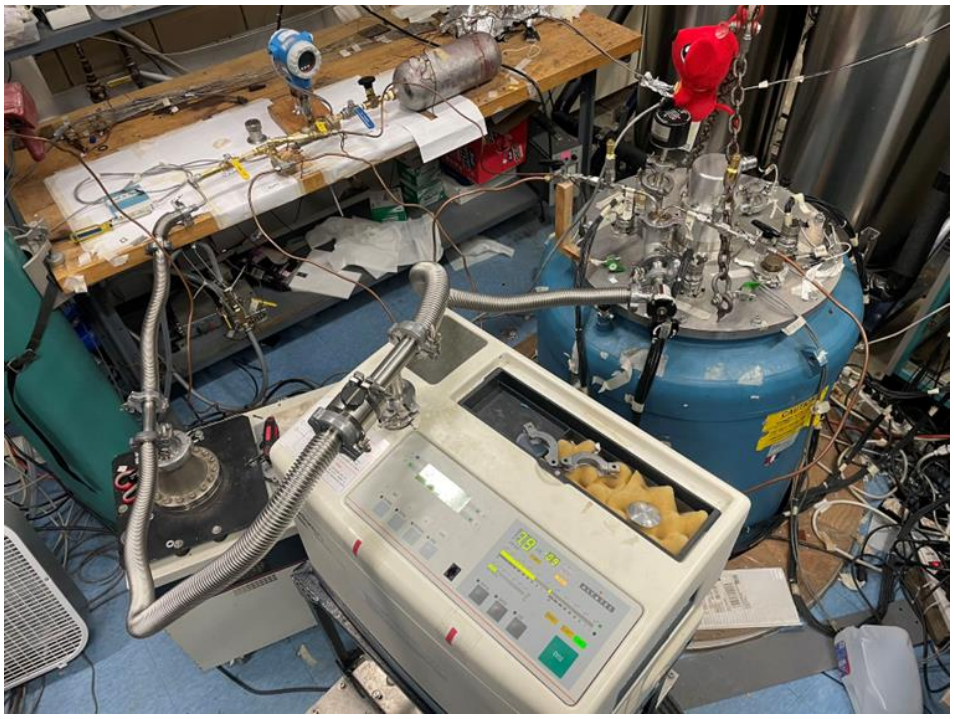

Figure 4-3 The leak detector is connected to the vacuum chamber for leak checking the vacuum chamber. When we do the leak detection of the gas line at the room temperature side, the gate valve that connects the leak detector to the vacuum chamber will be closed while the gate valve that connects the gas line of the PHP will be open.

Then we will perform a leak test of the gas line at the room temperature side by connecting the leak detector to the gas line of the PHP and spraying the helium to the all the pipelines and the fittings on the table and the top flange of the vacuum chamber. Eventually, we will perform the last leak check procedure by filling the helium into the PHP core and checking the leak rate of the leak detector that connects to the vacuum chamber. If there is a leak on the

gas line or on the PHP within the vacuum chamber, a spike of leak rate will be identified when helium is charged into the PHP. We also charge the helium into the PHP at different to see if the leak rate changes on the leak detector. If the leak rate on the leak detector increases after the pressure of the helium charged into the PHP increased, there is a leak either on the gas line or on the PHP within the vacuum chamber.

4.2 Calibration of the PRT and Pressure Transducer

The resistance of the PRT is measured when submerged in boiling liquid nitrogen at ambient pressure. The real ambient pressure of the environment is read from a mercury barometer. The resistance of the PRT is also measured when submerged in an ice-water bath. The resistance measured in the boiling liquid nitrogen and in the ice-water bath are fitted into the standard Callendar-Van Dusen polynomial

$$\mathrm{T} = (\frac{1}{2B})(-A + \sqrt{A^2 - 4B\left(1 - \frac{R}{R_0}\right)}) + 273.15 \qquad (3)$$

because the Lakeshore PT-100 series temperature sensors follow the IEC-751 standard. Here the coefficient B is -5.775×10^{-7}, and R_0 is the resistance of the PRT at the ice-water bath. The coefficient A is found by substituting the resistance and the temperature of the PRT measured in the boiling LN2 bath into the polynomial. The calibration for temperature sensor is listed in Table 4-2 below.

Table 4-2 Temperature sensor calibration data

Temperature Sensor Name	Coefficient A	R_0
T1	0.0039473948	99.7171800000
T2	0.0039526598	99.6368900000
T3	0.0039541804	99.6759200000
T4	0.0039608603	100.0855000000

T5	0.0039486425	99.2670300000
T6	0.0039561672	99.9878200000
T7	0.0039535455	100.1181000000
T8	0.0039543663	99.9030900000
T9	0.0039593637	99.6634700000
T10	0.0039839880	99.6774400000
T11	0.0039493842	99.7011400000
T12	0.0039496506	99.8128000000

All Endevco pressure transducers are calibrated with respect to the Endress & Hauser pressure gauge at the gas line. And the Endress & Hauser pressure gauge is calibrated with respect to the mercury barometer before calibrating the pressure transducers. The calibration range of the pressure gauge is between 25 kPa to 350 kPa. The voltage output from each pressure transducer and the corresponding pressure read from the Endress & Hauser pressure gauge are substituted into the equation

$$P = C_1 V_{transducer} + C_2 + P_{offset} \quad (4)$$

the coefficients C_1 and C_2 are calculated from the linear fit of the pressure readings and corresponding output voltage signals. Because the Endevco pressure transducer has a thermal sensitive drift, each pressure transducer is calibrated after each dry-out. The drift of the pressure measurement is then offset by the value of $P_{offset.}$ Table 4-3 shows the summary of the calibrated result for the pressure transducers.

Table 4-3 Pressure transducer calibration result.

Pressure Transducer Location	Coefficient C_1 [psi/mV]	Coefficient C_2 [psi]
Buffer Tank	+1.4743	+10.2765
Evaporator	+2.2921	-1.4748
Condenser	-1.8716	+15.8254

4.2 Experimental Procedure

4.2.1 Gas Evacuation and Filling Process

The gas molecules within the Dewar are evacuated by the mechanical/turbo pump station to reduce the heat transfer loss between the cold radiation shield and the Dewar wall at room temperature.

Figure 4-4 Mechanical/turbo pump station for evacuating the gas line and the vacuum chamber and the of the vacuum Dewar pressure is at 1.4x10^-6 Torr ion-gauge during the experiment.

The gas line and the buffer tank are purged with nitrogen gas four to five times to remove the contaminations within the system. Then the buffer tank is charged from the nitrogen gas cylinder to a specific pressure P_1. The entire gas line is maintained under a vacuum level of 10^{-6} Torr during the entire cool-down process. Once the condenser temperature reaches the target temperature, the tank valve is opened allowing the nitrogen gas to fill into the core of the cold PHP subsection. The tank valve will be closed when the pressure of the buffer tank drops to a specified pressure P_2 corresponding to the required condenser temperature and fill ratio.

The amount of nitrogen gas filled into each PHP section and the gas line assembly of the room temperature is defined by the idea gas law

$$m_{supply} = \frac{(P_1 - P_2)V_{tank}}{RT_{room}} \quad (5)$$

Each PHP section will be filled independently to avoid the possibility that most of the liquid or vapor stays in a certain portion of one PHP section. The mass balance for each PHP is given by:

$$m_{supply} = m_{assembly} + m_{PHPamb} + m_{amb-cold} + m_{PHPcold} \quad (6)$$

Here $m_{assembly}$ is the nitrogen gas within the gas line assembly in the ambient environment (between PHP valves, tank valve and the valve to the pump station. m_{PHPamb} is the mass of gas in the pipeline that is from the PHP valve to the dewar top plate. $m_{amb-cold}$ is the total amount of gas within the pipeline that extends between the dewar top plate and the PHP cold side. The nitrogen gas in the capillary tubes that extend between the pressure transducer and the PHP core is counted as part of $m_{amb-cold}$ for PHP1. $m_{assembly}$, $m_{PHPamb,}$ and $m_{amb-cold}$ are estimated by the ideal gas law. The ambient room temperature and the target condenser temperature are defined as T_{amb} and T_{cold}.

Table 4-4 The summary of the volume for the corresponding mass parameters for 1-turn PHP

Location	Volume [m^3]	Temperature	Corresponding Mass Parameter
V_{tank}	3.607E-3	T_{amb}	m_{supply}
$V_{assembly}$	1.051E-4	T_{amb}	$m_{assembly}$
V_{PHPamb} (PHP1)	7.589E-6	T_{amb}	m_{PHPamb} (PHP1)
$V_{amb-cold}$ (PHP1)	1.403E-6	$(T_{amb} + T_{cold})/2$	$m_{amb-cold}$ (PHP1)
$V_{PHPcold}$ (PHP1)	5.429E-7	T_{cold}	$m_{PHPcold}$ (PHP1)
V_{PHPamb} (PHP2)	7.628E-6	T_{amb}	m_{PHPamb} (PHP2)
$V_{amb-cold}$ (PHP2)	9.343E-7	$(T_{amb} + T_{cold})/2$	$m_{amb-cold}$ (PHP2)
$V_{PHPcold}$ (PHP2)	4.943E-7	T_{cold}	$m_{PHPcold}$ (PHP2)

The mass conserved within the cold PHP core is given by

$$m_{PHPcold} = \rho_{liq} Vol_{liq} + \rho_{vap}(Vol_{total} - Vol_{liq}) \quad (7)$$

where ρ_{liq} and ρ_{vap} are the densities of saturated liquid and vapor at the corresponding condenser temperature and Vol_{total} is the total volume of the cold PHP.

The volume of the gas line at the room temperature and between the room temperature and the cold side is the same for all configurations. The volume of the cold PHP core is different for 1-turn, 3-turn, 5-turn and 7-turn PHP configurations and is listed in Table 4-5 below.

Table 4-5 The summary of the volume for the PHP core for all PHP configurations

Configuration	$V_{PHPcold}$ (PHP1) [m^3]	$V_{PHPcold}$ (PHP2) [m^3]
1-turn	5.429E-7	4.943E-7
3-turn	1.496E-6	1.447E-6
5-turn	2.448E-6	2.397E-6
7-turn	3.398E-6	3.348E-6

4.2.2 Applying Heat Load on the Evaporator

Once the PHP reaches a steady state after the filling process, an identical heat load is applied to the evaporator of both PHPs. The magnitude of the heat load is increased to a higher level if the temperature of the PHP reaches a steady state for at least 20 mins. The heat load is increased successively until the dry-out condition is reached. The dry-out condition occurs when the temperature of the evaporator is above the critical point and pressure oscillations are no longer observed. The heat transfer performance deteriorates, and the evaporator temperature increases rapidly when dry-out is reached. Figure 4-5 below presents the PHP1 in 3-turn configuration dried out when the heat load increased from 3.86 W to 4.08 W. The evaporator temperature reached the critical point of nitrogen at around 111400 sec and the pressure started to drop significantly at around 10600 sec.

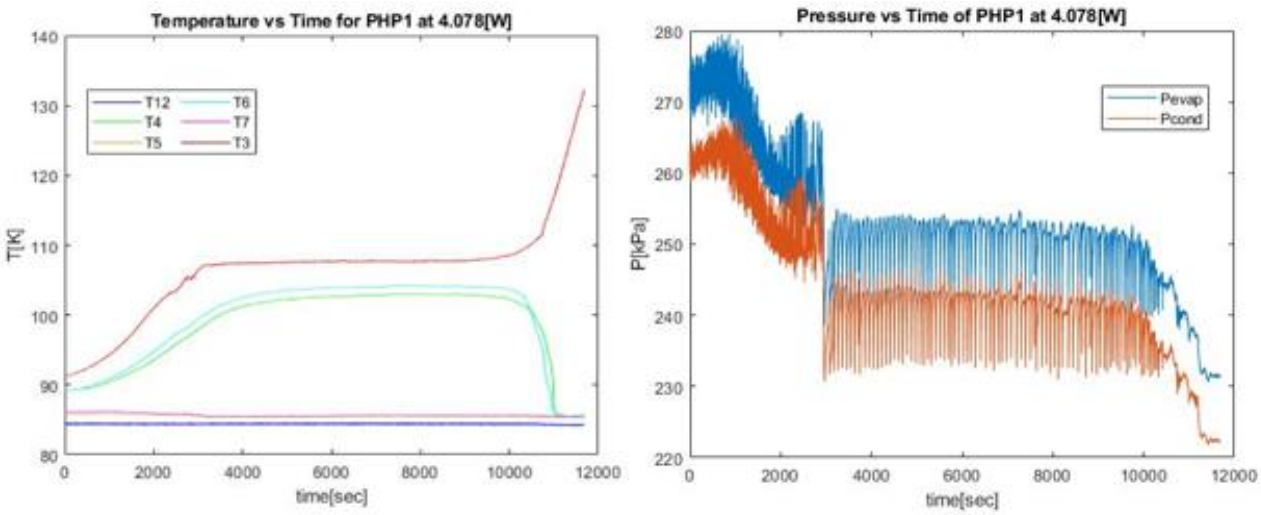

Figure 4-5 The temperature profile of the 3-turn PHP1 after the heat load on the evaporator increased from 3.86 W to 4.08 W (left). And the corresponding pressure profile of the condenser and the evaporator pressure transducers after the heat load on the evaporator increased from 3.86 W to 4.08W (right).

If the dry-out condition is observed in one of the PHPs at a relatively low heat load, it is most likely a local dry-out in a certain portion of the PHP propagating through the entire PHP and the fluid motion within the PHP cannot be sustained. The experiment is then 'rebooted' by applying zero heat load and then repeating the same heat load which caused the dry-out. Once the PHP reaches steady-state conditions after removing the heat load on the evaporator, the heat load that causes the previous dry-out condition is again applied to the evaporator. If the PHP still dries out at this heat load level, it is identified as the dry-out limit for the specified condenser temperature and the initial fill ratio. It is possible that the local dry-out in a certain portion of a multi-turn PHP would not affect the fluid motion of the entire system as much as for a single-turn PHP because the effect of the dry-out is distributed across the numerous tubes of the PHP. This dry-out at moderate heat load is mostly observed in 1-turn PHP experiments. From the 3-turn, 5-turn and 7-turn PHP experiment, we started to introduce the repeat tests by applying the same specified heat load on the PHP starting from a zero heat-load condition to verify the repeatability of the PHP.

4.3 Uncertainty Analysis

The heat transfer performance of the PHP is evaluated by the effective thermal conductivity

$$k_{eff} = \frac{QL}{NA_c(\bar{T}_e - \bar{T}_c)} \tag{8}$$

Where Q is the heat load on the evaporator, L is the adiabatic length of the PHP, A_c is the internal cross-sectional area of the capillary tube. N is the number of capillary tubes for each PHP, N is 2 for the single-turn pulsating heat pipes. $\bar{T}_e$ and $\bar{T}_c$ are the time-averaged temperature of the evaporator and the condenser. A 20-minute steady-state temperature measurement will be used for estimating the effective thermal conductivity of each head load. The uncertainty of the effective thermal conductivity is defined by the equation

$$\mu_{k_{eff}} = \sqrt{\left(\frac{\partial k_{eff}}{\partial Q}\mu_Q\right)^2 + \left(\frac{\partial k_{eff}}{\partial \bar{T}_e}\mu_{\bar{T}_e}\right)^2 + \left(\frac{\partial k_{eff}}{\partial \bar{T}_c}\mu_{\bar{T}_c}\right)^2} \tag{9}$$

μ_Q is the uncertainty of the applied heat on the evaporator, $\mu_{\bar{T}_e}$ is the uncertainty of the time-average evaporator temperature measurement and $\mu_{\bar{T}_c}$ is the uncertainty of the time-average condenser temperature measurement. The accuracy of the Lakeshore PT-102 temperature sensors with two-point calibration method is ±250 mK. The uncertainty of the applied heat is calculated as

$$\mu_Q = \sqrt{\left(\frac{\partial Q}{\partial I}\mu_I\right)^2 + \left(\frac{\partial Q}{\partial V}\mu_V\right)^2} \tag{10}$$

where μ_I and μ_V are the uncertainty of the current and voltage measurement of the evaporator heater. The current is measured by Agilent 3620A which has an accuracy of ±0.5% of the

measurement. And the voltage across the resistive heater on the evaporator is measured by HP34401A multimeters, which has an accuracy of 0.0035% of the measurement.

5. Experimental Results and Discussion

The condenser temperature and the initial fill ratio that have been tested for each PHP configuration are listed in Table 5-1 below. For the 1-turn and 3-turn PHP configurations, experimental results revealed optimum performance (highest effective thermal conductivity) between 50% and 75% fill ratio. However, optimum performance results for the 5-turn and 7-turn PHP occurred at fill ratios below 50%. Therefore no tests were carried out at the 75% fill ratio for these configurations. Furthermore, due to time limitations with the 7-turn PHP configuration only the 50% fill ratio case has been tested at the condenser temperature of 84.5 K.

Table 5-1 Initial fill ratio conditions that are tested at the condenser temperature of 77.4K and the condenser temperature of 84.5K for all the PHP configurations are listed below

Configuration	Initial Fill Ratio tested at T_{cond}~ 77.4K	Initial Fill Ratio tested at T_{cond}~ 84.5K
1-turn (2 tubes)	50%, 63%, 75%	50%, 63%, 75%
3-turn (6 tubes)	50%, 63%, 75%	50%, 63%, 75%
5-turn (10 tubes)	38%, 44%, 50%, 56.5%, 63%	38%, 50%, 63%
7-turn (14 tubes)	30%, 38%, 50%, 63%	50%

Figure 5-1 shows the locations of each temperature and pressure sensor. We will use the number in this schematic to discuss the experimental results in this section. For example, T3 refers to the temperature sensor installed at the center of the evaporator of PHP1; T6 refers to the temperature sensor installed at the left adiabatic section which is 0.25 m away from the evaporator. Pcond refers to the pressure transducer that is about 10 mm away from the condenser on the left adiabatic section on PHP1. The two nominally identical PHPs, PHP1 and PHP2 are

mounted to the same condenser in a parallel configuration and only PHP1 has pressure transducers near the condenser and evaporator.

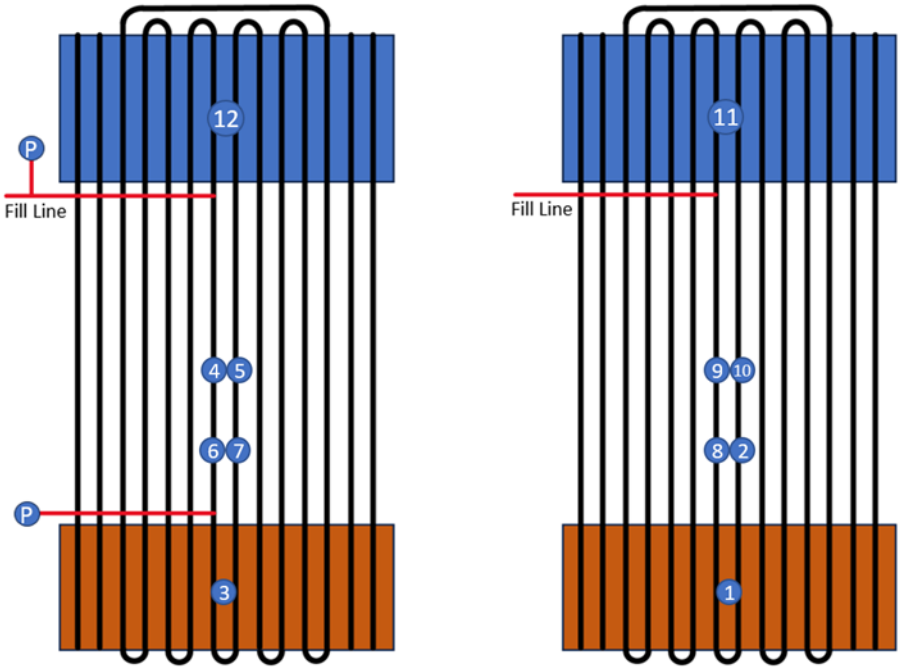

Figure 5-1 The location and numbering of each temperature and pressure sensor.

In the following subsections, I will discuss and analyze the data for each configuration (1-turn, 3-turn, 5-turn and 7-turn) and then compare the results across different configurations.

5.1 1-Turn PHP Experimental Results

5.1.1 Summary of the 1-turn PHP Experimental Results

The dry-out limit versus the initial fill ratio for the 1-Turn PHP experiment is shown in Figure 5-2 below. The dry-out limit is the maximum amount of heat load that can be applied to the PHP without causing a thermal run-away. Except for the test at the condenser temperature of

77.4 K and the fill ratio of 75%, a positive linear relationship between the fill ratio and the dry-out limit can be observed.

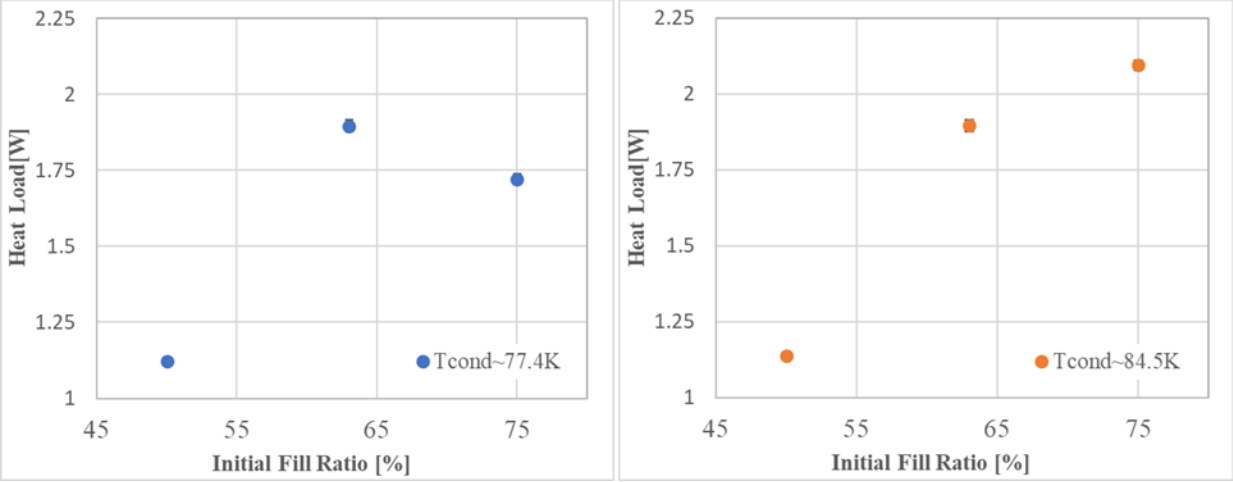

Figure 5-2 The dry-out limit versus the initial fill ratio for the condenser temperature of 77.4 K and 84.5 K.

The optimal effective thermal conductivity versus the initial fill ratio for the 1-turn PHP experiment is shown in Figure 5-3 below. The optimal heat transfer performance for PHP1 and PHP2 vary considerably over all the different fill ratio and condenser temperature cases. They are only close to each other at the test condition with the condenser temperature of 84.5K and the initial FR of 50%. In other test conditions, the optimal performance of the two PHPs are closest at the condenser temperature of 84.5 K and the initial fill ratio of 63% where the optimal effective thermal conductivity of PHP1 is about 25% higher than PHP2. The most significant difference in the optimal effective thermal conductivity between the two PHPs is observed at the condenser temperature of 77.4 K and the initial fill ratio of 75%. For this case, the optimal effective thermal conductivity for PHP1 is 643000 W/m-K which is about 3 times the optimal effective thermal conductivity of PHP2 212000 W/m-K. Note that although the lowest effective thermal conductivity of PHP2 (212000 W/m-K) determined with the intial fill ratio of 75% and a condenser temperature of 77.4 K is much lower than the effectiver thermal conductivities

observed in all other cases, it is still much higher than the thermal conductivity of other conventional thermal links. For comparison, the thermal conductivity of the copper with RRR values ranging between RRR=10 and RRR=2000 is only about 550 W/m-K at 77.4 K.

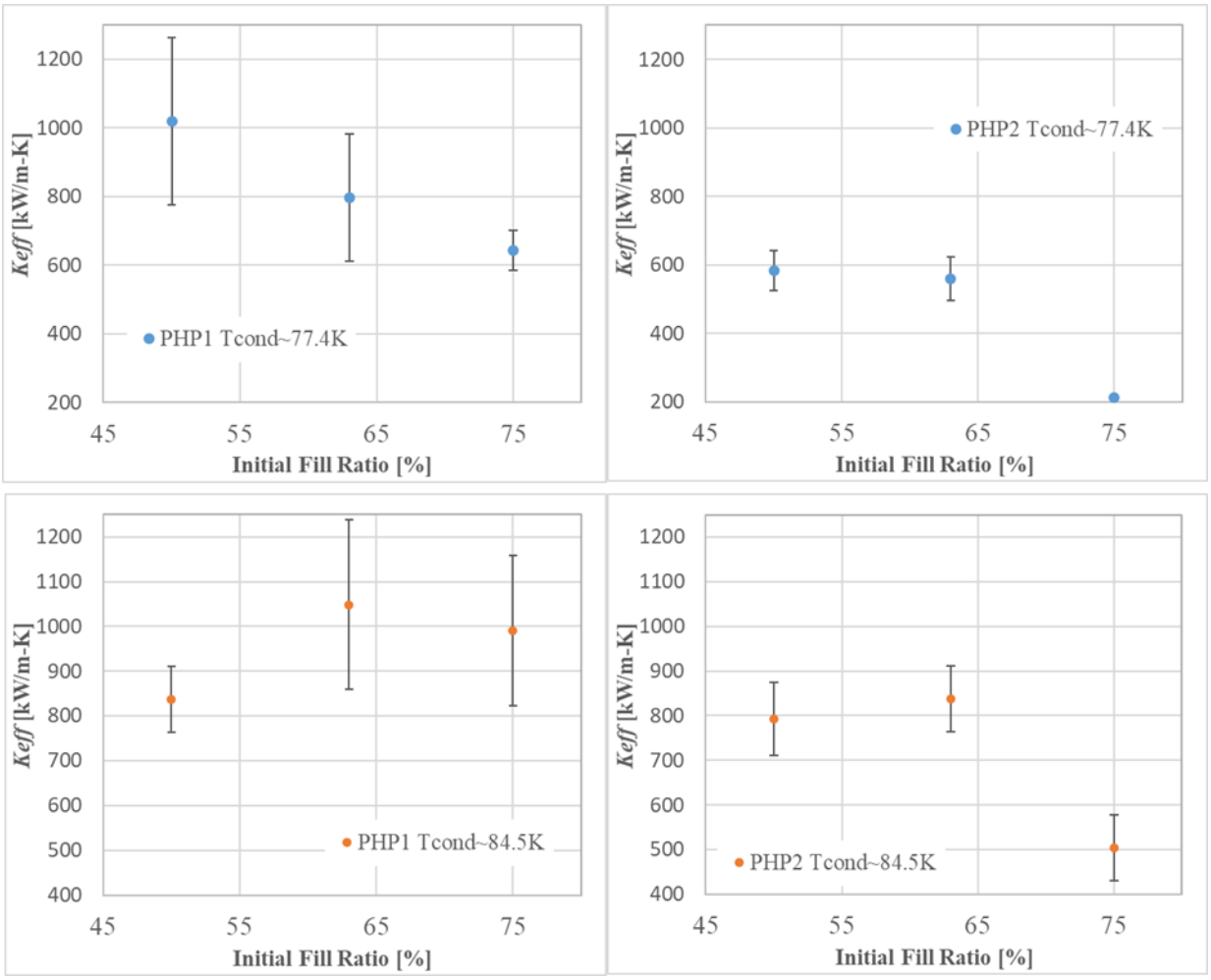

Figure 5-3 The optimal effective thermal conductivity versus the fill ratio for the PHP1 (top left) PHP2 (top right) at the condenser temperature of 77.4 K. And the optimal effective thermal conductivity versus the fill ratio for the PHP1 (lower left) PHP2 (lower right) at the condenser temperature of 84.5 K.

The difference in the thermal performance between PHP1 and PHP2 may be caused by unintended manufacturing variations, such as the slight difference in the curvature of the bending in the capillary tubes. A flow visualization experiment for a room temperature PHP with methonal as the working fluid has shown that liquid mass can accumulate at the bottom of the u-

bend of a tube forming a new liquid slug, blocking the flow of the vapor and resulting in a momentary increase of the vapor pressure [23]. The vapor pressure eventually grows to a level such that the liquid flows out of the lower section of the u-bend and compresses the downstream section of the vapor plug thereby causing a pressure oscillation [23]. Small variations in the radius of curvature can therefore influence the pressure perturbations that occur during operation.

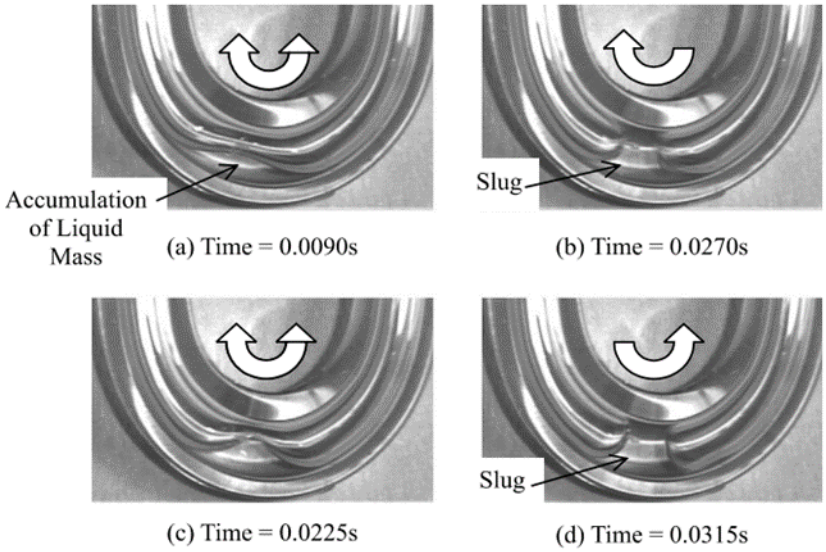

Figure 5-4 The liquid accumulated at the bottom of the U-bend of the PHP [23].

During the PHP fabrication process, we improved the bending technique for the capillary tube of the PHP and we only used the good capillary tube bent as shown in the picture Figure 5-5 below to reduce the influence of the curvature of the tube bending. A quantitative study of the fabrication factors, such as the curvature of the tube bending and the clogging of the capillary tubes, that affect the performance of the PHP could be conducted in the future.

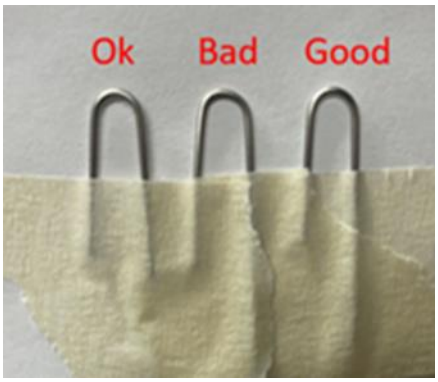

Figure 5-5 The acceptable, bad, and good examples of the U-bend of the capillary tubes. Only good examples are used for fabricating the PHP.

Another possible cause for the difference in the heat transfer performance between PHP1 and PHP2 is that PHP1 includes the extra volume associated with the capillary tubes that extend from the pressure transducers to the points where they tap into the evaporator and the condenser. The total volume of these tubes is estimated to be around 441.4 mm^3, representing about 75% of the total volume of the PHP core for the 1-turn PHP configuration. This extra space on PHP1 likely influences the vapor and liquid distribution of the working fluid. The same volume associated with the pressure transducers represents about 29%, 18%, and 13% of the total volume of the 3-turn, 5-turn, and 7-turn PHP respectively. In the following subsections that discuss the experimental results of the 3-turn, 5-turn, and 7-turn configuration, we will observe that the difference in the heat transfer performance between the PHP1 and PHP2 becomes smaller. In certain operating conditions, the heat transfer performance of PHP1 and PHP2 is within the uncertainty error of each other.

5.1.2 Initial Dry-out and the Reboot of the PHP (Tcond~84.5K and FR=63% case)

Both PHP1 and PHP2 exhibit dry-out behavior at moderate heat loads but can be rebooted with subsequent performance to higher heat loads, and exceptionally high values of effective thermal conductivity are observed for the 1-turn PHP experimental tests. In the

remainder of this subsection, we will present the moderate dry-out behavior and reboot process as measured at the condenser temperature of 84.5 K and the initial fill ratio of 63%. Similar behavior is observed at the other conditions of condenser temperature and fill ratio for the 1-turn PHP.

At the condenser temperature of 84.5 K and the initial fill ratio of 63%, PHP1 exhibits a dry-out condition when the heat load is increased to 1.43 W to the evaporator from the previous heat load of 1.32 W. The temperature profiles and the pressure traces at this condition are shown in Figure 5-3 below. The evaporator temperature of PHP1, T3, was above the critical temperature of the nitrogen after 10,000 sec in this run indicating a dry-out condition. T6 and T4 on the left adiabatic section of PHP1 were maintained at around 85.2 K and 85.81 K while T7 of the right adiabatic section was following the trend of the evaporator temperature during the dry-out process. These temperatures suggest that the left adiabatic section was full of liquid while the right adiabatic section was full of vapor. At around 6500 sec, T7 starts to drop and eventually decreases to around 85 K while the evaporator temperature T3 increases above 103 K. Fluid is pushed into the left adiabatic section from the evaporator due to the gas expansion and liquid from the condenser likely extends down to the location of T7. The slope of the T3 becomes much steeper when T3 approaches 105 K suggesting an absence of liquid in the evaporator anymore.

The evaporator and condenser pressure reduced sharply when the slope of the T3 becomes steeper between 4000 sec and 6000 sec, and after around 9000 sec. Such behavior suggests that more of the liquid /vapor interfaces are pushed into the condenser, thereby lowering the saturation temperature and pressure. Even though both the evaporator and condenser pressure dropped during this run, the pressure difference between the evaporator and the condenser

remained constant at around 1.5 kPa. Additionally, PHP2 reached a steady state at around 1000 sec. The effective thermal conductivity of PHP2 was around 732000 W/m-K.

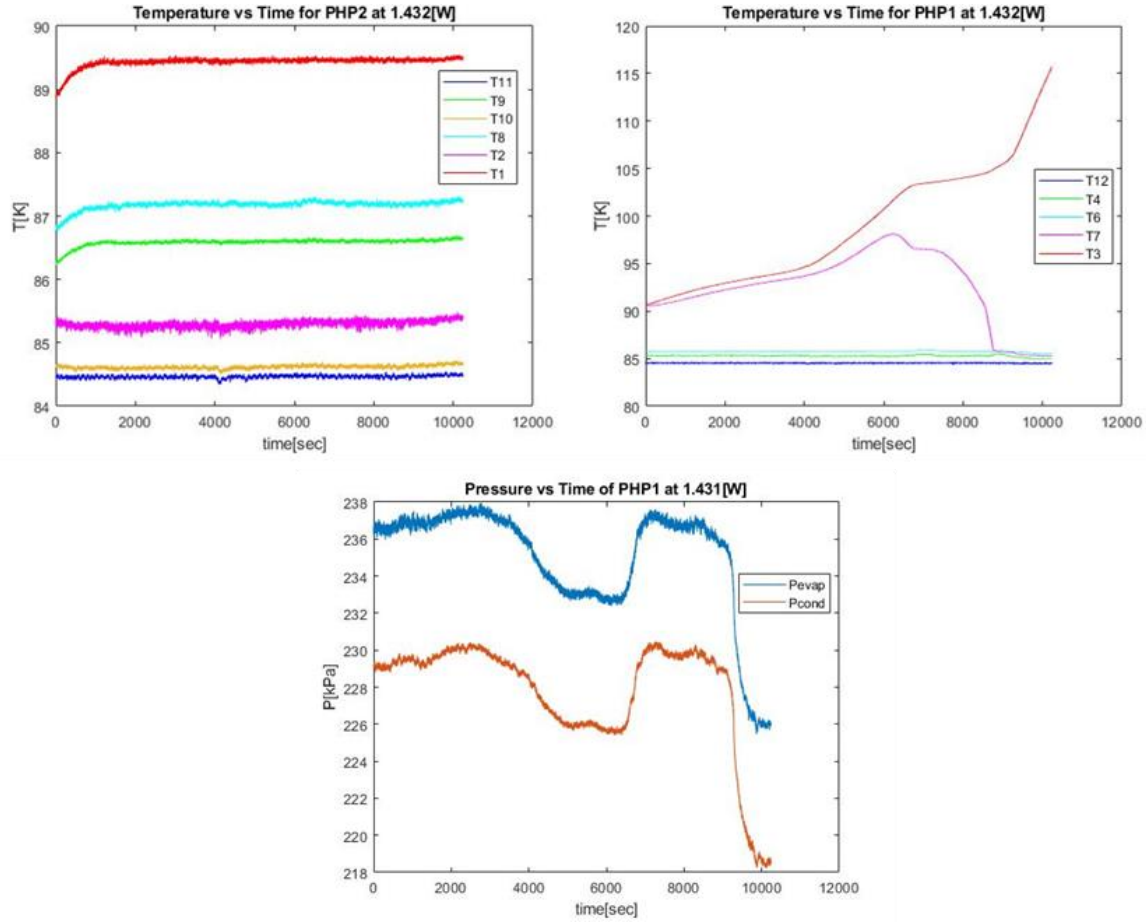

Figure 5-6 Temperature and Pressure profiles of the PHP when the initial dry-out is observed at the heat load of 1.43 W.

After the dry-out, the evaporator heaters on both PHPs were shut off. When the steady state of the PHPs was observed at zero heat load, the evaporator heaters were again increased to 1.43 W, a so called ‘reboot’ process. After the PHPs are rebooted from zero heat load, both PHPs reach a steady state at around 1400 sec. The effective thermal conductivity of PHP1 and PHP2 become 658000 W/m-K and 740000 W/m-K respectively. After the PHPs have been ‘rebooted’, both PHP sections can operate with increasing heat load until the dry-out limit of 1.90 W is reached on each PHP evaporator.

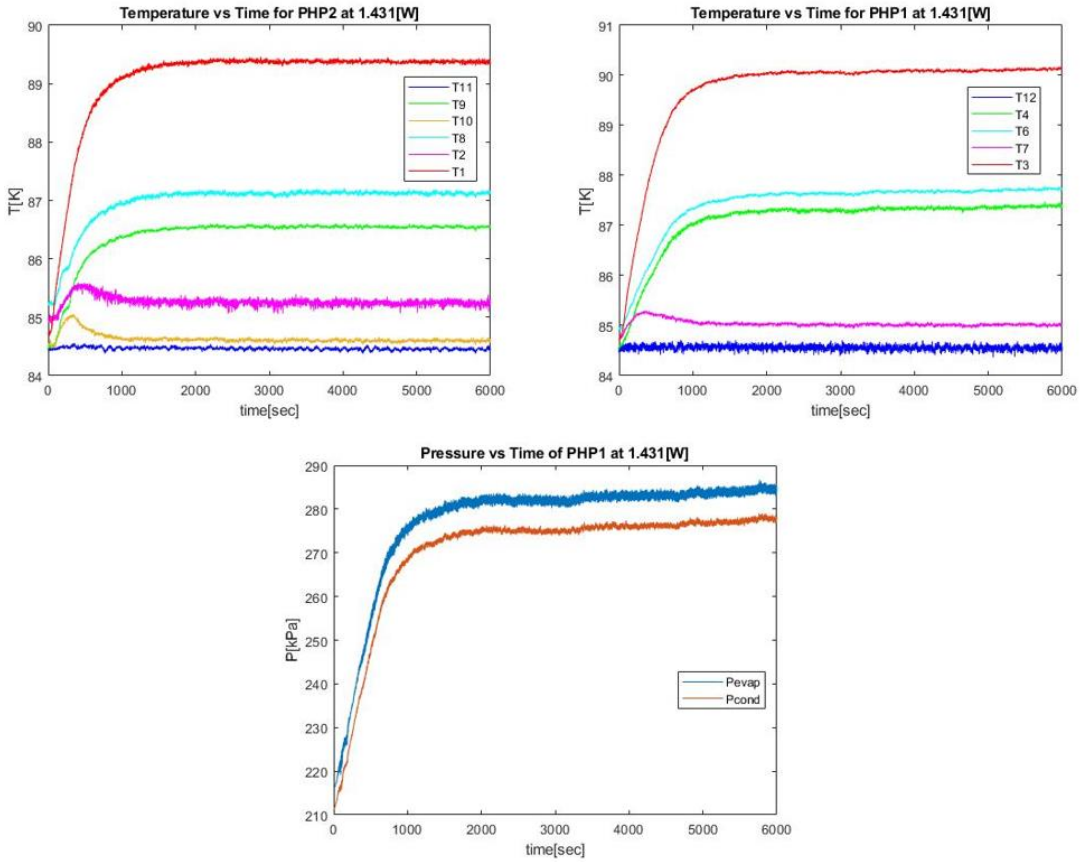

Figure 5-7 Temperature and Pressure profiles of the PHP when 'rebooted' at the heat load of 1.43 W.

Figure 5-8 summarizes the effective thermal conductivity versus heat load of PHP1 at the condenser temperature of 84.5 K and initial fill ratio of 63%. During the first ramp-up of heat, PHP1 dried out at 1.32 W and was then successfully rebooted from a lower heat load. PHP1 dried out again at 1.43 W after the first reboot but was rebooted again at 1.43W and then continued to operate to a higher heat load, eventually drying out at around 1.90 W on the evaporator.

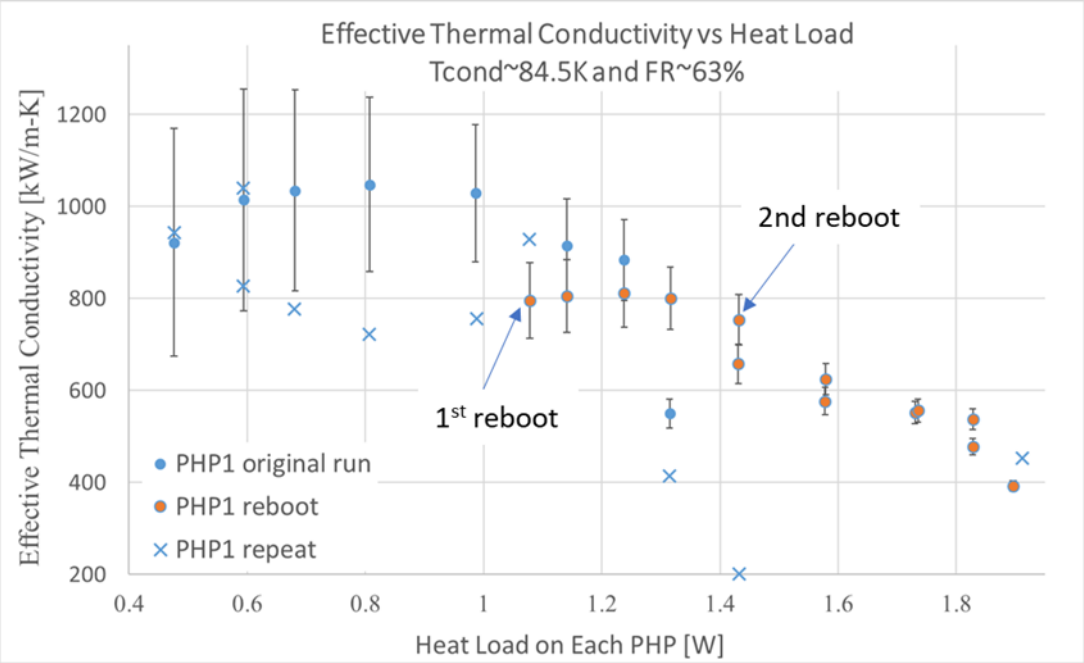

Figure 5-8 Effective Thermal Conductivity vs Heat Load for PHP1 at the condenser temperature of 84.5 K and the initial fill ratio of 63% (1-turn PHP).

5.2 3-Turn PHP Experimental Results

5.2.1 Summary of the 3-turn PHP Experimental Results

The dry-out limit versus the initial fill ratio for the 3-turn PHP experiment is shown in Figure 5-9 below. The dry-out limit is the maximum amount of heat load that can be applied to each PHP evaporator without drying out. In the 3-turn PHP experiments, the PHP only experience initial dry-out at heat load at 3.76 W at the condenser temperature of 84.5 K with the initial fill ratio of 50% and at 3.45 W at the condenser temperature of 77.4 K with the initial fill ratio of 75%. The heat level of the initial dry-out observed for the 3-turn PHP is very close to the real dry-out limit of the PHP unlike the initial dry-out for 1-turn PHP is usually observed at moderate heat load. The heat load initial dry-out for the condenser temperature of 84.5 K and the intial fill ratio of 50% is 3.76 W that is only 3.1% lower than the real dry-out limit 3.88 W. Even two intial dry-out observed, but they are very close to the maximum heat load that can be applied

on the evaporator. Thus 3-turn PHP has a better stability than 1-turn PHP. A positive linear relationship between the fill ratio and the dry-out limit can be observed for both condenser temperature conditions.

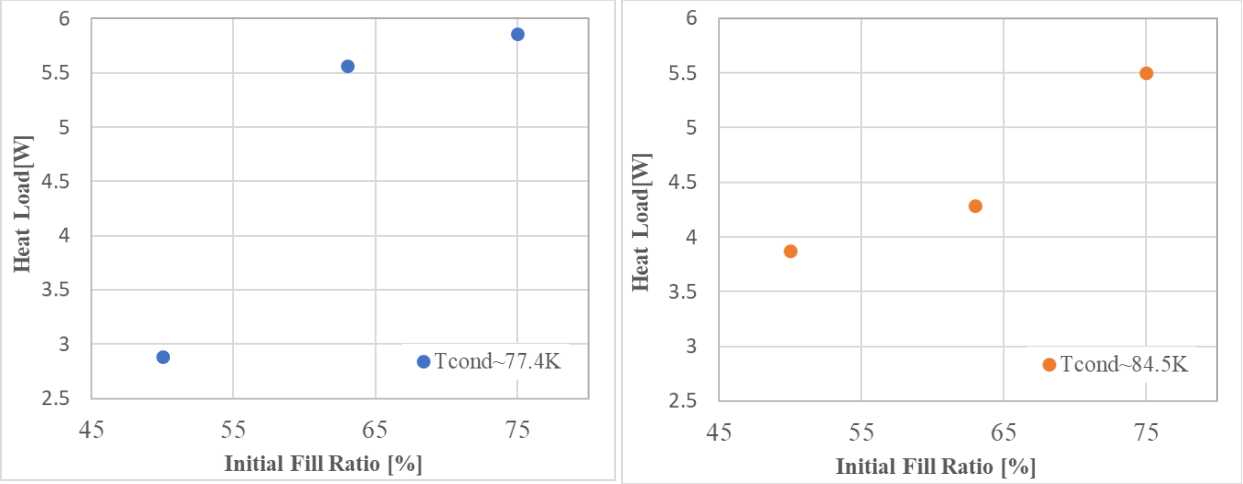

Figure 5-9 The dry-out limit versus the initial fill ratio of the 3-turn PHP for the condenser temperature of 77.4 K (left) and 84.5 K (right).

The optimal effective thermal conductivity versus the initial fill ratio for the 3-turn PHP experiment is shown in Figure 5-10 below. The best effective thermal conductivity of PHP1 and PHP2 is 851000 W/m-K and 789000 W/m-K respectively. They are both observed at the condenser temperature of 84.5 K at the initial fill ratio of 50%. The difference between the optimal effective thermal conductivity of PHP1 and PHP2 is only about 9.1% and 7.9% for the initial fill ratio of 50% at the respective condenser temperature of 77.4 K and 84.5 K. The difference in the optimal effective thermal conductivity between PHP1 and PHP2 is only about 30% and 15% for the initial fill ratio of 63% at the respective condenser temperature of 77.4 K and 84.5 K. The optimal effective thermal conductivity of PHP1 is about 2.2 times and 2.1 times larger than the effective thermal conductivity of PHP2 for the initial fill ratio of 75% at the

respective condenser temperature of 77.4 K and 84.5 K. The difference in the optimal heat transfer performance between PHP1 and PHP2 for the 3-turn configuration is less significant when compared with the results observed in the 1-turn PHP tests. However, it is still true that the performance of PHP1 is much better than PHP2 at both of 75% fill ratio results. It is possible the better performance of PHP1 at high fill ratios may be attributed to the extra space associated with the taps connected to the pressure transducers. The influence of the extra space on the degree of freedom for the bubble distribution is more significant at the high fill ratio conditions in agreement with observations from Khandekar's parametric study of pulsating heat pipes [19].

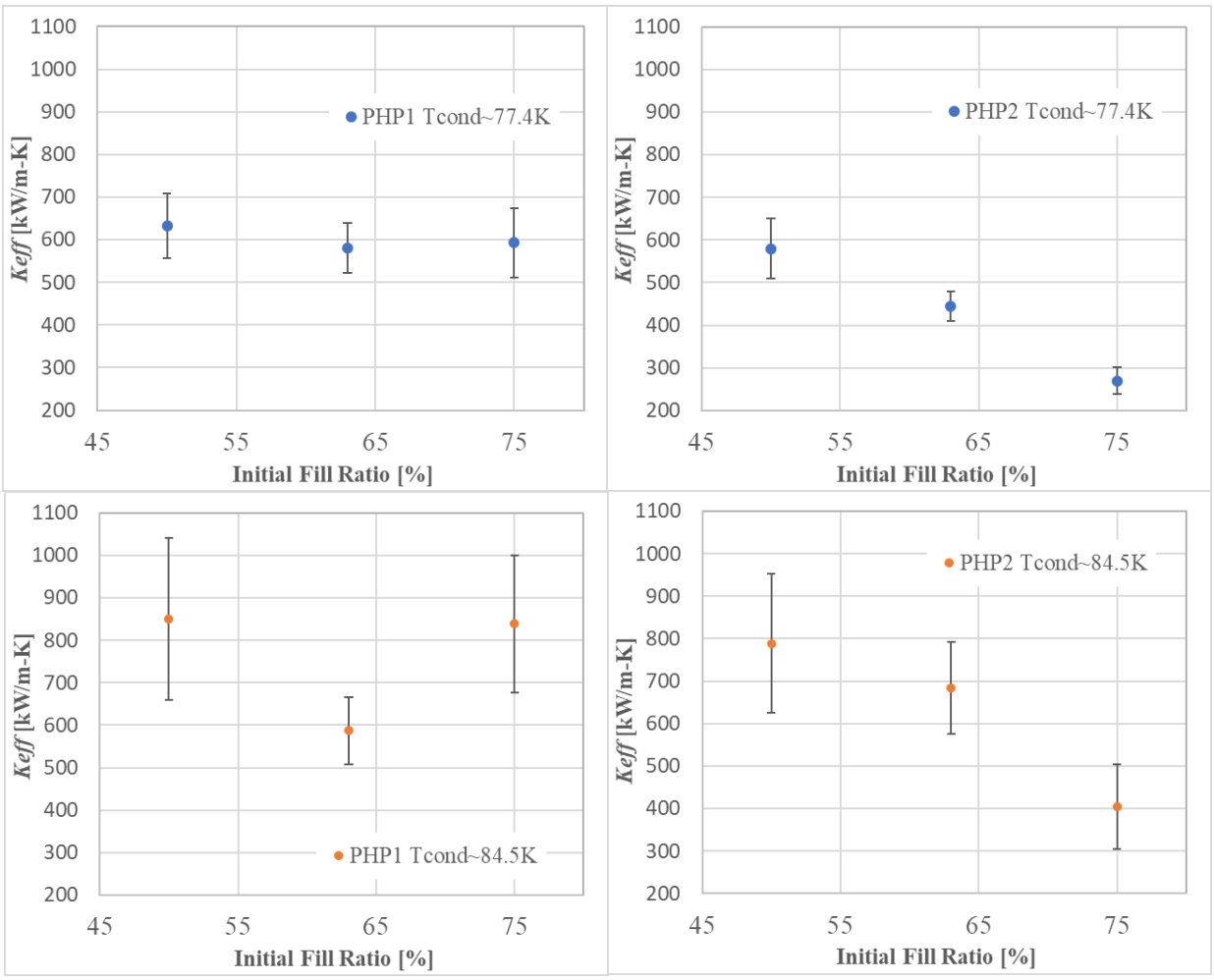

Figure 5-10 The optimal effective thermal conductivity versus the fill ratio for the 3-turn configuration PHP1 (top left) PHP2 (top right) at the condenser temperature of 77.4 K. And the optimal effective thermal conductivity versus the fill ratio for the 3-turn configuration PHP1 (lower left) PHP2 (lower right) at the condenser temperature of 84.5 K.

5.2.2 3-turn PHP Experimental Results at Tcond~77.4 K and FR=50%

Figure 5-11 below summarizes the effective thermal conductivity versus heat load at the condenser temperature of 84.5 K and the initial fill ratio of 63%. Both PHP1 and PHP2 show a greater than 500 kW/m-K effective thermal conductivity performance from 1.58W to 2.88 W.

The results of the repeat tests are all within the uncertainties of the effective thermal conductivities measured during the initial (sequential) heat load test.

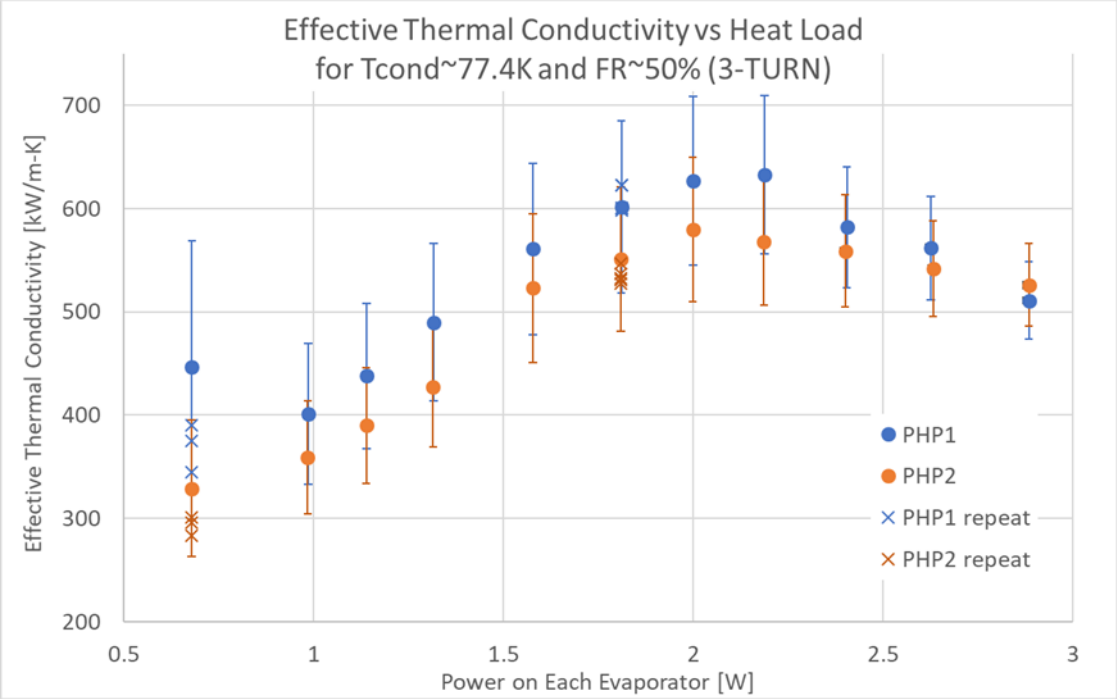

Figure 5-11 Effective thermal conductivity versus the heat load for the PHP1 and PHP2 at the condenser temperature of 77.4 K with the initial fill ratio of 50%.

The combined measurements from the temperature sensors mounted in the adiabatic sections and the pressure transducers on the 7th tube of PHP1, enable a richer set of information regarding PHP1 such as the thermodynamic state of the fluid in the adiabatic sections and the flow direction. Figure 5-12 below summarizes the temperature in the adiabatic section of the 7th and 8th tube of PHP1 and the saturation temperatures corresponding to the condenser and evaporator pressure transducer measurements in the sequential heat load runs. ‘T_left’ in the plot

is the average of temperature of the T4 and T6 and ‘T_right’ is the average temperature of the T5 and T7 on the PHP1.

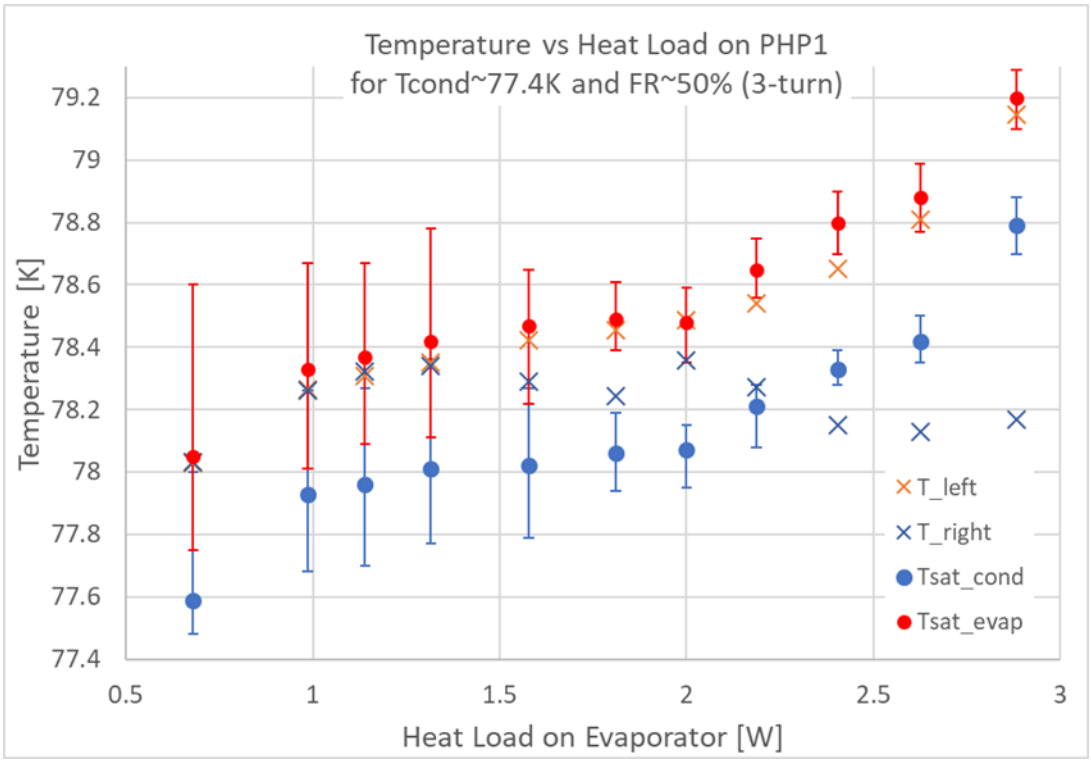

Figure 5-12 The temperature vs heat load plot for PHP1 for the condenser temperature of 77.4 K and the initial fill ratio of 50%. T_left is the average of T4 and T6 at the 7th adiabatic tube, and T_right is the average of the T5 and T7 on the adiabatic tube as shown in Figure 5-1.

When the evaporator heat load is smaller than 1.5W, both left and right leg of the adiabatic section are at the same thermodynamic state and tracking the saturation temperature of the evaporator pressure transducer. The working fluid is two-phase and the heat transfer relies on the latent heat. A clock-wise unidirectional flow is formed when the heat load reaches 1.58 W. At this, and higher, heat loads the fluid in the right adiabatic section approaches a subcooled state, eventually becoming subcooled when the heat load exceeds 2W. The corresponding decrease in thermal performance of the PHP may reflect the reduced heat transfer coefficient

related to single phase flow compared to that associated with two-phase flow. As the heat load increases further, the thermal performance of PHP decreases.

5.2.2 3-turn PHP Experimental Results at Tcond~77.4 K and FR=75%

In the 3-turn PHP experiment, both PHPs display dry-out behavior at a moderate heat load and require rebooting to operate at a higher heat load when the condenser temperature is 77.4 K and the initial fill ratio is 75%. PHP dry out at a moderate heat load during an increasing heat load test does not occur for any of the 5-turn or 7-turn tests. PHP1 initially dries out at 3.45 W, however both PHPs reach a maximum heat load of 5.86 W on the evaporator after reboot. Figure 5-13 below presents the effective thermal conductivity as a function of the heat load for this test condition.

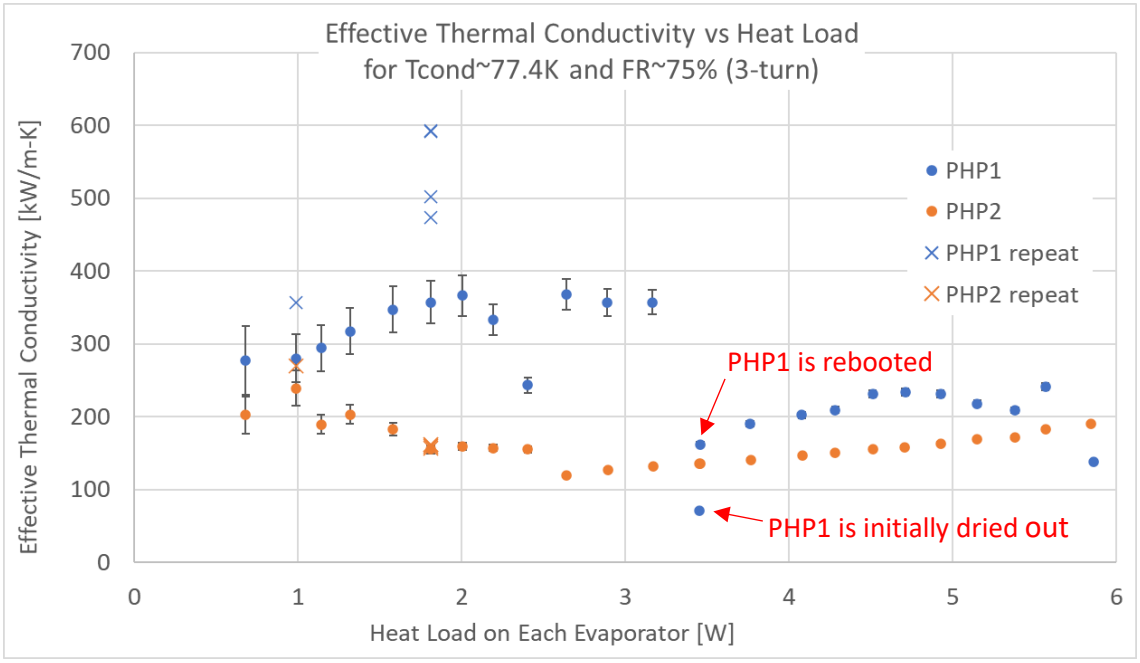

Figure 5-13 Effective thermal conductivity versus the heat load for the PHP1 and PHP2 at the condenser temperature of 77.4 K with the initial fill ratio of 75%.

After the reboot, the heat transfer performance of PHP1 dropped significantly. The effective thermal conductivity of PHP1 at 3.46 W (the first test after reboot) is only 162000 W/m-K which is only 45% of the effective thermal conductivity of the PHP1 at 3.16 W (the last test before reboot).

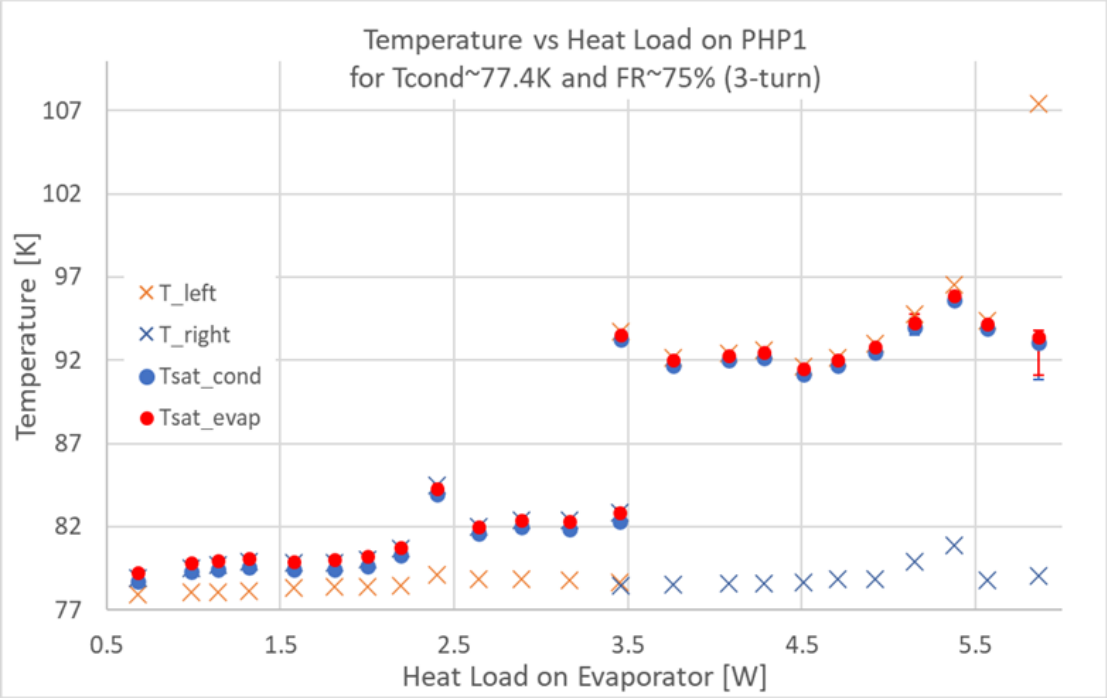

Figure 5-14 The temperature vs heat load plot for PHP1 for the condenser temperature of 77.4 K and the initial fill ratio of 75%. T_left is the average of T4 and T6 at the 7th adiabatic tube, and T_right is the average of the T5 and T7 on the adiabatic tube as shown in Figure 5-1.

Figure 5-14 summarizes the temperature of the adiabatic section at the 7th and 8th tube of PHP1 and the saturation temperatures corresponding to the condenser and evaporator pressure transducer measurements in the sequential heat load runs. We will refer to the adiabatic section that has a higher temperature than the other as the hot side and the adiabatic section with a lower temperature as the cold side in the following analysis. Prior to the reboot process, the right adiabatic section (hot side) of the PHP is very close to, but slightly below, the saturation temperature of the evaporator pressure, meaning it is not superheated.

After the reboot process, the flow direction changes from counterclockwise to clockwise. Figure 5-14 also shows that the saturation temperatures associated with both pressure transducers increase drastically after the reboot. Furthermore, the temperature of left adiabatic section (now the hot side) is higher than the saturation temperature of the evaporator meaning the left adiabatic section is superheated and therefore carrying a large amount of the heat load.

The left side and the right side in Figure 5-14 are the cold side of the PHP before the reboot and after the reboot respectively. The cold side is also in a subcooled state before and after the reboot, and the temperature difference between the cold side and the saturation temperature of the condenser pressure transducer after the reboot is much higher than the temperature difference before the reboot. The significant temperature difference between the saturation temperature of the pressure transducer and the cold side temperature means the condenser section of the PHP is flooded with the subcooled liquid. The left adiabatic section is full of superheated vapor and the right adiabatic section is full of the subcooled liquid which is an extreme vapor and liquid distribution scenario. There is no two-phase fluid after the reboot based on the observation of Figure 5-14, the heat transfer coefficient of the PHP drops significantly and the effective thermal conductivity displayed in Figure 5-13 also decreases. In the experiments of the PHP at other test conditions and configurations, we also find similar behavior at high heat loads, suggesting that in such cases the hot adiabatic section is full of superheated vapor and the cold adiabatic section is full of subcooled liquid. The heat transfer performance is usually within the range of 150000 W/m-K and 300000 W/m-K in these cases.

Figure 5-15 shows the temperature of the left adiabatic section, right adiabatic section, saturation temperature of the evaporator pressure transducer, and the saturation temperature of the condenser pressure transducer as a function of the effective thermal conductivity for PHP1 at

1.81 W. It includes the results of PHP1 at 1.81 W from both the sequential heat load test and the repeat tests. This plot characterizes three distinct vapor and liquid distribution scenarios, and we will call these three scenarios as case 1, case 2 and case 3 as highlighted in Figure 5-15. In case 1, the left leg of the adiabatic section is subcooled liquid and the right adiabatic section is full of of a saturated fluid. The fluid pressure is the greatest in this case but the heat transfer performance is the worst. In case 2, the right leg is saturated vapor but the temperature is not as hot as in the case 1 and it is possible that the fluid in the cold leg of the adiabatic section is slightly subcooled liquid. In case 3, the temperatures of both adiabatic sections are within the saturation temperature of the evaporator and the condenser pressure measurements suggesting the existence of interfaces between the liquid and vapor in both adiabatic sections. The fluid in both adiabatic sections is two-phase vapor and liquid in this case.

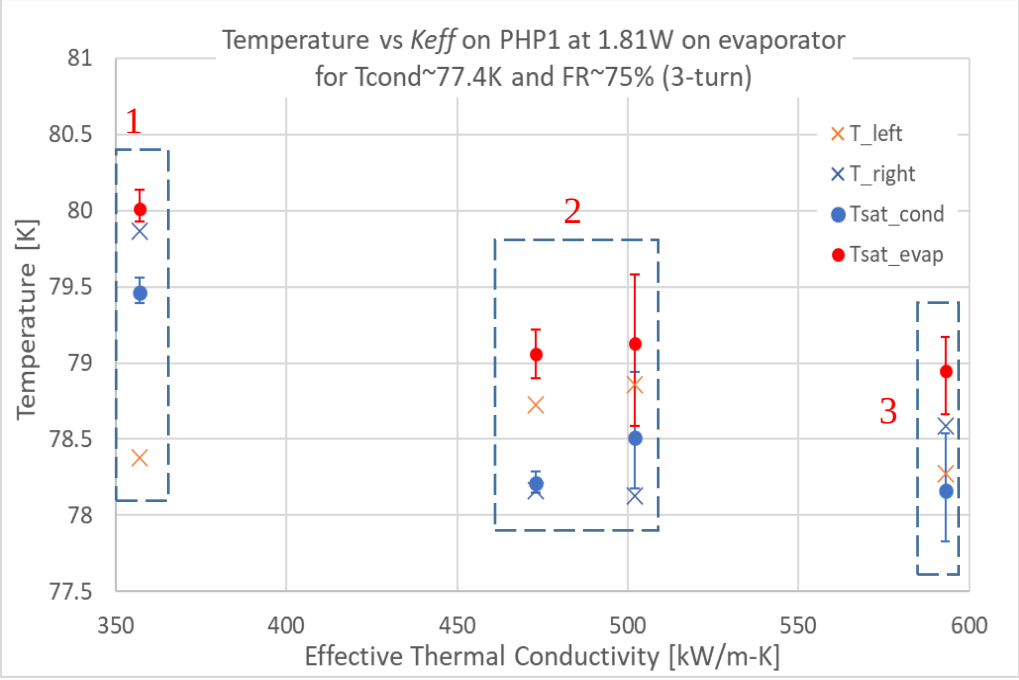

Figure 5-15 The temperature versus the effective thermal conductivity for the PHP1 tested at 1.81 W. The result corresponds to the effective thermal conductivity of 357kW/m-K is the measurement from the original increasing heat load test, the other results are from the repeat heat

load test at 1.81 W. The temperature highlighted in the three dashed boxes are the three distinct vapor and liquid distribution cases.

The heat transfer performance is the greatest when the fluid is saturated vapor and liquid in both legs. From case 1 to case 3, the heat transfer mechanism transitions from the sensible heat to latent heat as the heat transfer coefficient performance increases even though the heat load applied on the evaporator is the same.

In summary the best heat transfer performance of the PHP occurs when the fluid in both adiabatic sections is comprised of a two-phase mixture of vapor and liquid. When the adiabatic section is occupied by either super-heated vapor, subcooled liquid or both, the heat transfer performance degrades.

5.3 5-Turn PHP Experimental Results

5.3.1 Summary of the 5-turn PHP Experimental Results

In the 5-turn PHP experiment, PHPs do not display dry-out at moderate heat load, nor require the reboot process for operating at a higher heat load as was the case for the 1-turn and 3-turn PHP experiments. The dry-out limit versus the initial fill ratio for the 5-Turn PHP experiment is displayed in Figure 5-16 below. The dry-out limit is the maximum amount of heat load that can be applied to each PHP evaporator without either of them drying out. The maximum dry-out limit that can be applied on the evaporator of the PHP has a positive relationship with the initial fill ratio for the 5-turn PHP configuration. It is worth noting that the maximum heat load that can be applied to the PHP at the condenser temperature of 77.4 K is about 8.11 W for the intial fill ratio of 63% while the maximum heat load that can be applied on the PHP at the condenser temperature of 84.5K is 7.80W for the intial fill ratio of 63%. A similar trend exists in the experimental results with the 3-turn configuration. In that case the

maximum dry-out limit that can be applied to the PHP at 84.5K is lower than that at 77.4 K for the maximum fill ratio tested (75%). One impotrant driving force for the PHP operation is the contraciton and the expansion of the fluid when the fluid flows throught the condenser and the evaporator. And $(dP/dT)_{sat}$ is about 11.99 kPa/K and 21.27 kPa/K at 77.4 K and 84.5 K, our physical intuition tells us that 84.5 K is expected have a higher dry-out limit if (dP/dT)sat is the dominant driving force. In the following subsections, we will try to explain why the PHP with lower condenser temperature have a higher dry-out limit. But we also need to keep in mind there are many other factors might need to be considered such as the temperature dependt viscosity of the liquid, the magnitude of the gravtional force between two adiabatic secitons and the temperature dependent latenet,etc

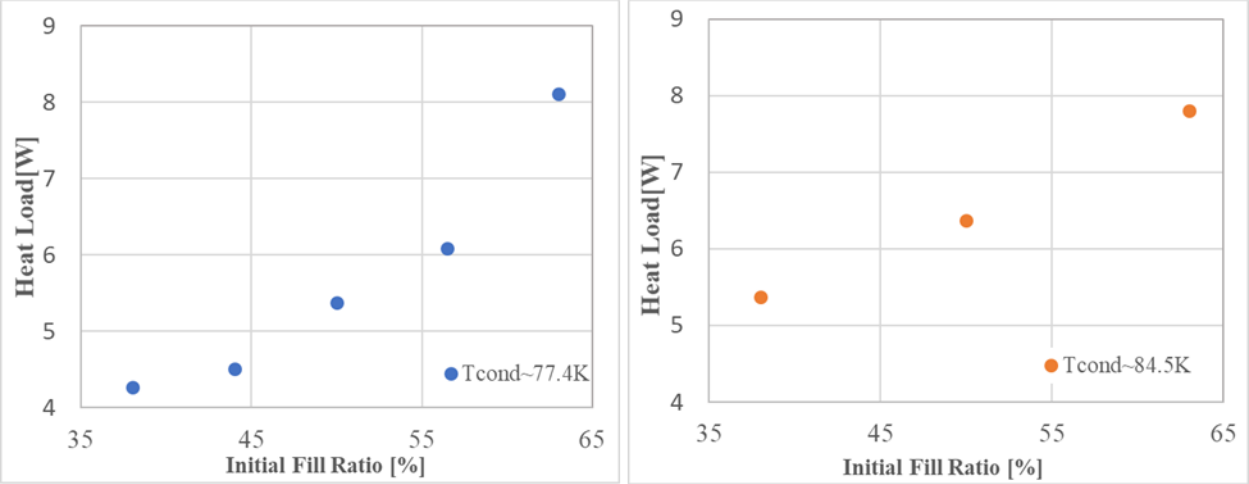

Figure 5-16 The dry-out limit versus the initial fill ratio of the 5-turn PHP for the condenser temperature of 77.4 K (left) and 84.5 K (right).

Figure 5-17 and Figure 5-18 below present the optimal effective thermal conductivity as a function of the initial fill ratio for the 5-turn PHP at the condenser temperature of 77.4 K and 84.5 K. The fill ratios have been chosen so that an optimum value could be determined, that is the fill ratio enabling the maximum effective thermal conductivity.

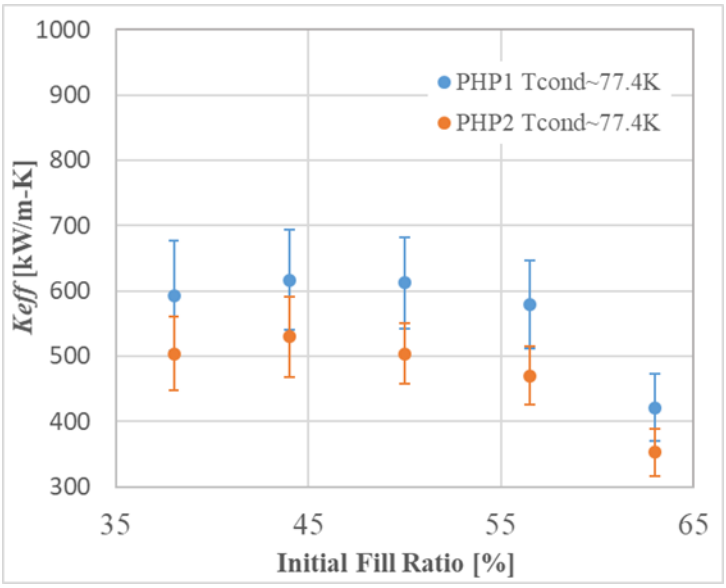

Figure 5-17 Optimal effective thermal conductivity versus the fill ratio for the 5-turn PHP experiments with the initial fill ratio between 38% and 63%.

It is worth noting that the PHP2 has the same the trend as the PHP1 for the effective thermal conductivity as function of the fill ratio. The optimal effective thermal conductivity of the PHP2 is about 16% to 23% lower than that of PHP1 at each fill ratio for the condenser temperature of 77.4 K. And optimal effective thermal conductivity of PHP2 is about 17%, 19% and 27% lower than that of PHP1 at the fill ratio of 38%, 50%, and 63% for the condenser temperature of 84.5 K. For the 5-turn configuration at both condenser temperatures, the heat transfer performance of PHP1 and PHP2 is within the uncertainty error of each other.

In the plots of effective thermal conductivity as a function of the fill ratio for the 1-turn PHP (Figure 5-3) and 3-turn PHP (Figure 5-10), PHP1 and PHP2 not only do not have the same trend but also have significantly different values of optimal effective thermal conductivity at the same test condition. As mentioned in the chapter describing the 1-turn PHP, it is possible that the extra volume associated with the capillary tubes that extend from the pressure transducers to the points where they tap into the evaporator and the condenser on PHP1 becomes less significant as

the number of turns increases. For the 5-turn PHP, the extra volume in PHP1 might still promote the heat transfer performance by influencing the distribution of the vapor and liquid, but the influence is not sufficiently significant to determine an optimum fill ratio. The absence of any early dry-out events for the 5-turn PHP may be attributed to the large enough number of turns that provide a more even distribution of the vapor and liquid. The larger number of turns also gives more chance for liquid flowing into the evaporator to overcome the local hot spot that caused the initial dry-out observed in the 1-turn experiments and occasionally in 3-turn PHP experiments.

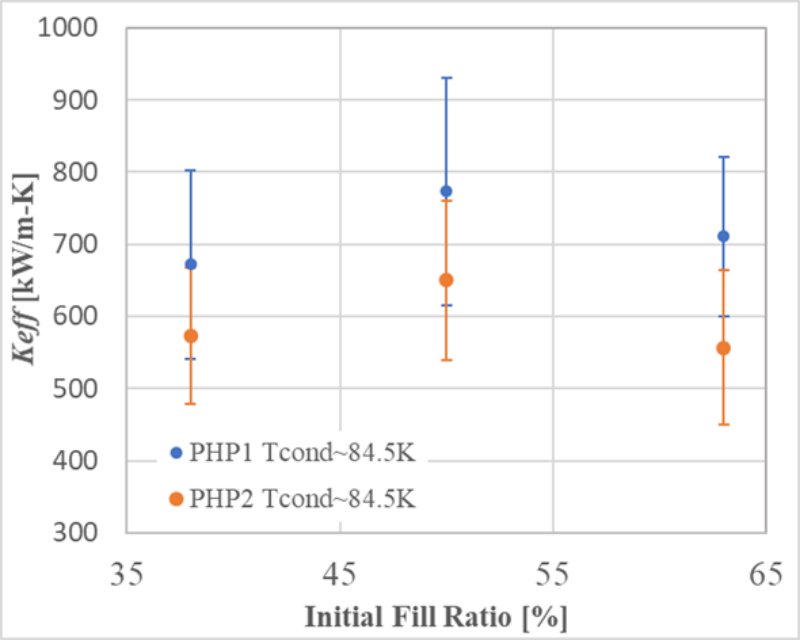

Figure 5-18 Optimal effective thermal conductivity versus the fill ratio for the 5-turn PHP experiments with the initial fill ratio between 38% and 63%.

5.3.2 5-turn PHP Experimental Results at FR=63% for Tcond~77.4 K and Tcond~84.5 K

Figure 5-19 summarizes the effective thermal conductivity as a function of the heat load on the evaporator for PHP1 at the condenser temperature of 77.4 K and 84.5 K with the intial fill ratio of 63%. The value of $(dP/dT)_{sat}$ at 84.5 K is about 77% higher than the value of $(dP/dT)_{sat}$ at 77.4K, a factor that contributes to the higher heat transfer performance at the condenser temperature of 84.5 K as compared to that at 77.4 K with the same intial fill ratio.

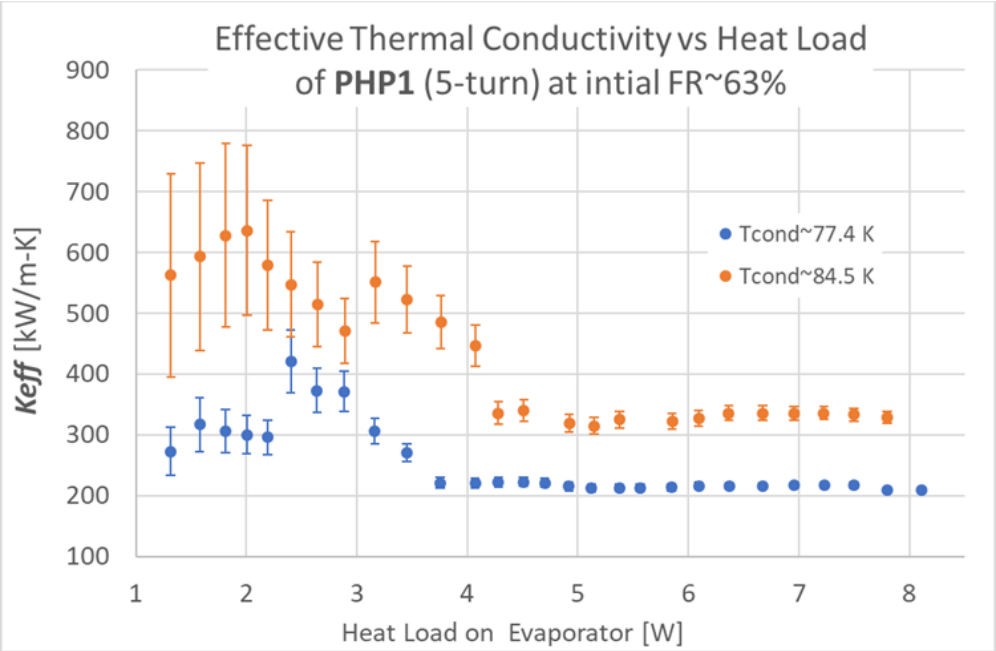

Figure 5-19 Effective thermal conductivity as a function of the heat load on the PHP1 evaporator for the condenser temperature of 77.4 K and the condenser temperature of 84.5 K at the initial fill ratio of 63%.

Figure 5-20 and Figure 5-21 below summarize the temperature in the adiabatic section of the 7th tube (left) and 8th tube (right) of PHP1 and the saturation temperatures corresponding to the condenser and evaporator pressure transducer measurements in the sequential heat load runs at the initial fill ratio of 77.4 K and 84.5 K respectively. In the case with the condenser temperature of 77.4 K, the fluid within the right adiabatic section becomes superheated from 1.81 W to 2.20 W. When the heat load increased from 2.20 W to 2.40 W, the flow direction

changed counter-clockwise to clockwise. For the step of heat load at 2.40 W, 2.64 W and 2.89 W, the working fluid in both adiabatic sections is most likely two-phase as the greatest effective thermal conductivities occur at these three heat loads (see Figure 5-19). The effective thermal conductivity starts to decrease after the heat load is greater than 3 W. For the same range of heat load, the right adiabatic section is not two-phase, but subcooled.

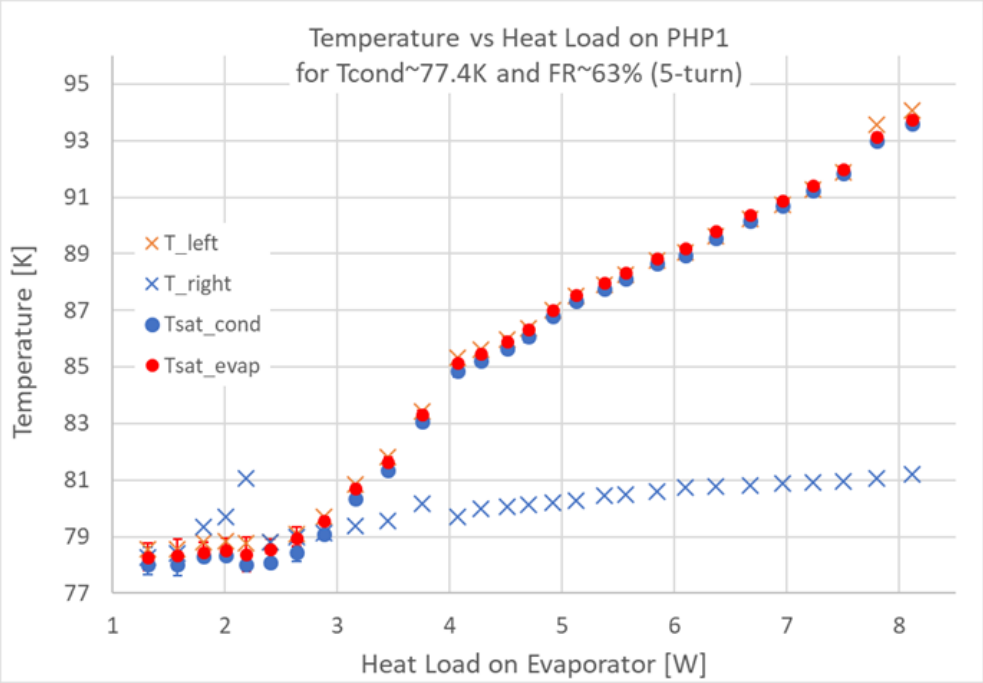

Figure 5-20 The temperature vs heat load plot for PHP1 for the condenser temperature of 77.4 K and the initial fill ratio of 63%. T_left is the average of T4 and T6 at the 7th adiabatic tube, and T_right is the average of the T5 and T7 on the adiabatic tube as shown in Figure 5-1.

In the case with a condenser temperature of 84.5 K, the working fluid in both the left and right adiabatic sections is two-phase during the heat load range from 1.32 W to 2.00 W (see Figure 5-21) and a positive trend of the heat transfer performance as a function of the heat load is displayed in Figure 5-19. From 2.00 W to 2.89 W, the working fluid in the left adiabatic section becomes superheated and the right adiabatic section becomes subcooled. In the same range the heat transfer performance decreases as shown in Figure 5-19. The saturation temperature of the condenser and the evaporator increases drastically when the heat load is above 4 W.

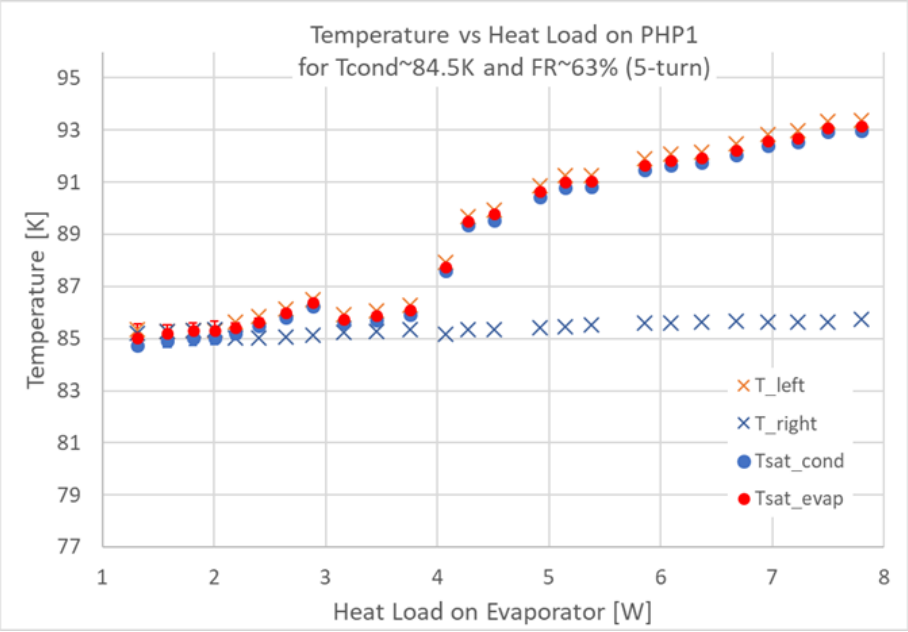

Figure 5-21 The temperature vs heat load plot for PHP1 for the condenser temperature of 84.5 K and the initial fill ratio of 63%. T_left is the average of T4 and T6 at the 7th adiabatic tube, and T_right is the average of the T5 and T7 on the adiabatic tube as shown in Figure 5-1.

As shown in Figure 5-20 and Figure 5-21 the working fluid in the right adiabatic section of PHP1 is subcooled when the heat load is greater than 3 W at the condenser temperature of 77.4 K experiment and when the heat load is greater than 4 W at the condenser temperature of 84.5 K. Furthermore, the temperature difference between the subcooled liquid in the cold adiabatic section and the saturated temperature is much greater with the condenser temperature of 77.4 K than with the condenser temperature of 84.5 K. The temperature difference between the subcooled liquid in the right adiabatic section and the saturation temperature determined from the pressure transducer is about 12.4 K at the maximum heat load of 8.1 W for the condenser temperature of 77.4 K case and is about 7.25 K at the maximum heat load of 7.8 W for the condenser temperature of 84.5 K case. Even though both cases have the same initial fill ratio, the larger ΔT suggests that more liquid has accumulated in the condenser (and less vapor exists in the evaporator) for the 77.4 K condition than the 84.5 K condition. A higher quantity of

the subcooled liquid in the condenser could explain why the 5-turn PHP has a higher dry-out limit for the condenser temperature of 77.4K than for the condenser temperature of 84.5 K.

5.3.2 5-turn PHP Experimental Results at FR=44% for Tcond~77.4 K

Figure 5-22 summarizes the effective thermal conductivity as a function of heat load on the evaporator for PHP1 and PHP2 at the condenser temperature of 77.4 K with the initial fill ratio of 44%. The effective thermal conductivity of PHP1 reaches a maximum of 617000 W/ m-K when the heat load is 3.46 W during a repeat test and the effective thermal conductivity of PHP2 reaches a maximum of 530000 W/m-K at 3.17 W during the sequential heat load test. Both the maximum thermal conductivities observed here are the best heat transfer performance of PHP1 and PH2 at the condenser temperature of 77.4 K in the 5-turn configuration experiments.

For PHP2, the heat transfer performance decreases as the heat load increases from 2.40 W to 2.89 W during the sequential heat load test. Repeat tests conducted at 2.40 W, 2.64 W, 2.89 W produce effective thermal conductivities that match the trend of the effective thermal conductivity as a function of heat load over the entire sequential heat load test, except for the data observed from 2.40 W to 2.89 W.

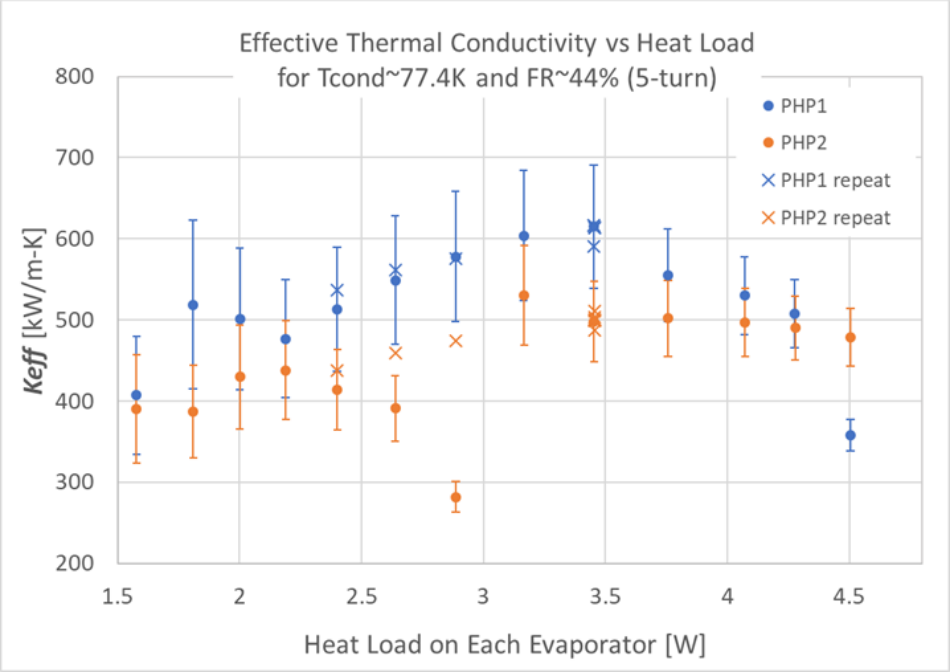

Figure 5-22 Effective thermal conductivity as a function of the heat load on the evaporator for the condenser temperature of 77.4 K at the initial fill ratio of 44% for PHP1 and PHP2.

Figure 5-23 presents the temperature profiles of PHP2 when the heat load increases from 2.64 W to 2.89 W and when the heat load increases from 2.89 W to 3.17 W during the sequential heat load tests. The data reflects a local dry out at 2.89 W in the right adiabatic section causing the temperature of T10 to jump to nearly to the same temperature as the evaporator. After the heat load increased to 3.17 W, the driving force is large enough that the local dry out recovers: T1 (the evaporator) and T10 (right adiabatic section) increase rapidly to a peak temperature and subsequently drop to 80.3 K and 78.2 K respectively. PHP2 reaches a new steady state at around 3000 sec.

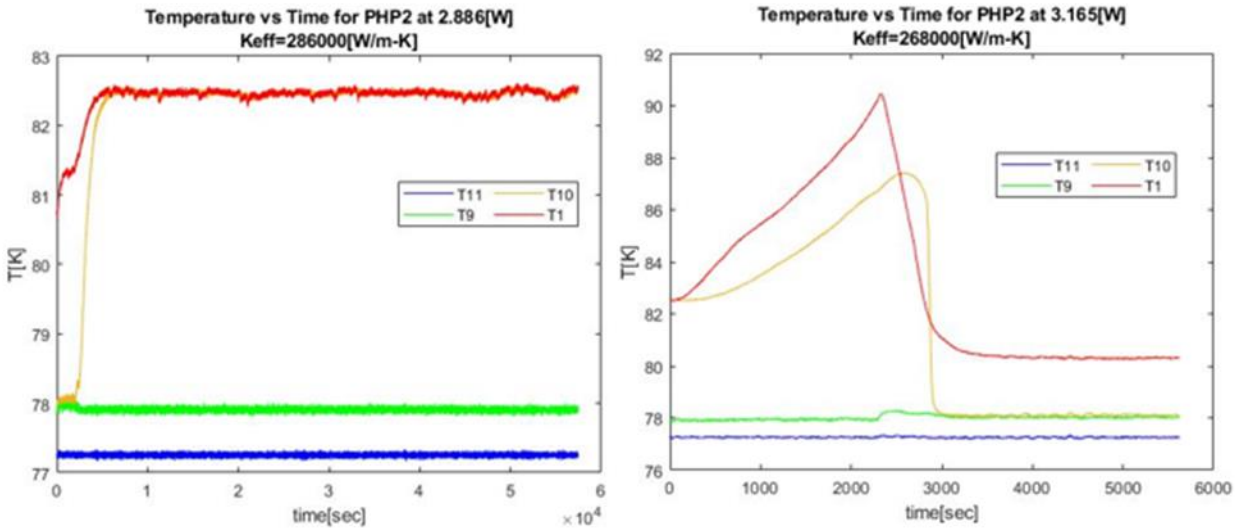

Figure 5-23 Temperature profiles of PHP2 when the heat load increased from 2.64 W to 2.89 W (left) and when the heat load increased from 2.89 W to 3.17 W (right).

The decay of the heat transfer performance of the PHP2 between 2.40 W and 2.89 W might be casued by a random local hot spot or dry out condition when the heat load is at 2.20 W in the initial sequential heat load test. Furthermore, the thermal performance deteroriates so that the right adiabatic section eventually becomes as hot as the evaporator because of the unfavorable flow condution from previous heat loads. Because each repeat test re-applies the specified heat load from the 0 W steady state, the results of repeat tests are not affected by the unfavorable vapor-liquid distribution from prior history. The repeat test results at 2.40 W, 2.64 W, 2.89 W likely produce the more favorable distribution in PHP2 than the results from the initial sequential heat load tests. Further repeat the tests at 2.40W, 2.64 W and 2.89 W could provide a statistical characterization of favorable and unfavorable distributions. Overall, the measurements show fairly good repeatability at the condenser temperature of 77.4 K and the initial ratio of 44%.

5.3.4 5-turn PHP Experimental Results at initial fill ratio of 38% and 50% for Tcond~77.4 K

Figure 5-24 and Figure 5-25 present the effective thermal conductivity as a function of heat load on the evaporator of PHP1 and PHP2 for the condenser temperature of 77.4 K at the initial fill ratio of 38% and 50% respectively. In both fill ratio cases, PHP1 and PHP2 demonstrate good repeatability at their optimal thermal conductivity condition – a very similar heat load as for the 44% fill ratio case. Furthermore, the shape of the trendline for the fill ratios of 38%, 44% and 50% also look similar.

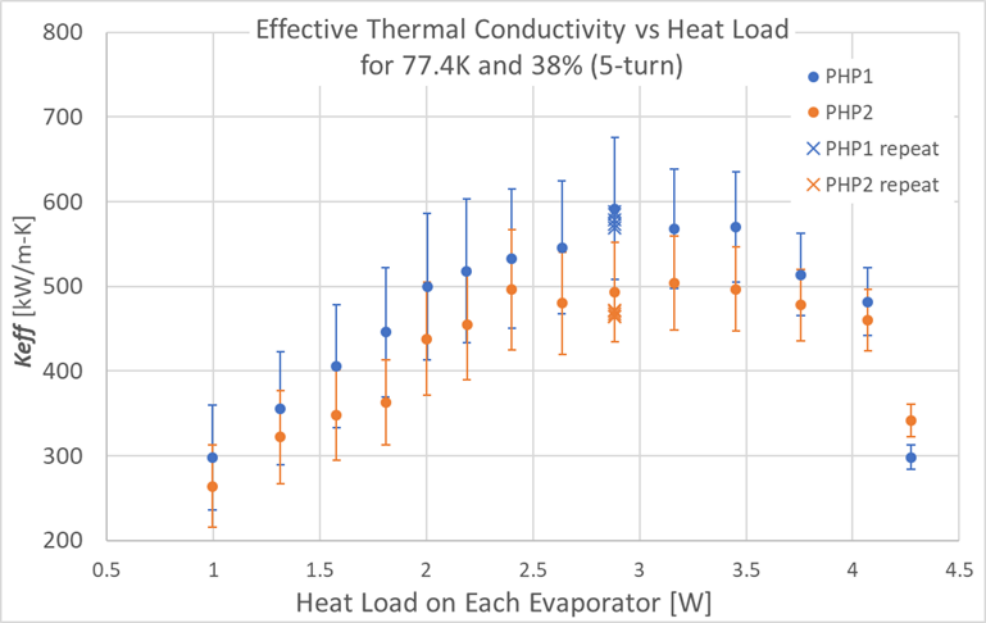

Figure 5-24 Effective thermal conductivity as a function of the heat load on the evaporator for the condenser temperature of 77.4 K at the initial fill ratio of 38% for PHP1 and PHP2.

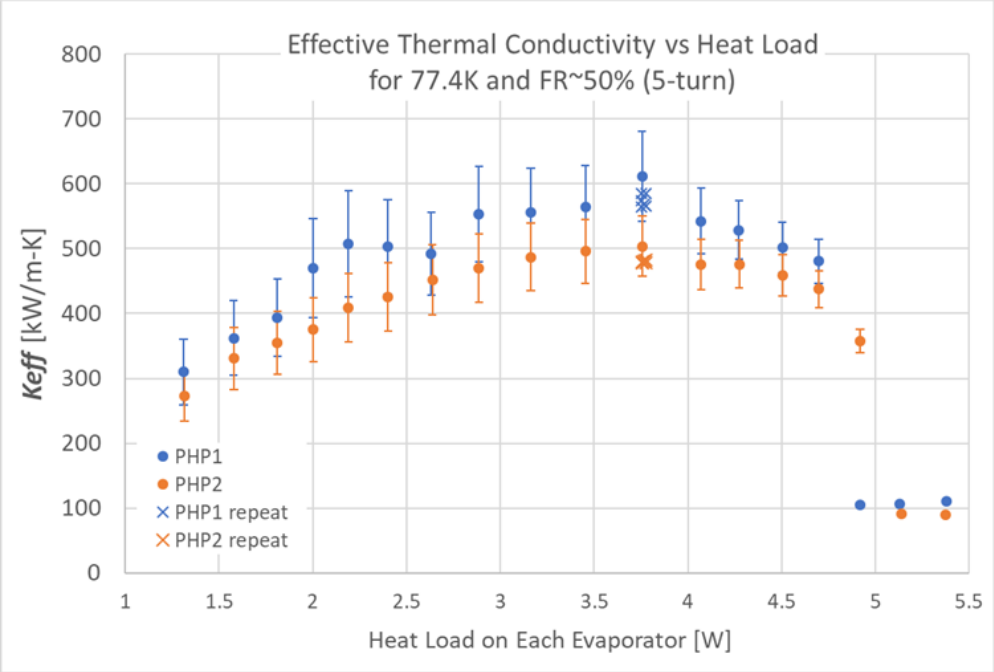

Figure 5-25 Effective thermal conductivity as a function of the heat load on the evaporator for the condenser temperature of 77.4 K at the initial fill ratio of 50% for PHP1 and PHP2 (5-turn).

5.3.4 5-turn PHP Experimental Results at initial fill ratio of 56.5% for Tcond~77.4 K

Figure 5-26 displays the effective thermal conductivity as a function of heat load on the evaporator of PHP1 and PHP2 for the condenser temperature of 77.4 K at the initial fill ratio of 56%. In this case, the repeat test results are more scattered than those observed in the 38%, 44% and 50% cases. The optimal effective thermal conductivity of PHP1 and PHP2 are 579000 W/m-K and 470000 W/m-K and both are observed in the repeat tests at 3.46 W on the PHP evaporator. A positive trend exists before the heat load of optimal heat transfer performance and a decreasing trend after the heat load of optimal effective thermal conductivity as observed with the other 5-turn runs at 77.4 K.

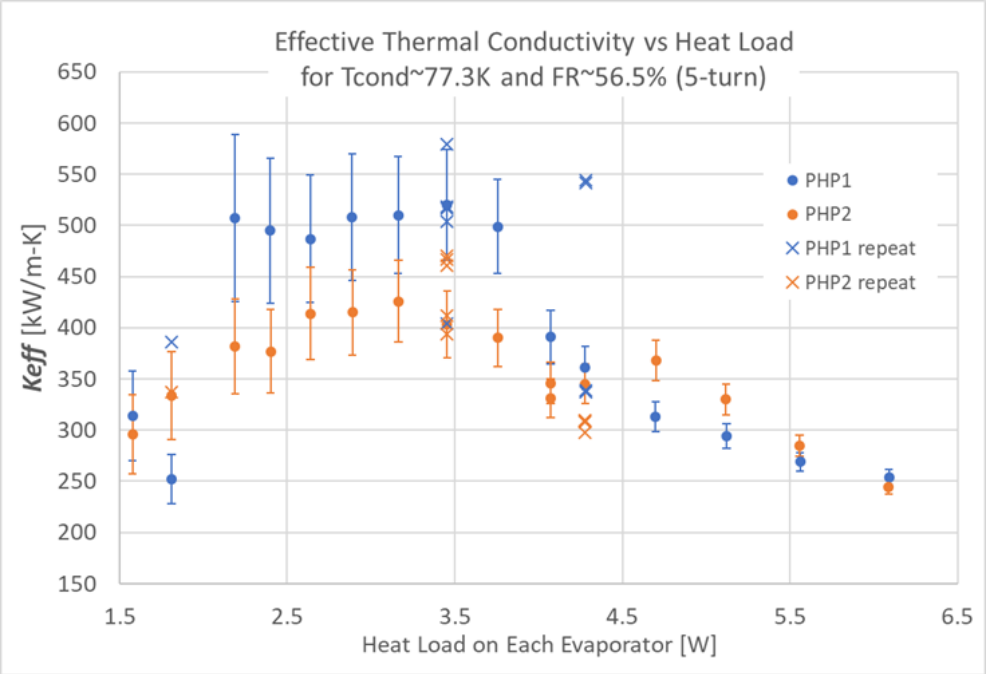

Figure 5-26 Effective thermal conductivity as a function of the heat load on the evaporator for the condenser temperature of 77.4 K at the initial fill ratio of 50% for PHP1 and PHP2 (5-turn).

For the 5-turn PHP, the heat load of the optimal thermal conductivity increases as the fill ratio increased from 38% to 50% and then decreased as the fill ratio increases as is presented in Figure 5-27. The optimum condition with the initial fill ratio of 56.5% is nearly at the same heat load as that with the initial fill ratio of 44%, but the PHP at the initial fill ratio of 44% has better repeatability, a higher optimal effective thermal conductivity and a wider range of decent heat transfer performance. PHP1 at the condenser temperature of 77.4 K and the initial fill ratio of 44% has a 1.88 W range of heat load where the effective thermal conductivity is above 500000 W/m-K. However, PHP1 at the condenser temperature of 77.4 K and the initial fill ratio of 56.5% only has a 1.27 W range of heat load where the effective thermal conductivity is above 500000 W/m-K. In a real application, a fill ratio equal to or less than 50% is a preferable condition for operating the 5-turn PHP at the condenser temperature of 77.4 K if the possible heat load on the evaporator will not be greater than 6 W.

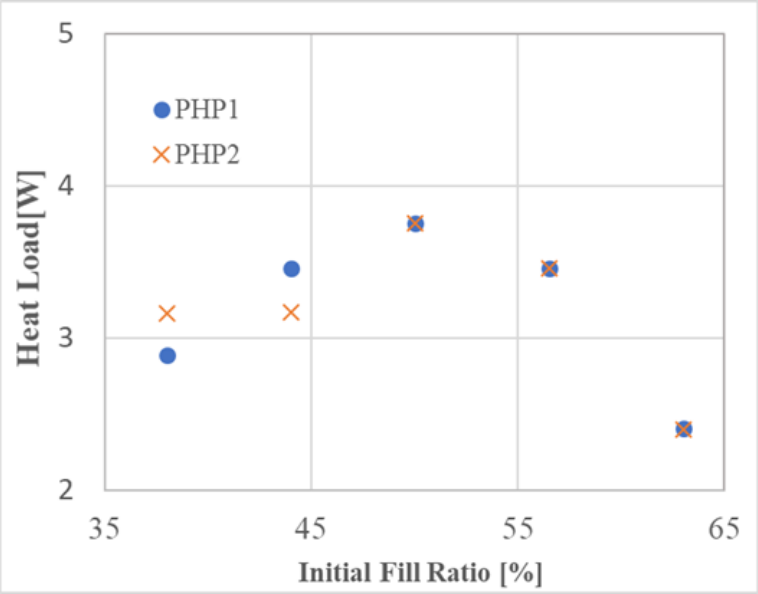

Figure 5-27 Heat load on the evaporator when the optimal effective thermal conductivity is observed as a function of initial fill ratio for PHP1 and PHP2 for the condenser temperature of 77.4 K experiments.

5.4 7-Turn PHP Experimental Results

5.4.1 Summary of the 7-turn PHP Experimental Results

The dry-out limit versus the initial fill ratio for the 7-turn PHP experiment at the condenser temperature of 77.4 K is shown in Figure 5-28 below. The 7-turn PHP experiment has also been conducted at one fill ratio, the initial fill ratio of 50%, for the condenser temperature of 84.5 K. The maximum heat that can be applied on the evaporator of the PHP is 8.50 W without dry-out at the condenser temperature of 84.5 K and the initial fill ratio of 50%. The maximum dry-out limit that can be applied on the evaporator of the PHP has a positive linear relationship with respect to the initial fill ratio for the 7-turn PHP configuration at the condenser temperature of 77.4 K.

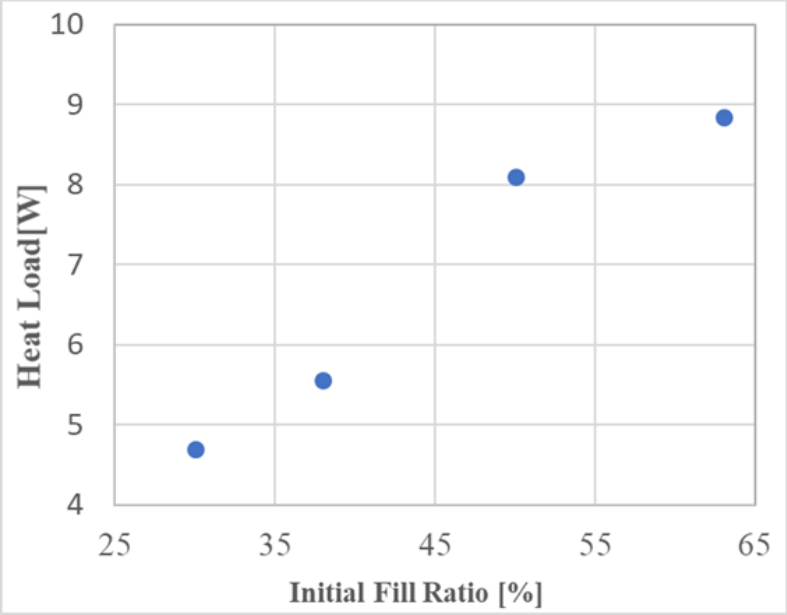

Figure 5-28 The dry-out limit versus the initial fill ratio of the 7-turn PHP for the condenser temperature of 77.4 K. This is the maximum of the heat load can be applied on the evaporator of the PHP without drying out.

Figure 5-29 below summarizes the optimal effective thermal conductivity as a function of the initial fill ratio for the 7-turn PHP at the condenser temperature of 77.4 K. The optimal effective thermal conductivity of PHP1 is about 993000 W/m-K for the initial fill ratio of 30% at the condenser temperature of 77.4 K. This is the third highest heat transfer performance observed among all the experiments conducted in this study. An effective thermal conductivity near 1000000 W/m-K has been observed twice with the 1-turn PHP experiment. In the 1-turn PHP experiments, the optimal effective thermal conductivity for PHP1 is measured at 1048000 W/m-K and 1020000 W/m-K at the condenser temperature of 84.5 K and the initial fill ratio of 63% and at the condenser temperature of 77.4 K and the initial fill ratio of 50%. Although the best heat transfer performance from the 1-turn PHP configuration is comparable or even slightly higher than the best heat transfer performance from the 7-turn PHP configuration, the dry-out limit of the 1-turn PHP configuration in which we observed the best heat transfer performance is much smaller than that observed for the 7-turn configuration. The 1-turn PHP also experienced

an initial dry-out in these test conditions whereas the 7-turn PHP exhibits good stability and repeatability. Further comparisons across all four configurations will be presented in a later chapter.

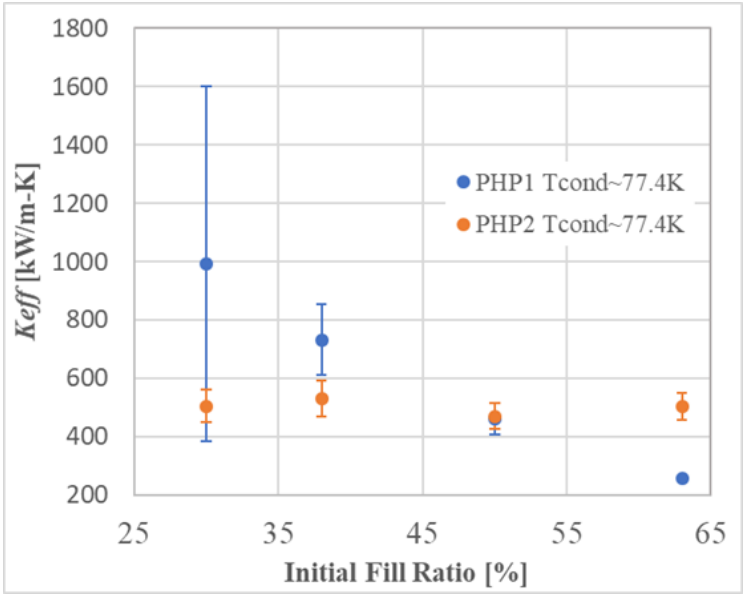

Figure 5-29 Optimal effective thermal conductivity versus the fill ratio for the 7-turn PHP experiments at the condenser temperature of 77.4 K.

In Figure 5-29, the optimal effective thermal conductivity has a negative linear relationship with respect to the initial fill ratio for PHP1. It is worth noting that the optimal effective thermal conductivity of PHP2 is in the range of 470000 W/m-K and 530000 W/m-K in all four initial fill ratio conditions. The optimal effective thermal conductivity of PHP2 is about half of the optimal effective thermal conductivity of PHP1 at the initial fill ratio of 30%, but the optimal effective thermal conductivity of PHP2 is about 95% higher than that of PHP1 at the initial fill ratio of 63%. The uncertainty error bar for PHP1 at the 30% fill ratio case looks much more significant than the others is due to the temperature difference between the condenser and the evaporator is only 0.577 K and the uncertainty errors of the PRT temperature sensor with 2-point calibration method is $\pm$0.250 K.

The optimal effective thermal conductivity of the 7-turn PHP at the initial fill ratio of 50% at the condenser temperature of 84.5 K is about 759000 W/m-K and 732000 W/m-K respectively for PHP1 and PHP2. This increase of the optimal thermal conductivity at the 84.5 K condition compared to that at 77.4 K is similar to that observed for the 5-turn configuration.

5.4.2 7-turn PHP Experimental Results at initial fill ratio of 30% for Tcond~77.4 K

Measurements of the effective thermal conductivity for the 7-turn PHP experiment with the condenser temperature of 77.4 K and the initial fill ratio of 30% test condition are shown in Figure 5-30. The optimal effective thermal conductivity of PHP1 is 993000 W/m-K and the optimal effective thermal conductivity of PHP2 is 709000 W/m-K.

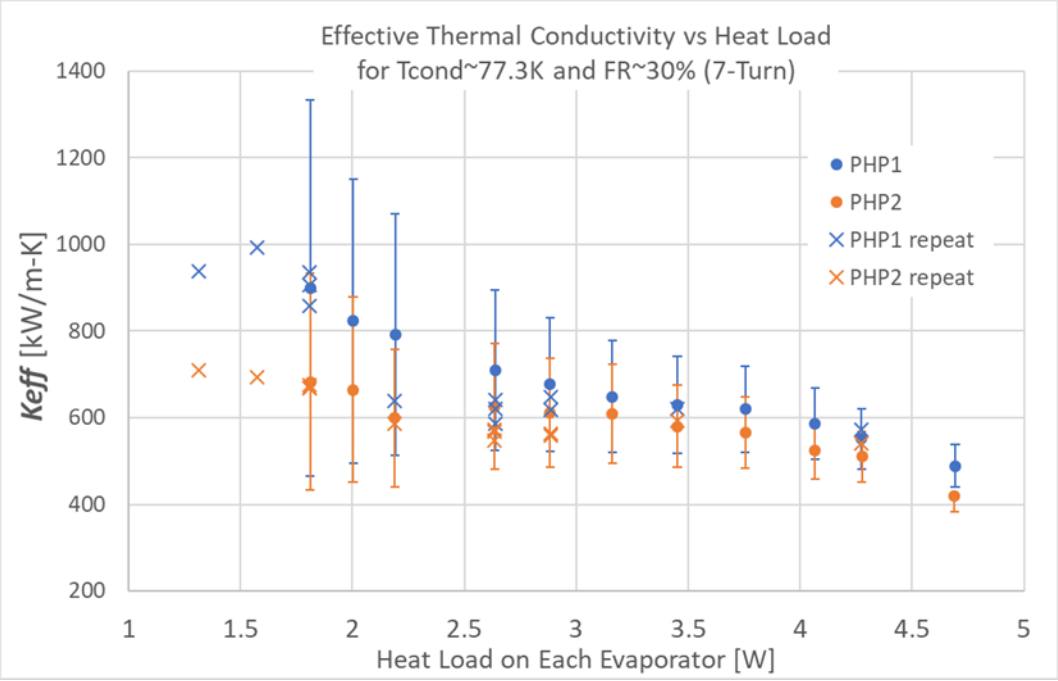

Figure 5-30 Effective thermal conductivity as a function of the heat load on the evaporator for the condenser temperature of 77.4 K at the initial fill ratio of 30% for PHP1 and PHP2 (7-turn).

Based on the monotonic decrease of the effective thermal conductivity for PHP2 shown in Figure 5-30 it is possible that the optimal effective thermal conductivity of PHP2 might be at a

lower heat load than the minimal tested condition of 1.32 W. However, at such a low heat load the PHP exhibits a pseudo steady-state modulating between a short-lived steady state followed periodically by a sudden rise in temperature. In Figure 5-31 below, the duration of the steady state increases with the heat load on the evaporator, and PHP2 eventually is able to maintain a steady state permanently when the heat load on the evaporator is 2.64 W. Thus, it is possible that PHP2 can reach an effective thermal conductivity around 1000000 W/m-K, but the duration for such performance in steady state might be very short.

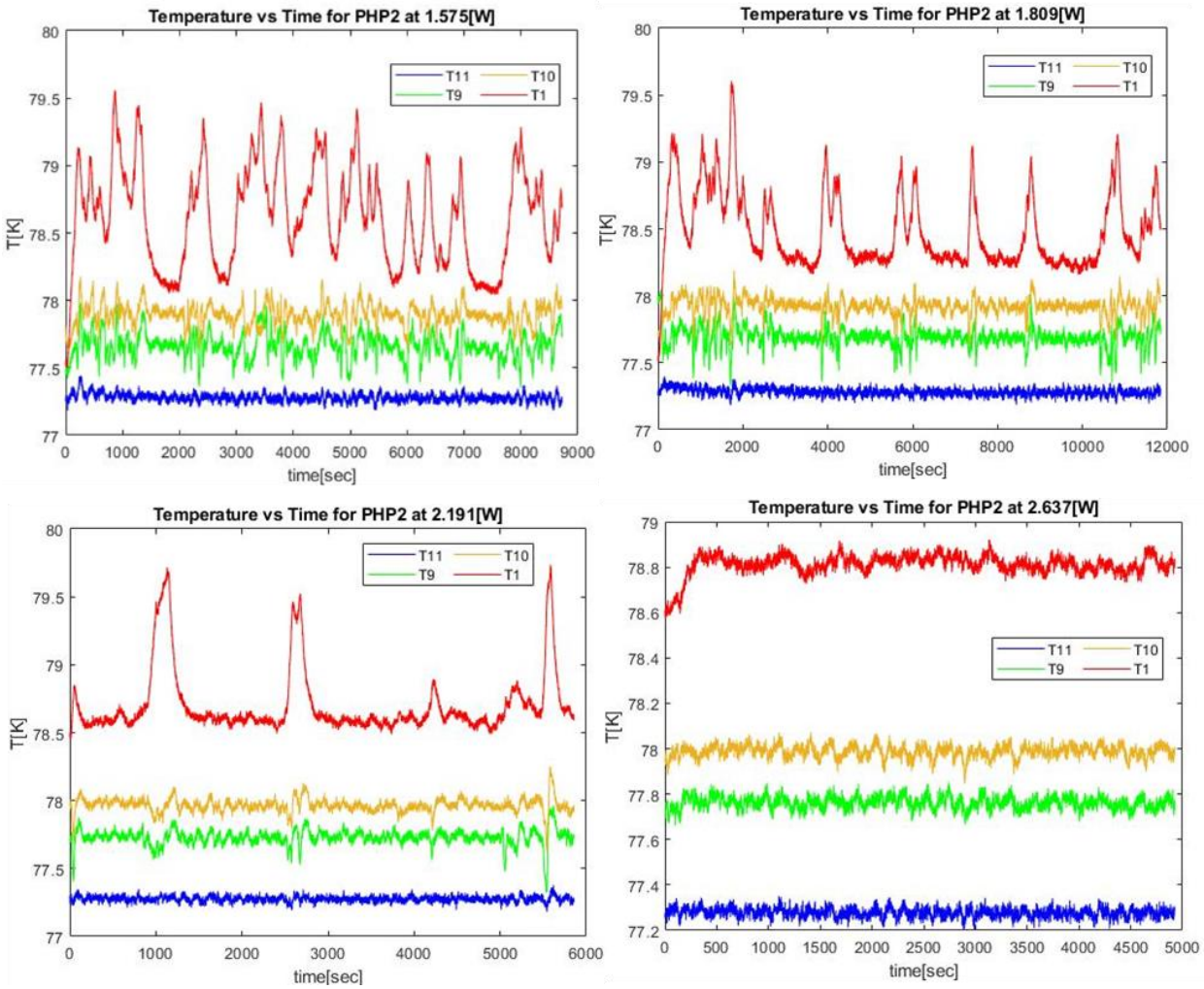

Figure 5-31 Temperature profiles of PHP2 at the heat load of 1.58 W (top left), 1.81 W (top right), 2.20 W (lower left) and 2.64 W (lower right). The duration of the steady state increases as the heat load on the evaporator increases.

A similar pseudo steady state behavior is observed in PHP1, however PHP1 maintains the period of steady state for a longer time than PHP2 and sometimes can even permanently recover from the pseudo steady state as shown in Figure 5-32. PHP1 exhibits a pseudo steady state at 1.58 W and begins transitioning into a steady state at about 5600 sec, achieving an effective thermal conductivity of 993000 W/m-K. A small amount of liquid inventory and a weak driving force are two possible factors producing the pseudo steady state exhibited by PHP1 and PHP2 at low heat load conditions. It is also possible that the 7-turn PHP has a large enough number of turns and therefore a high probability for liquid flowing into the evaporator to resolve any hot spots within the evaporator. Thus the 7-turn PHP exhibits the pseudo steady state that includes a temperature spike and periodic recovery. Such behavior is impossible to occur in PHPs with a small number turns and such small initial fill ratios.

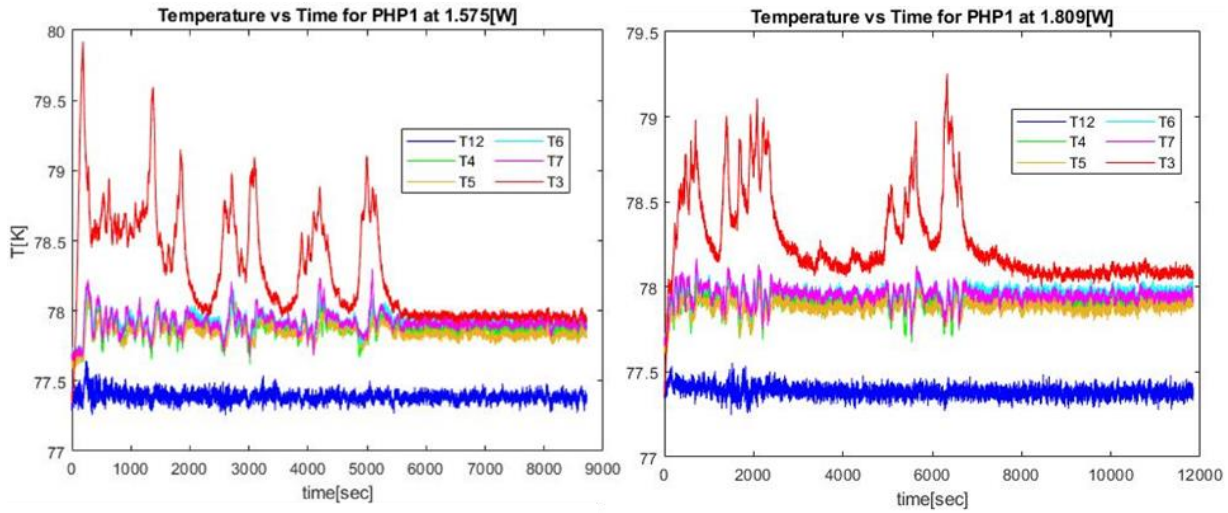

Figure 5-32 Temperature profiles of PHP1 at the heat load of 1.58 W (left), 1.81 W (right).

Figure 5-30 also demonstrates that the repeat test results are all within the uncertainties of the results from the sequential heat load runs at small, moderate and high heat loads. The repeatability of PHP1 and PHP2 is good for the condenser temperature of 77.4 K and the initial fill ratio of 30%.

5.4.3 7-turn PHP Experimental Results at initial fill ratio of 38% for Tcond~77.4 K

Figure 5-33 displays the effective thermal conductivity as a function of heat load on the evaporator of PHP1 and PHP2 for the condenser temperature of 77.4 K at the initial fill ratio of 38%. The difference of the effective thermal conductivity between PHP1 and PHP2 is between 4% to 23% in the sequential heat load runs.

Furthermore, the effective thermal conductivities measured from the repeat tests are either within the uncertainties of the sequential heat load tests or outperform the sequential heat load runs.

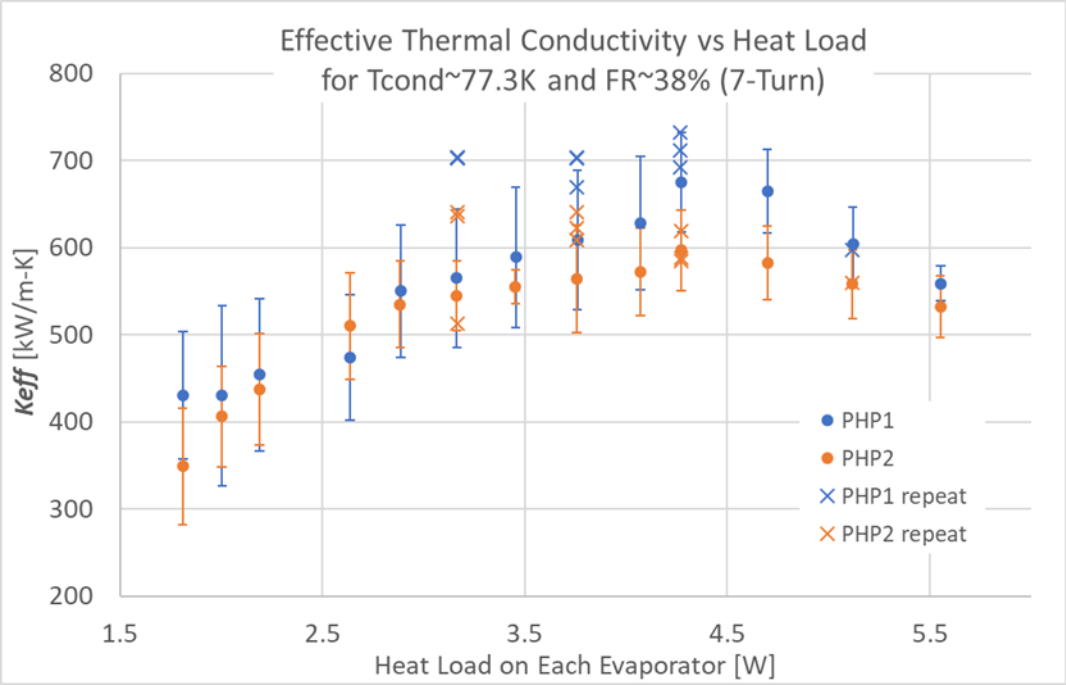

Figure 5-33 Effective thermal conductivity as a function of the heat load on the evaporator for the condenser temperature of 77.4 K at the initial fill ratio of 38% for PHP1 and PHP2 (7-turn).

As shown in Figure 5-34, the thermodynamic state of the working fluid is slightly superheated (hot adiabatic section) and subcooled (cold adiabatic section) for heat load values less than 5.5 W. At the maximum heat load of 5.56 W the PHP is transitioning to a dry-out

condition. The effective thermal conductivity for both PHP1 and PHP2 exceeds 500000 W/m-K between the heat load range of 2.67 W and 2.64 W. The initial fill ratio of 38% is a desirable operating condition for the 7-turn PHP at the condenser temperature of 77.4 K.

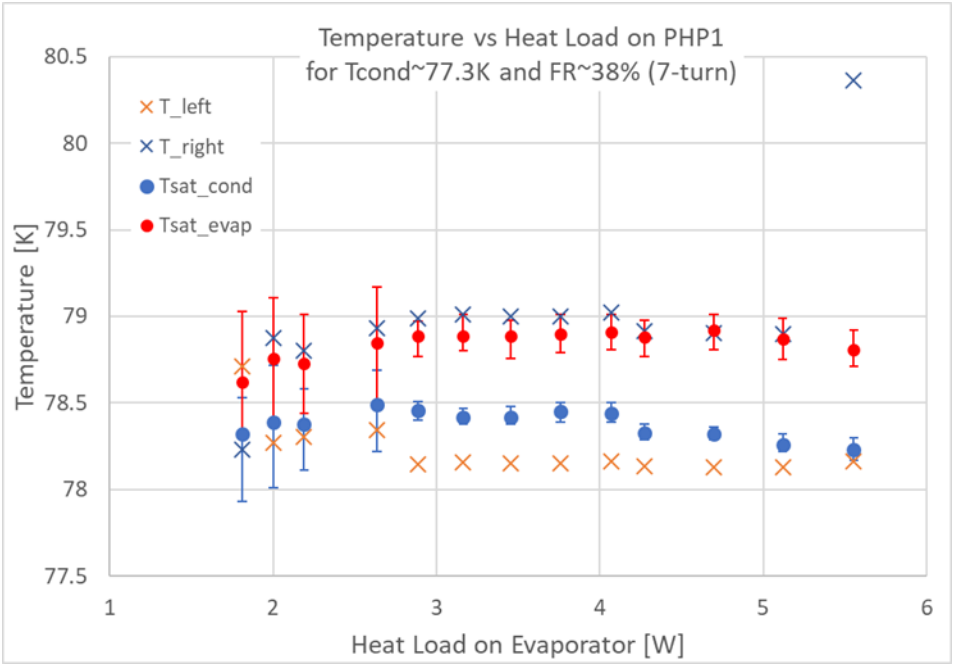

Figure 5-34 The temperature vs heat load plot for PHP1(7-turn) for the condenser temperature of 77.4 K and the initial fill ratio of 38%. T_left is the average of T4 and T6 at the 7th adiabatic tube, and T_right is the average of the T5 and T7 on the adiabatic tube as shown in Figure 5-1.

5.4.4 7-turn PHP Experimental Results at initial fill ratio of 50% for Tcond~84.5 K

Figure 5-35 displays the effective thermal conductivity as a function of heat load on the evaporator of PHP1 and PHP2 for the condenser temperature of 84.5 K at the initial fill ratio of 50%. The effective thermal conductivity of PHP1 and PHP2 are within the uncertainty error of each other over the entire range of applied heat load. The repeat test results also fall within the uncertainty errors of the effective thermal conductivity from the sequential heat load tests. Both PHP1 and PHP2 exhibit effective conductivity values greater or near 600000 W/m-K over the entire range of applied heat load, up to 8.1 W. Although the heat transfer performance drops

below 600000 W/m-K when the heat load is increased to 8.50 W, both PHPs sill perform great exhibiting effective thermal conductivity values more than 500000 W/m-K.

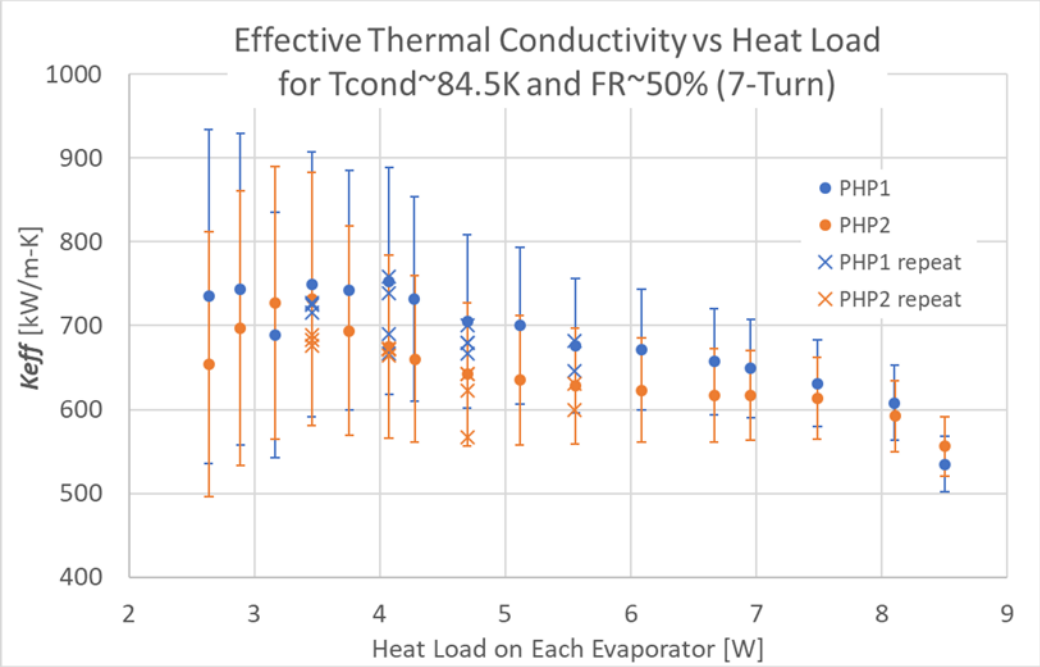

Figure 5-35 Effective thermal conductivity as a function of the heat load on the evaporator for the condenser temperature of 84.5 K at the initial fill ratio of 50% for PHP1 and PHP2 (7-turn).

Figure 5-36 shows that the working fluid in the right adiabatic section is slightly super-heated from 2.64 W to 7.49 W. The working fluid in the left adiabatic section also is slightly super-heated over the entire range of applied heat load. If we consider the ±250 mK accuracy of the platinum temperature sensor within the 73 K to 305 K temperature range [24], it is possible that the working fluid in the left adiabatic section is two-phase.

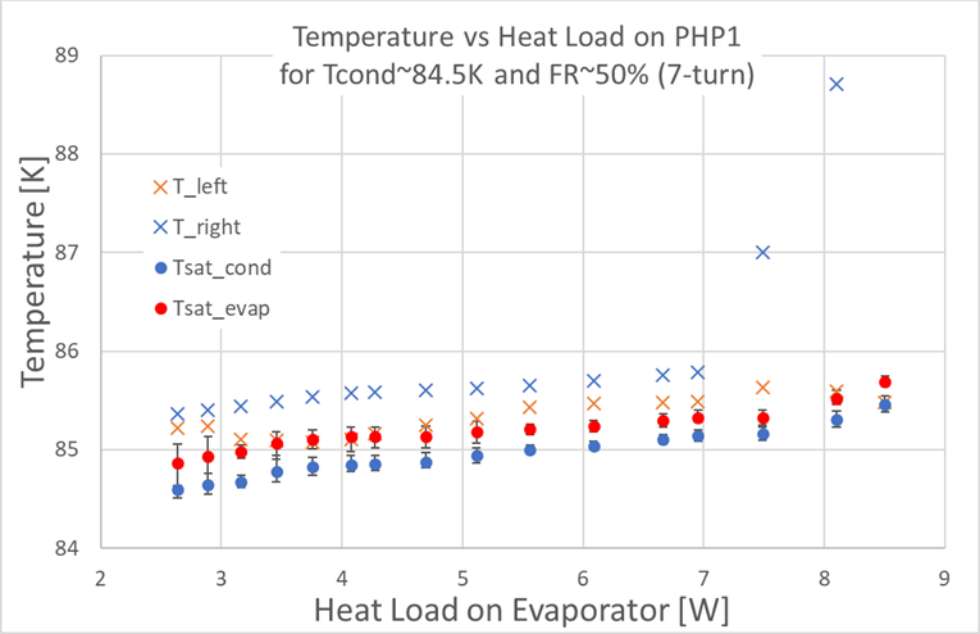

Figure 5-36 The temperature vs heat load plot for PHP1(7-turn) for the condenser temperature of 84.5 K and the initial fill ratio of 50%. T_left is the average of T4 and T6 at the 7th adiabatic tube, and T_right is the average of the T5 and T7 on the adiabatic tube as shown in Figure 5-1.

The 7-turn PHP at the condenser temperature of 84.5 K and the initial fill ratio of 50% exhibits a wide range of outstanding effective thermal conductivity performance (greater than 500000 W/m-K effective thermal conductivity through the entire range of applied heat load) and a good repeatability. The maximum heat load applied on the evaporator exceeds 8 W. Although the 7-turn PHP at the condenser temperature of 77.4K can also operate at a higher applied heat load than 8 W without drying out with a fill ratio of 63% and 50%, the effective thermal conductivity is less than 300000 W/m-K. Thus, a 7-turn PHP operating at the condenser temperature of 84.5 K and the initial fill ratio of 50% is a preferable operating condition.

5.4.5 7-turn PHP Experimental Results at initial fill ratio of 63% for Tcond~77.4 K

Figure 5-37 displays the effective thermal conductivity as a function of the heat load on the evaporator of PHP1 and PHP2 for the condenser temperature of 77.4 K at the initial fill ratio of 63%. Effective conductivity results of PHP1 and PHP2 differ significantly during the initial sequential heat load test over the full range. A set of repeat test results ranging sequentially from 3.76 W to 6.09 W reveal closer values of effective conductivity for PHP1 and PHP2.

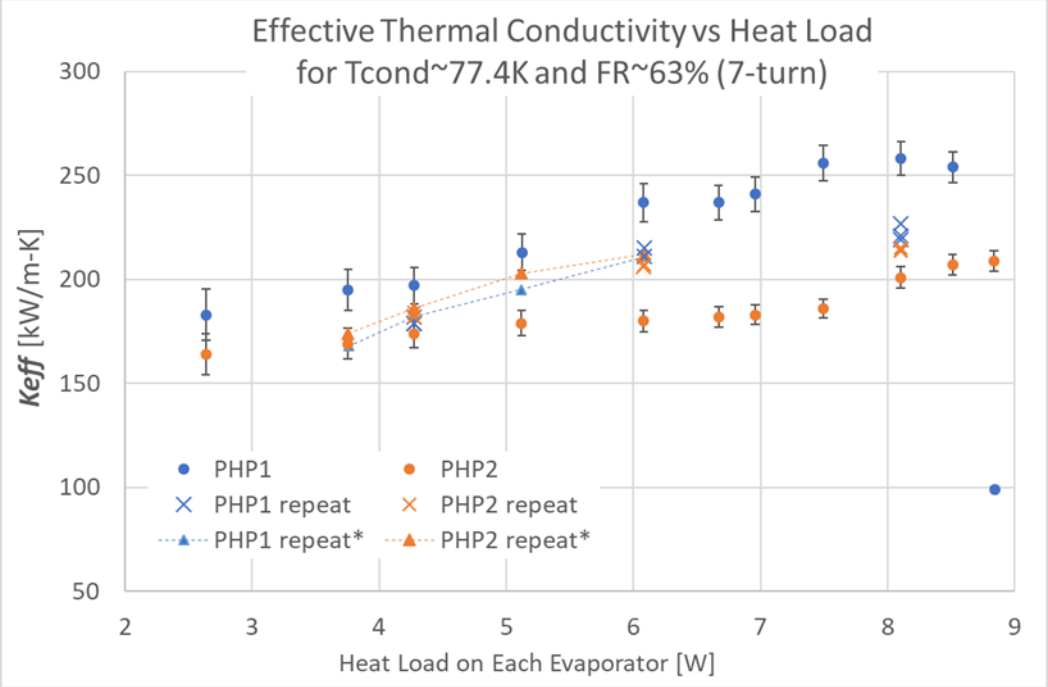

Figure 5-37 Effective thermal conductivity as a function of the heat load on the evaporator for the condenser temperature of 77.4 K at the initial fill ratio of 63% for PHP1 and PHP2 (7-turn).

An additional single repeat test at 8.1 W follows the trend of the second sequential heat load test. The percentage difference of effective thermal conductivity between PHP1 and PHP2 is less than 3% in the second sequential heat load runs from 3.76 W to 6.09 W. In the original sequential heat load runs, the percentage difference of the effective thermal conductivity between PHP1 and PHP2 ranges between 13% to 32% over the same heat load range.

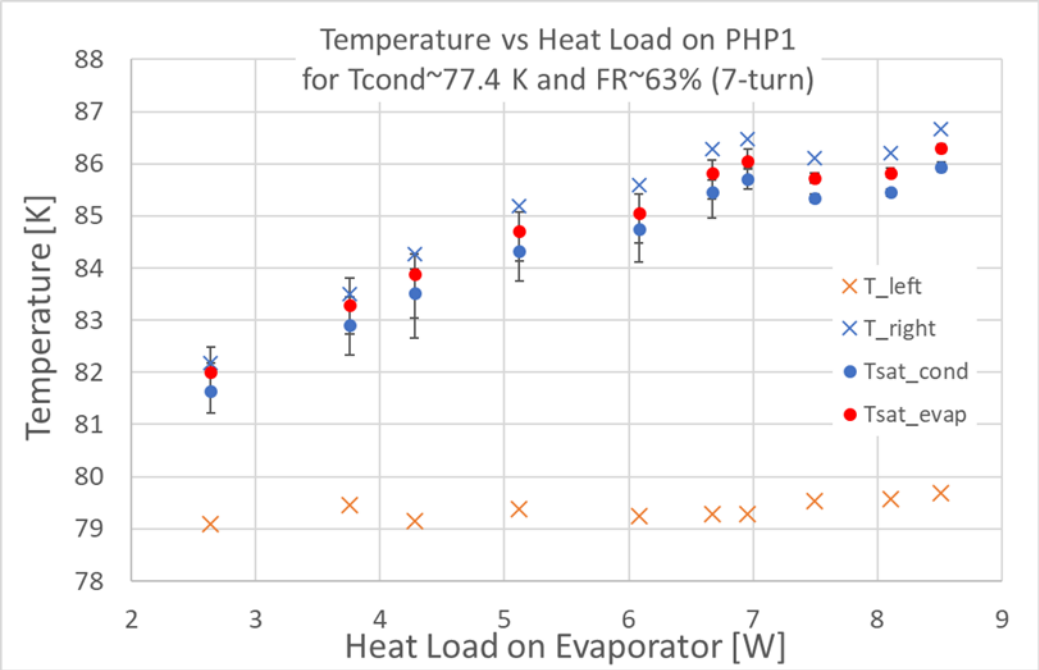

Figure 5-38 The temperature vs heat load plot for PHP1(7-turn) for the condenser temperature of 77.4 K and the initial fill ratio of 63%. T_left is the average of T4 and T6 at the 7th adiabatic tube, and T_right is the average of the T5 and T7 on the adiabatic tube as shown in Figure 5-1.

From Figure 5-38 above, we see that the working fluid in the hot adiabatic section is already in the super-heated state and the fluid in the cold adiabatic section is subcooled liquid from the beginning of the sequential heat load test. The same conditions of subcooled liquid in the cold adiabatic section and superheated vapor in the hot adiabatic section exist in the repeat tests, however it is entirely possible that the distribution of liquid and vapor sections is slightly different during the repeat tests. The relatively low effective thermal conductivity of the PHP at the condenser temperature of 77.4 K and the initial fill ratio of 63% can be attributed to the single-phase conditions in the cold and hot regions.

6. Comparison of the Experimental Results across Configurations

Based on the results presented above, one may observe that the 1-turn and 3-turn PHP will not perform well if the fill ratio is below 50%. Furthermore, the 5-turn and 7-turn PHP show

good heat transfer performance at low fill ratios such as 38% and 30%, but the maximum heat capacity and the effective thermal conductivity for the PHP in these two configurations are not desirable at the fill ratio of 63%. In view of these observations, the following subsections will mainly focus on the fill ratio of 50% at the condenser temperature of 77.4 K and the 84.5 K test conditions for which the PHP can operate well in all configurations.

6.1 Maximum Heat Capacity

The maximum heat capacity (dry-out limit) is the maximum heat that can be applied on each PHP without drying out. The dry-out limit is usually the same for both PHP1 and PHP2 like the case shown in Figure 6-1. Here both PHP subsections dry out when the heat load increases from 8.50 W to 8.92 W at the condenser temperature of 84.5 K and the initial fill ratio of 50%. Thus, 8.50 W is the maximum heat capacity that can be applied to the 7-turn PHP with a condenser temperature of 84.5 K and an initial fill ratio of 50%.

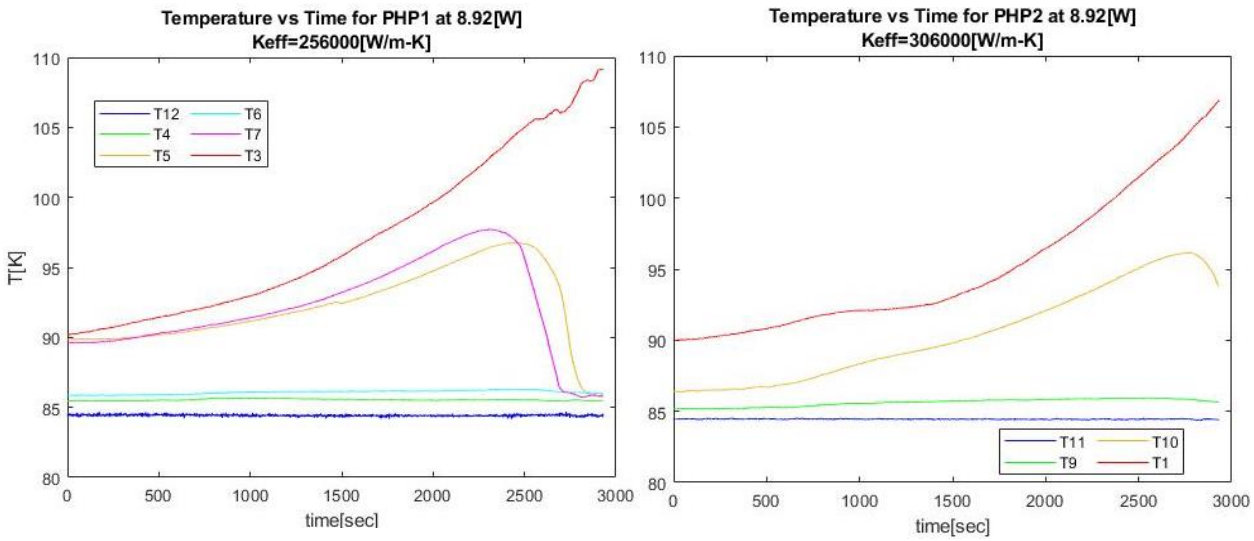

Figure 6-1 The temperature profiles above present the dry-out of the PHP subsection in the 7-turn PHP experiment at the condenser temperature of 84.5 K and the initial fill ratio of 50%.

Occasionally one of the PHP subsections will dry out while the other one will not. However, if the tests are repeated the PHP that is first to dry out switches. For example, Figure 6-2 displays a case when PHP2 dries out when the heat load increased from 1.12 W to 1.24 W. Subsequently PHP1 dries out but PHP2 does not when the PHPs are rebooted from zero heat load steady state. For such data, 1.12 W is identified as the maximum heat capacity (dry-out limit) of both PHPs. Thus, we treat the maximum heat capacity listed in Figure 6-3 and Figure 6-4 below as the maximum heat capacity of both PHPs.

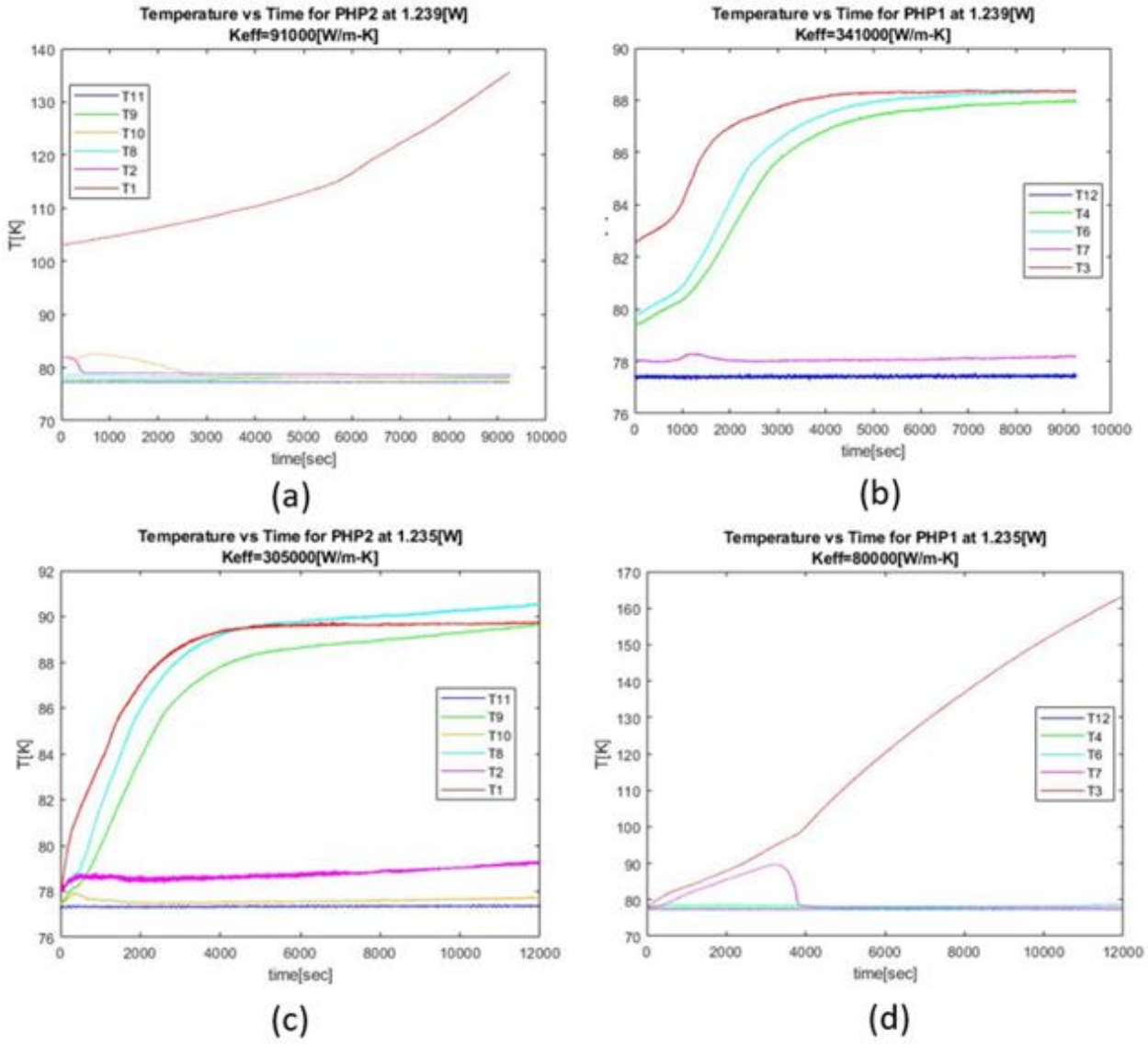

Figure 6-2 The temperature profiles above present the dry-out of the PHP subsection in the 1-turn PHP experiment at the condenser temperature of 77.4 K and the initial fill ratio of 50%. The temperature profile of the PHP1 (b) and PHP2 (a) after the heat load increased from 1.12 W to 1.24 W. And the temperature profile of the PHP1 (d) and PHP2 (c) after the PHP was rebooted from zero heat load to 1.24 W on each PHP evaporator.

Figure 6-3 below summarizes the maximum heat capacity of the PHP as a function of the number of turns at the initial fill ratio of 50% for the condenser temperature of 77.4 K and the condenser temperature of 84.5 K test condition. In both cases, we observed a positive linear relationship between the maximum heat capacity and the number of turns of the PHP. The

uncertainty of maximum heat capacity on the 7-turn PHP at the condenser temperature of 84.5 K and the intial fill ratio of 50% is about ± 607 mW, which is about a order of magnitude higher than the uncertainties of the maximum heat capacity that can be applied on the PHP with other configurations at the same test condition.

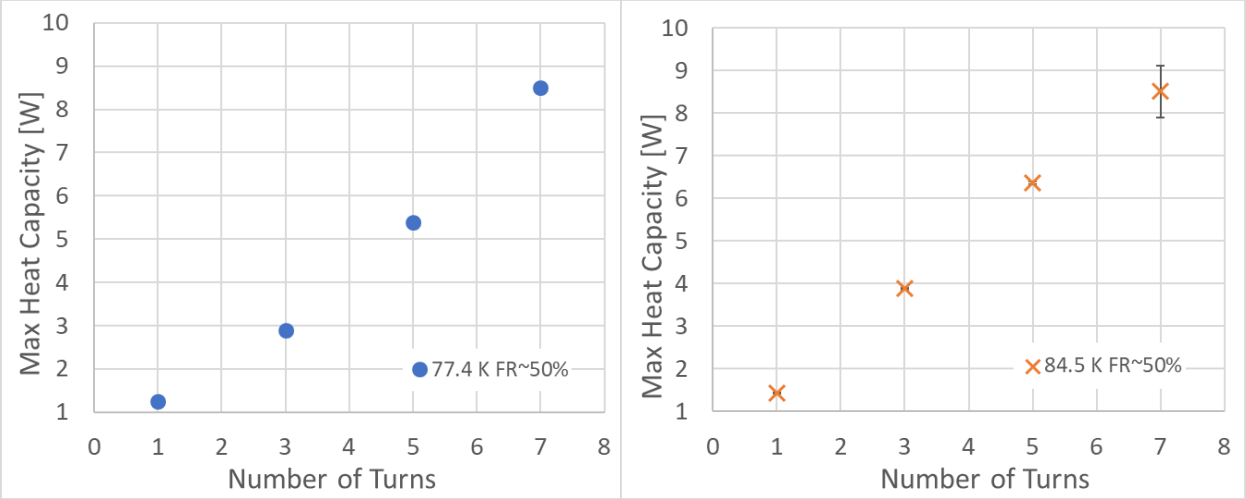

Figure 6-3 The maximum heat capacity on the PHP as a function of the PHP configuration (number of turns) at the condenser temperature of 77.4 K and the initial fill ratio of 50% (left) and at the condenser temperature of 84.5 K and the initial fill ratio of 50% (right).

Figure 6-4 below presented the maximum heat capacity **per turn** on the PHP as a function of the PHP configuration. There is no obvious trend observed in Figure 6-4 for the maximum heat capacity per turn respective to the number of turns.

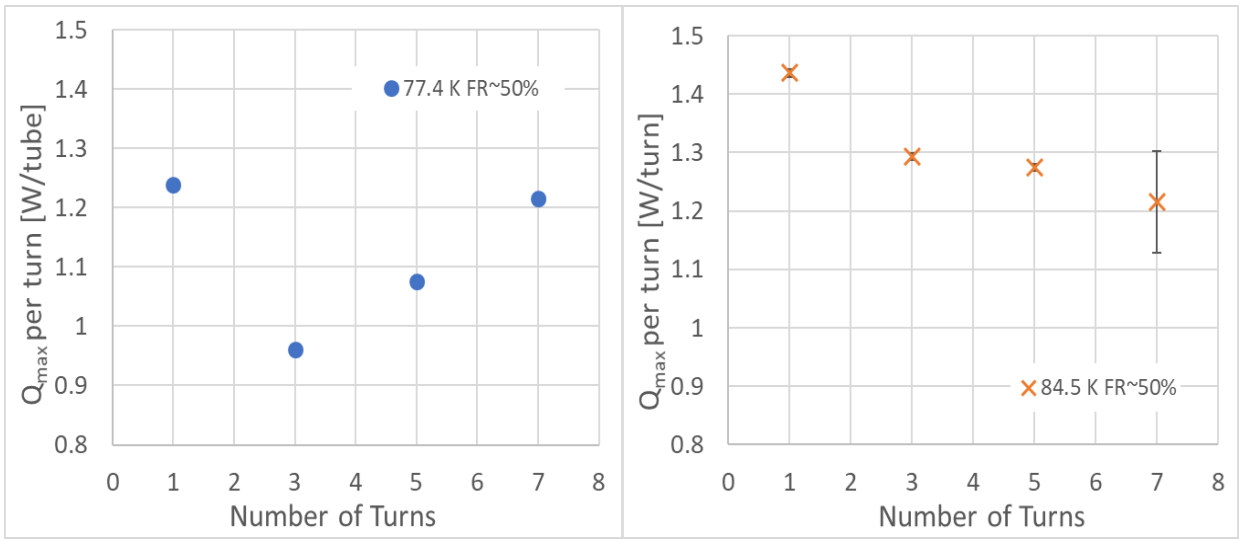

Figure 6-4 The maximum heat capacity **per turn** on the PHP as a function of the PHP configuration (number of turns) at the condenser temperature of 77.4 K and the initial fill ratio of 50% (left) and at the condenser temperature of 84.5 K and the initial fill ratio of 50% (right)

Notice that the greatest maximum heat capacity per turn is only about 29% and 18% higher than the lowest maximum heat capacity per turn for the respective condenser temperatures of 77.4 K and 84.5 K. These results stand in contrast to similar measurements gathered with a helium PHP [22] for which the maximum heat capacity per turn of an 8-turn helium PHP is about 6.4 times larger than the maximum heat capacity per turn of a 48-turn PHP. Additionally, the maximum heat capacity per turn of the 1-turn PHP in this study is only about 1.8% and 18% higher than that of the 7-turn PHP at the respective condenser temperature of 77.4 K and 84.5 K. It is also interesting to notice that the variation in the maximum heat capacity per turn for the nitrogen PHP is much smaller than the variation observed for the 8-turn and 48-turn helium PHP even though the ratio of the number of turns in our study (7:1) is greater than that for the helium PHP study (6:1).

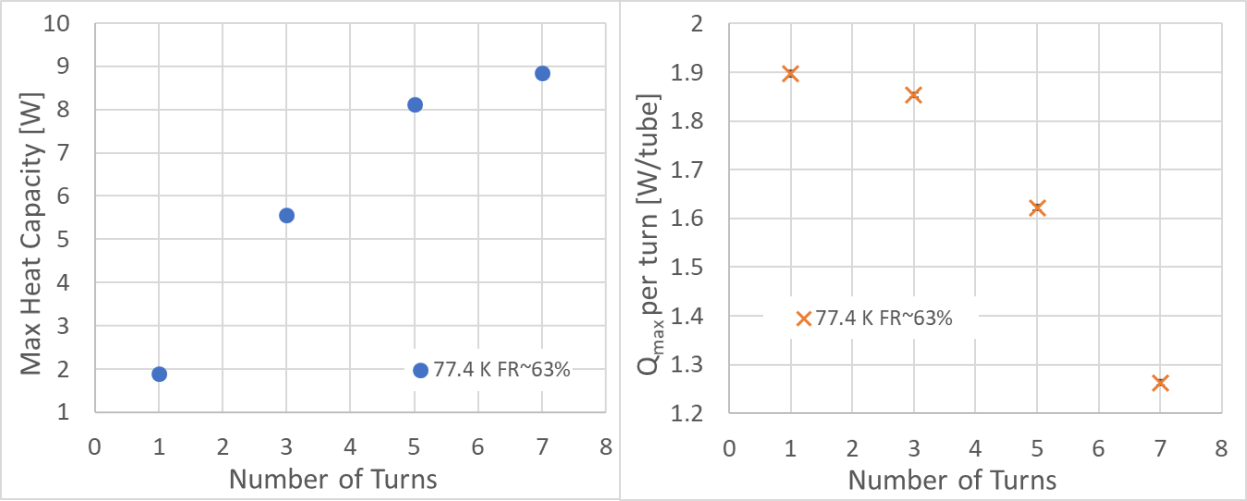

Figure 6-5 The maximum heat capacity (left) on the PHP as a function of the PHP configuration (number of turns) and the maximum heat capacity **per turn** (right) on the PHP as a function of the PHP configuration (number of turns) at the condenser temperature of 77.4 K and the initial fill ratio of 63%.

Figure 6-5 demonstrates that at the condenser temperature of 77.4 K and the initial fill ratio of 63%, a negative trend of the maximum heat capacity per turn is observed. The maximum heat capacity per turn of the 1-turn PHP configuration is about 50% higher than the maximum heat capacity per turn of the 7-turn PHP configuration at the condenser temperature of 77.4 K and the initial fill ratio of 63% test condition.

For the test condition with an initial fill ratio of 50% and condenser temperatures of 77.4 K and 84.5 K, there is no clear trend for the maximum heat capacity per turn as a function of the number of turns. There is a negative trend for the initial fill ratio of 63% test condition at both 77.4 K condenser temperature condition. From the data gathered in this study, one can conjecture that for each configuration the PHP has a different ideal fill ratio. A PHP with a small number of turns is likely to dry-out from a local spot and needs a higher fill ratio to wet the evaporator. In contrast, a PHP with a large number of turns has more probability for the liquid to flow into the evaporator and cool the hot area than a PHP with a small number of turns, so it does not benefit

from a high fill ratio like the PHP with a small number of turns. In the study comparing the 8-turn and 48-turn helium PHP, both PHP configurations are charged to about a 70% fill ratio [22]. It is possible that the difference of the maximum heat capacity per turn between the 8-turn and 48-turn would be reduced if the comparison is conducted with differing, but optimal fill ratios.

Comparing the experimental results in the present study of a nitrogen PHP with varying number of turns to the experimental results of the 8-turn and 48-turn helium PHP, it is helpful to keep in mind that the adiabatic section of the nitrogen PHP is 1000 mm while the adiabatic length of the helium PHP is only 100 mm. In addition, the fluid properties of the nitrogen in our experiment and helium in Li's comparison study are drastically different.

Table 6-1 The fluid properties of the nitrogen and helium at their normal boiling point.

	Nitrogen at NBT (77.4 K)	Helium at NBT (4.2 K)
ρ_sat_liq [kg/m^3]	807.7	125.4
ρ_sat_vap[kg/m^3]	4.4	16.5
surface tension [N/m]	0.00896	0.0000908
viscosity [kg/m-s]	0.0001629	0.000003182

where ρ_sat_liq is the density of the saturated liquid of the working fluid, ρ_sat_vap is the density of the saturated vapor. One important driving force for the PHP oscillation is from the contraction and expansion of the working fluid when flows into the condenser and the condenser. The ratio of the volume contraction and expansion of the saturated working fluid when flowing into the condenser and the evaporator in nitrogen PHP will be much more significant than the helium PHP. Because the ratio of the density of the saturated vapor and saturated liquid is about 183.6 for nitrogen fluid while the ratio of density of the saturated vapor and liquid is only about 7.6.

The following sections analyze the optimal effective thermal conductivity across the number of turns. Here one finds that the fill ratio producing the optimal heat transfer performance shifts across different configurations.

6.2 Effective Thermal Conductivity as a function of Heat Load per turn

Figure 6-6, 6-7 and 6-8 summarize the effective thermal conductivity as a function of the heat load per turn on PHP1 at the condenser temperature of 77.4 K and the initial fill ratio of 50%, at the condenser temperature of 84.5 K and the initial fill ratio of 50%, and at the condenser temperature of 77.4 K and the initial fill ratio of 63% respectively.

At the condenser temperature of 77.4 K and the initial fill ratio of 50%, the optimal effective thermal conductivity of the 1-turn, 3-turn and 5-turn configurations are very close to each other. The heat load per tube producing the optimal effective thermal conductivity is also very consistent over all the configurations, ranging between 0.68 W/turn to 0.75 W/turn. Although the maximum heat capacity per turn of the 7-turn PHP is only about 1.8% lower than that of the 1-turn PHP, the optimal effective thermal conductivity of the 7-turn PHP is significantly lower (~ 33% lower) than that of the 1-turn, 3-turn and 5-turn PHP when the heat load per turn is between 0.38 W/turn and 0.95 W/turn.

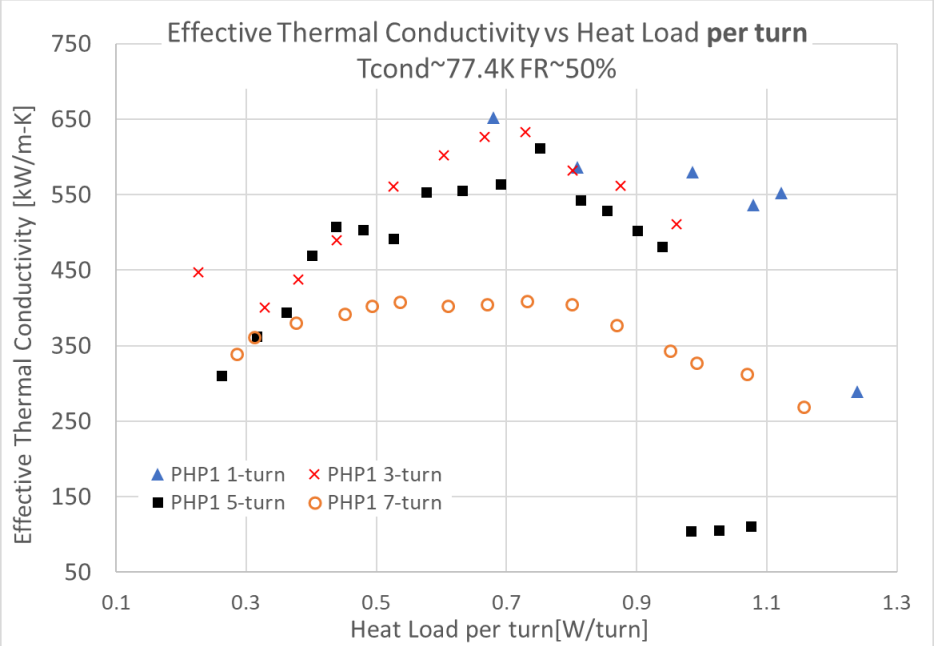

Figure 6-6 Effective thermal conductivity as a function of heat load **per turn** for PHP1 at the condenser temperature of 77.4 K and the initial fill ratio of 50%.

At the condenser temperature of 84.5 K and the initial fill ratio of 50%, the 3-turn, 5-turn and 7-turn PHPs display a similar trend. The 1-turn PHP performs well when the heat load per turn is high, while the other three configurations reach their respective optimal heat transfer performance when the heat load is about 0.5 W/turn. The effective thermal conductivity vs. the heat load per turn generally deceases with increasing number of turns for this condition.

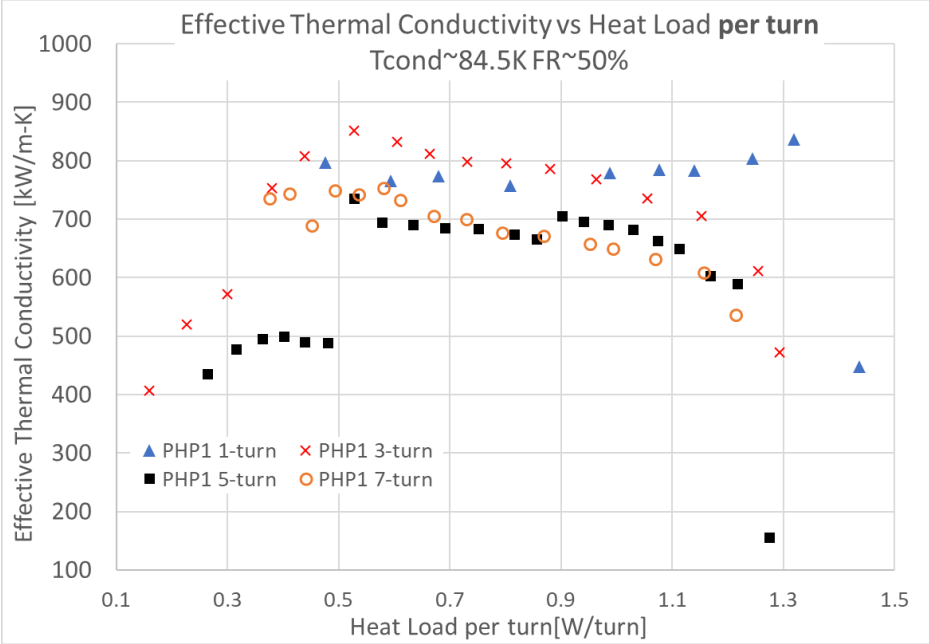

Figure 6-7 Effective thermal conductivity as a function of heat load **per turn** for PHP1 at the condenser temperature of 84.5 K and the initial fill ratio of 50%.

At the condenser temperature of 77.4 K and the initial fill ratio of 63%, the 1-turn PHP exhibits an effective thermal conductivity of 796000 W/m-K and 761000 W/m-K at 0.48 W/turn and at 1.08 W/turn respectively. However, the 1-turn PHP dries out when the heat load is increased to a heat load above 1.08 W/turn. After rebooting, the heat transfer performance of the 1-turn PHP decreased and the trendline of the 1-turn PHP performance is similar to the 3-turn and 5-turn PHP at this condition. The maximum heat capacity per turn also deceases with increasing number of turns for this condition.

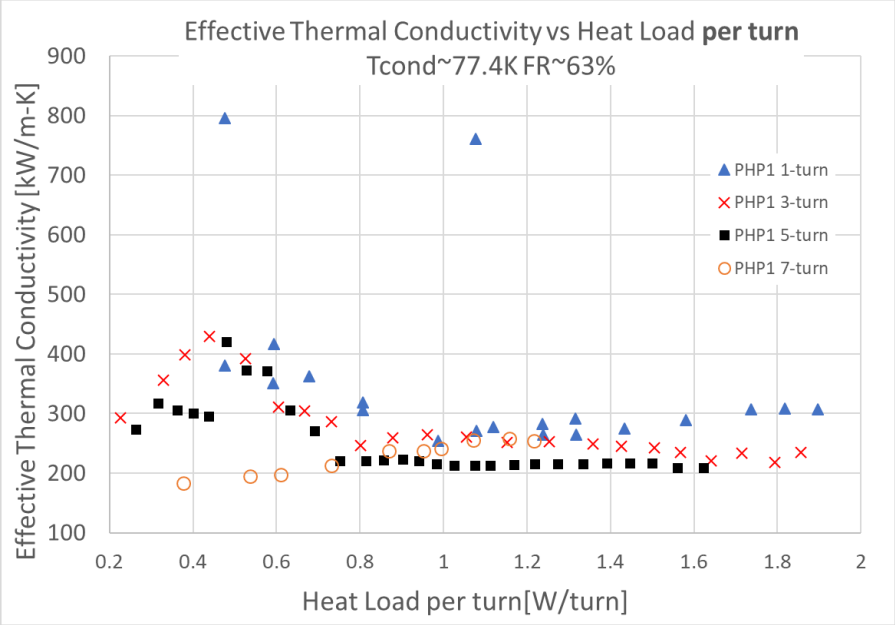

Figure 6-8 Effective thermal conductivity as a function of heat load **per turn** for PHP1 at the condenser temperature of 77.4 K and the initial fill ratio of 63%

6.3 Is it fair to compare the heat transfer performance across the configurations at the same fill ratio?

Figure 6-9 and Figure 6-10 below summarize the optimal effective thermal conductivity for all four configurations as a function of the initial fill ratio at the condenser temperature of 77.4 K for PHP1 and PHP2 respectively.

Each PHP configuration displays a unique dependence for the optimal effective thermal conductivity with respect to the initial fill ratio. Generally, the optimal heat transfer performance of the PHP displays a decreasing trend as a function of the fill ratio. However, the trendline shifts from the left (low fill ratio) to the right (high fill ratio) going from the 7-turn PHP to the 1-turn PHP. The red dashed boxes in Figure 6-9 highlight the optimal effective thermal conductivity at the initial fill ratio of 50% and 63%. In the 50% fill ratio case, the best optimal heat transfer performance of the 1-turn PHP, 3-turn PHP and the 5-turn PHP are compared with the second lowest optimal effective thermal conductivity of the 7-turn PHP. In the 63% fill ratio case, the

second-best optimal heat transfer performance of the 1-turn PHP is compared with the worst optimal heat transfer performance of the 5-turn and 7-turn PHP.

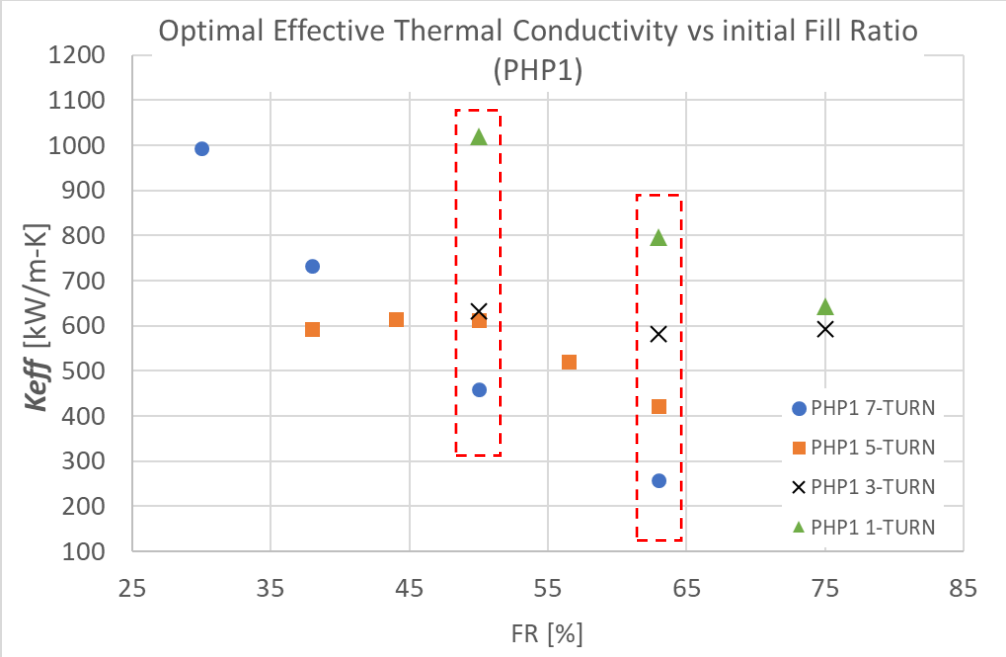

Figure 6-9 The optimal effective thermal conductivity as a function of the initial fill ratio at the condenser temperature of 77.4 K for PHP1.

So, the comparison presented in Chapter 6.2 of the effective thermal conductivity as a function of the heat load per turn at the initial fill ratio of 50% and 63% at the condenser temperature of 77.4 K might not be fair to the 7-turn PHP. One might also wonder if the comparison study between the 8-turn and 48-turn cryogenic helium PHP at the initial fill ratio of about 70% [22] is also a competition between the best fill ratio of the one configuration against the worst fill ratio of the other configuration.

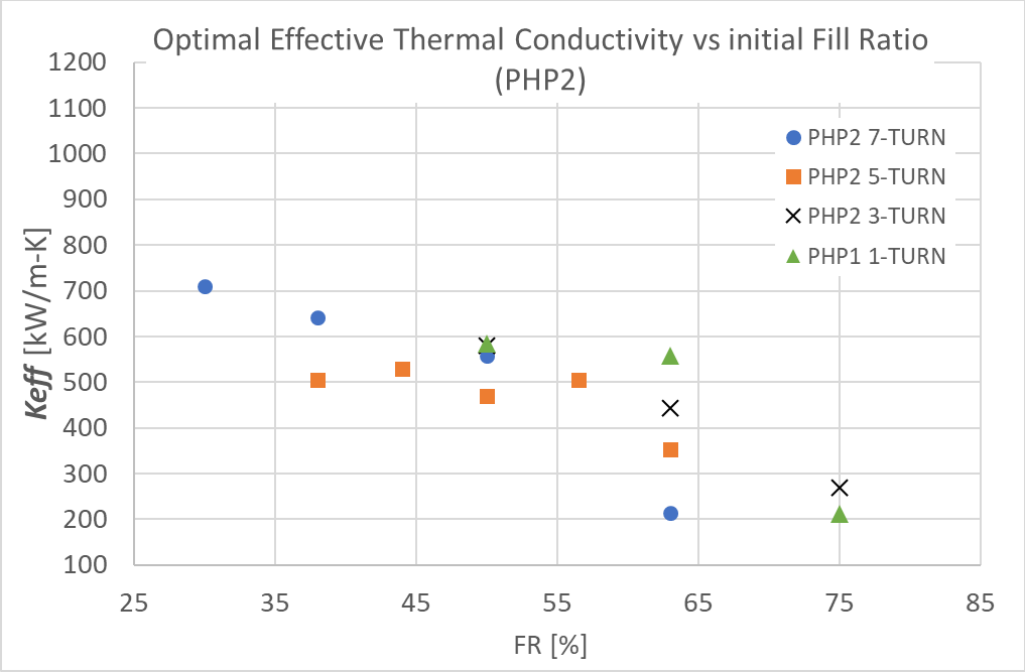

Figure 6-10 The optimal effective thermal conductivity as a function of the initial fill ratio at the condenser temperature of 77.4 K for PHP2.

Figure 6-11 below, compares the case with an initial fill ratio of 30% for the 7-turn PHP to the case with an initial fill ratio of 50% for the 1-turn, 3-turn and 5-turn PHP. The experimental data of each configuration in Figure 6-11 is at the fill ratio of their greatest optimal thermal conductivity. With this perspective, the thermal conductivity of the 7-turn configuration is much higher than that of the 1-turn, 3-turn and 5-turn configurations when the heat flux is below 0.58 W/turn.

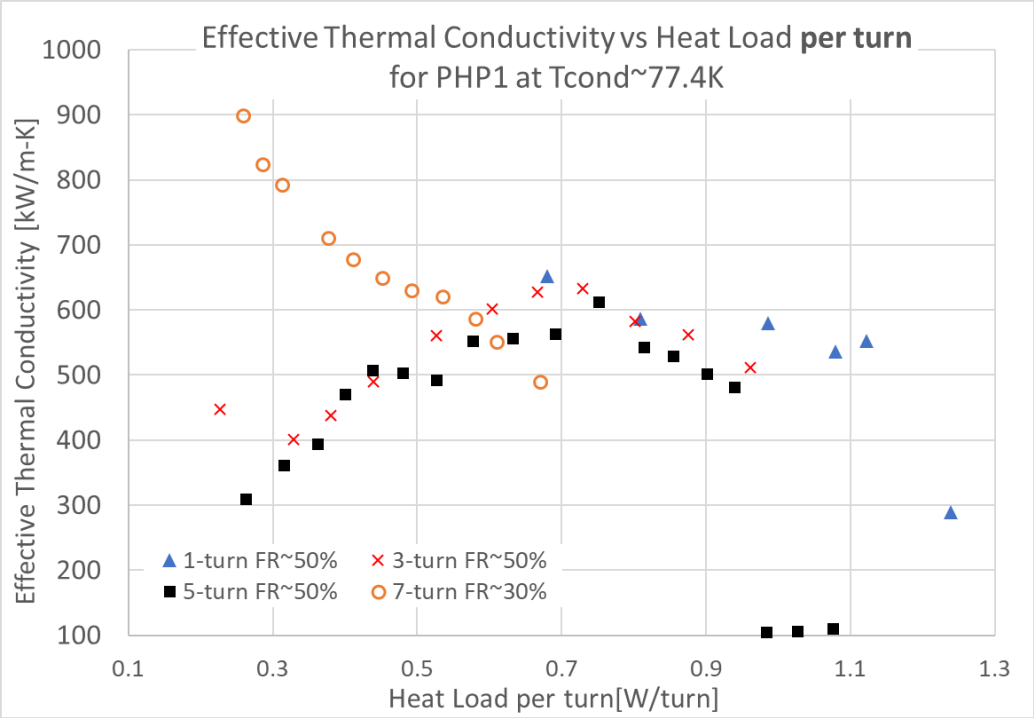

Figure 6-11 Effective thermal conductivity as a function of heat load **per turn** for PHP1 at the condenser temperature of 77.4 K and at the initial fill ratio of 50% for 1-turn, 3-turn and 5-turn PHP, but at the initial fill ratio of 30% for 7-turn PHP.

6.4 5-turn PHP is the recommended configuration from our study

Among all the configurations tested for our cryogenic nitrogen PHP experiment, the 5-turn PHP has the best stability and repeatability as discussed in the previous chapters. The difference of the heat transfer performance between PHP1 and PHP2 is small compared with the difference between PHP and PHP2 in other configurations. Although the 5-turn PHP does not produce an effective thermal conductivity approaching 1000000 W/m-K as observed for the 1-turn and 7-turn PHP, the 5-turn PHP has very good heat transfer performance over a wide range of fill ratios at both condenser temperatures. The 5-turn PHP has a very stable value of optimal effective thermal conductivity, about 600000 W/m-K for PHP1 and about 500000 W/m-K, between the initial fill ratio of 38% and 56.5% at the condenser temperature of 77.4 K. The 5-turn PHP also produces a very stable optimal effective thermal conductivity, about 670000 W/m-

K for PHP1 and about 550000 W/m-K between the initial fill ratio of 38% and 63% at the condenser temperature of 84.5 K. The other PHP configurations usually perform well in a much smaller fill ratio range as shown in Figure 6-9 and Figure 6-10. Although effective thermal conductivity values exceeding 1000000 W/m-K are sometimes observed when operating the 1-turn PHP at the condenser temperature of 77.4 K and the initial fill ratio of 50% and at the condenser temperature of 84.5 K and the initial fill ratio of 63%, these are not stable. The 1-turn PHP experienced dry out multiple times during the sequential heat load test at the condenser temperature of 77.4 K and the initial fill ratio of 50% and at the condenser temperature of 84.5 K and the initial fill ratio of 63%. In real life applications, it is not acceptable to sacrifice the stability for the peak performance. For example, if a 1-turn PHP is used to cool an HTS magnet, the additional heat generated from a local hot spot might make the PHP dry out and cause catastrophic consequence even though the performance during normal operating conditions is great. The 7-turn PHP exhibits pseudo steady state behavior at certain low and moderate heat load conditions at the initial fill ratios of 30% and 38%, exhibiting optimal effective thermal conductivity values around 1000000 W/m-K and 730000 W/m-K at these two fill ratios respectively. However, the heat transfer performance of the 7-turn PHP decays significantly when the initial fill ratio is greater than 50% at the condenser temperature of 77.4 K.

The heat load range where the 5-turn configuration performs well is also very wide when compared with other configurations at most test conditions. At the condenser temperature of 77.4 K and the initial fill ratio of 50% test condition, the 5-turn PHP1 provides an effective thermal conductivity greater than 400000 W/m-K between the heat load of 1.81 W and 4.70 W. Furthermore, the 5-turn PHP2 also exhibits an effective thermal conductivity value greater than 400000 W/m-K between the heat load of 2.19 W and 4.70 W.

Table 6-2 The heat load range and the magnitude of the heat load range where the effective thermal conductivity is above 400000 W/m-K for PHP1 and PHP2 for all the configurations tested at the condenser temperature of 77.4 K and the initial fill ratio of 50%.

	PHP1	PHP2
1-TURN	0.48 W to 1.12 W (0.64 W)	0.48 W to 0.81 W (0.33W)
3-TURN	0.99 W to 2.88 W (1.89 W)	1.32 W to 2.88 W (1.56 W)
5-TURN	1.81 W to 4.70 W (2.89 W)	2.19 W to 4.70 W (2.51 W)
7-TURN	3.46 W to 5.60 W (2.14 W)	3.76 W to 6.64 W (2.88 W)

Based on experimental data collected from the 1-turn, 3-turn, 5-turn and 7-turn configurations in this study, the 5-turn PHP provides the best configuration for decent heat transfer performance over a wide range of operable heat loads, good repeatability and stability.

7. Proposal for future work

The cryogenic nitrogen pulsating heat pipes characterized in this study included the 1-turn, 3-turn, 5-turn and 7-turn configurations at two different condenser temperatures and different fill ratios. The experimental data collected in the study demonstrates that nitrogen PHPs can achieve high heat transfer performance among all configurations tested. From the comparison of all four configurations, the 5-turn configuration proved to be the most practical choice from the perspective of the heat transfer performance, operable range, stability and repeatability. A limited range of initial fill ratio conditions have been conducted for the 7-turn PHP at the condenser temperature of 84.5 K.

Additional future parameters to study include variable adiabatic length, orientation with respect to the gravity, and the vibration measurement on the evaporator.

8. Appendix

8.1 **Table of Voltage and Current on the PHP1 and PHP2 Evaporator Heaters**

Table 8-1 Voltage and current measured on the evaporator heaters on PHP1 and PHP2 at Tcond~84.5 K and the initial FR of 50% (1-turn PHP)

Run	I PHP1[A]	V PHP1[V]	I PHP2[A]	V PHP2[V]
1	0.060	0.167	0.060	0.165
2	0.139	3.428	0.139	3.426
3	0.166	4.095	0.166	4.091
4	0.181	4.463	0.181	4.457
5	0.200	4.939	0.200	4.932
6	0.209	5.150	0.209	5.146
7	0.215	5.304	0.215	5.307
8	0.224	5.553	0.224	5.540
9	0.231	5.711	0.231	5.711
10	0.241	5.960	0.241	5.957
11	0.101	2.493	0.101	2.490
12	0.155	3.826	0.155	3.825

Table 8-2 Voltage and current measured on the evaporator heaters on PHP1 and PHP2 at Tcond~84.5 K and the initial FR of 63% (1-turn PHP)

Run	I PHP1[A]	V PHP1[V]	I PHP2[A]	V PHP2[V]
1	0.101	2.492	0.101	2.489
1	0.101	2.492	0.101	2.489
2	0.139	3.427	0.139	3.428
3	0.155	3.829	0.155	3.827
4	0.166	4.103	0.166	4.096
5	0.181	4.458	0.181	4.461
6	0.200	4.928	0.200	4.936
7	0.209	5.152	0.209	5.155
8	0.215	5.306	0.215	5.307
9	0.224	5.526	0.224	5.530
10	0.231	5.694	0.231	5.696
11	0.231	5.694	0.231	5.691
12	0.241	5.943	0.241	5.948
13	0.241	5.938	0.241	5.938
14	0.253	6.236	0.253	6.242
15	0.265	6.528	0.265	6.527
16	0.272	6.720	0.272	6.717
17	0.277	6.901	0.277	6.891
18	0.209	5.156	0.209	5.156

19	0.215	5.306	0.215	5.307
20	0.224	5.527	0.224	5.530
21	0.231	5.699	0.231	5.693
22	0.241	5.944	0.241	5.943
23	0.253	6.241	0.253	6.243
24	0.265	6.548	0.265	6.547
25	0.272	6.721	0.272	6.723
26	0.277	6.845	0.277	6.845
27	0.139	3.427	0.139	3.426
28	0.155	3.825	0.155	3.825
29	0.166	4.094	0.166	4.087
30	0.181	4.458	0.181	4.457
31	0.200	4.938	0.200	4.937
32	0.155	3.825	0.155	3.825

Table 8-3 Voltage and current measured on the evaporator heaters on PHP1 and PHP2 at Tcond~84.5 K and the initial FR of 75% (1-turn PHP)

Run	I PHP1[A]	V PHP1[V]	I PHP2[A]	V PHP2[V]
1	0.139	3.428	0.139	3.427
2	0.265	6.533	0.265	6.530
3	0.155	3.829	0.155	3.826
4	0.166	4.101	0.166	4.102
5	0.181	4.476	0.181	4.476
6	0.200	4.941	0.200	4.942
7	0.209	5.157	0.209	5.156
8	0.215	5.317	0.215	5.317
9	0.224	5.531	0.224	5.530
10	0.231	5.703	0.231	5.702
11	0.241	5.951	0.241	5.953
12	0.241	5.947	0.241	5.944
13	0.253	6.249	0.253	6.248
14	0.265	6.546	0.265	6.543
15	0.271	6.694	0.271	6.700
16	0.277	6.853	0.277	6.851
17	0.284	7.025	0.284	7.023
18	0.291	7.198	0.291	7.198
19	0.298	7.370	0.298	7.369

Table 8-4 Voltage and current measured on the evaporator heaters on PHP1 and PHP2 at Tcond~77.4 K and the initial FR of 50% (1-turn PHP)

Run	I PHP1[A]	V PHP1[V]	I PHP2[A]	V PHP2[V]
1	0.139	3.425	0.139	3.427
2	0.155	3.824	0.155	3.821
3	0.166	4.097	0.166	4.097
4	0.181	4.471	0.181	4.468
5	0.200	4.931	0.200	4.928
6	0.209	5.162	0.209	5.163
7	0.213	5.268	0.213	5.266
8	0.224	5.531	0.224	5.531
9	0.224	5.513	0.224	5.511

Table 8-5 Voltage and current measured on the evaporator heaters on PHP1 and PHP2 at Tcond~77.4 K and the initial FR of 63% (1-turn PHP)

Run	I PHP1[A]	V PHP1[V]	I PHP2[A]	V PHP2[V]
1	0.139	3.426	0.139	3.427
2	0.209	5.152	0.209	5.152
3	0.213	5.299	0.213	5.303
4	0.224	5.531	0.224	5.531
5	0.231	5.703	0.231	5.703
6	0.241	5.952	0.241	5.950
7	0.253	6.249	0.253	6.249
8	0.265	6.551	0.265	6.548
9	0.271	6.705	0.271	6.691
10	0.277	6.848	0.277	6.848
11	0.284	7.023	0.284	7.024
12	0.155	3.819	0.155	3.820
13	0.166	4.092	0.166	4.091
14	0.181	4.452	0.181	4.453
15	0.200	4.931	0.200	4.927
16	0.209	5.161	0.209	5.155
17	0.213	5.257	0.213	5.255
18	0.224	5.521	0.224	5.521
19	0.231	5.693	0.231	5.692
20	0.139	3.426	0.139	3.426
21	0.155	3.824	0.155	3.820
22	0.181	4.451	0.181	4.447

Table 8-6 Voltage and current measured on the evaporator heaters on PHP1 and PHP2 at Tcond~77.4 K and the initial FR of 75% (1-turn PHP)

Run	I PHP1[A]	V PHP1[V]	I PHP2[A]	V PHP2[V]
1	0.139	3.425	0.139	3.427

2	0.155	3.823	0.155	3.821
3	0.166	4.091	0.166	4.092
4	0.181	4.466	0.181	4.467
5	0.200	4.936	0.200	4.937
6	0.209	5.157	0.209	5.145
7	0.209	5.147	0.209	5.146
8	0.213	5.262	0.213	5.260
9	0.224	5.531	0.224	5.531
10	0.213	5.262	0.213	5.260
11	0.209	5.161	0.209	5.157
12	0.213	5.262	0.213	5.260
13	0.224	5.530	0.224	5.530
14	0.231	5.705	0.231	5.707
15	0.241	5.957	0.241	5.958
16	0.253	6.250	0.253	6.248
17	0.264	6.523	0.264	6.519
18	0.271	6.701	0.271	6.700

Table 8-7 Voltage and current measured on the evaporator heaters on PHP1 and PHP2 at Tcond~84.5 K and the initial FR of 50% (3-turn PHP)

Run	I PHP1[A]	V PHP1[V]	I PHP2[A]	V PHP2[V]
1	0.139	3.431	0.139	3.432
2	0.166	4.096	0.166	4.092
3	0.200	4.494	0.200	4.496
4	0.215	5.305	0.215	5.306
5	0.231	5.704	0.231	5.699
6	0.253	6.253	0.253	6.244
7	0.271	6.693	0.271	6.680
8	0.284	7.011	0.284	7.006
9	0.298	7.359	0.298	7.353
10	0.312	7.708	0.312	7.708
11	0.327	8.077	0.327	8.068
12	0.342	8.451	0.342	8.443
13	0.358	8.845	0.358	8.841
14	0.374	9.243	0.374	9.239
15	0.390	9.645	0.390	9.634
16	0.390	9.642	0.390	9.621
17	0.396	9.794	0.396	9.787
18	0.406	10.044	0.406	10.041

Table 8-8 Voltage and current measured on the evaporator heaters on PHP1 and PHP2 at Tcond~84.5 K and the initial FR of 63% (3-turn PHP)

Run	I PHP1[A]	V PHP1[V]	I PHP2[A]	V PHP2[V]
1	0.139	3.431	0.139	3.427
2	0.166	4.106	0.166	4.101
3	0.200	4.938	0.200	4.936
4	0.215	5.306	0.215	5.296
5	0.231	5.707	0.231	5.703
6	0.253	6.247	0.253	6.244
7	0.271	6.690	0.271	6.685
8	0.284	7.013	0.284	7.007
9	0.298	7.359	0.298	7.349
10	0.312	7.711	0.312	7.709
11	0.327	8.080	0.327	8.069
12	0.342	8.454	0.342	8.434
13	0.358	8.852	0.358	8.837
14	0.374	9.248	0.374	9.240
15	0.390	9.653	0.390	9.637
16	0.406	10.045	0.406	10.039
17	0.416	10.300	0.416	10.287
18	0.427	10.568	0.427	10.561
19	0.271	6.684	0.271	6.676
20	0.284	7.017	0.284	7.007
21	0.298	7.356	0.298	7.348
22	0.312	7.714	0.312	7.699
23	0.284	7.018	0.284	7.003
24	0.425	10.537	0.425	10.523

Table 8-9 Voltage and current measured on the evaporator heaters on PHP1 and PHP2 at Tcond~84.5 K and the initial FR of 75% (3-turn PHP)

Run	I PHP1[A]	V PHP1[V]	I PHP2[A]	V PHP2[V]
1	0.166	4.145	0.166	4.118
2	0.200	4.940	0.200	4.934
3	0.215	5.311	0.215	5.304
4	0.231	5.706	0.231	5.706
5	0.253	6.244	0.253	6.237
6	0.271	6.703	0.271	6.694
7	0.284	7.028	0.284	7.021
8	0.298	7.364	0.298	7.357
9	0.312	7.721	0.312	7.713
10	0.327	8.084	0.327	8.070

11	0.342	8.456	0.342	8.450
12	0.358	8.854	0.358	8.847
13	0.374	9.272	0.374	9.249
14	0.390	9.658	0.390	9.639
15	0.406	10.049	0.406	10.049
16	0.416	10.308	0.416	10.304
17	0.425	10.526	0.425	10.513
18	0.436	10.796	0.436	10.787
19	0.446	11.049	0.446	11.043
20	0.457	11.323	0.457	11.318
21	0.466	11.547	0.466	11.539
22	0.271	6.697	0.271	6.687
23	0.271	6.697	0.271	6.687
24	0.358	8.836	0.358	8.825
25	0.271	6.686	0.271	6.676
26	0.271	6.686	0.271	6.676
27	0.271	6.681	0.271	6.674
28	0.166	4.089	0.166	4.080
29	0.271	6.694	0.271	6.687
30	0.271	6.695	0.271	6.688
31	0.474	11.734	0.474	11.711
32	0.471	11.676	0.471	11.655

Table 8-10 Voltage and current measured on the evaporator heaters on PHP1 and PHP2 at Tcond~77.4 K and the initial FR of 50% (3-turn PHP)

Run	I PHP1[A]	V PHP1[V]	I PHP2[A]	V PHP2[V]
1	0.166	4.097	0.166	4.088
2	0.200	4.929	0.200	4.925
3	0.215	5.301	0.215	5.299
4	0.231	5.696	0.231	5.693
5	0.253	6.238	0.253	6.238
6	0.271	6.682	0.271	6.674
7	0.285	7.019	0.285	7.016
8	0.298	7.342	0.298	7.337
9	0.312	7.707	0.312	7.692
10	0.326	8.054	0.327	8.048
11	0.342	8.434	0.342	8.432
12	0.358	8.838	0.358	8.834
13	0.374	9.251	0.374	9.250
14	0.374	9.250	0.374	9.250
15	0.271	6.682	0.271	6.674
16	0.271	6.686	0.271	6.679
17	0.271	6.687	0.271	6.679

18	0.271	6.687	0.271	6.679
19	0.271	6.687	0.271	6.679
20	0.358	8.832	0.358	8.830
21	0.358	8.836	0.358	8.829
22	0.166	4.089	0.166	4.092
23	0.166	4.094	0.166	4.092
24	0.166	4.093	0.166	4.091
25	0.358	8.822	0.358	8.820

Table 8-11 Voltage and current measured on the evaporator heaters on PHP1 and PHP2 at Tcond~77.4 K and the initial FR of 63% (3-turn PHP)

Run	I PHP1[A]	V PHP1[V]	I PHP2[A]	V PHP2[V]
1	0.166	4.094	0.166	4.095
2	0.200	4.929	0.200	4.927
3	0.215	5.304	0.215	5.300
4	0.231	5.697	0.231	5.697
5	0.253	6.243	0.253	6.240
6	0.271	6.688	0.271	6.685
7	0.285	7.025	0.285	7.030
8	0.298	7.356	0.298	7.351
9	0.312	7.699	0.312	7.696
10	0.327	8.067	0.327	8.065
11	0.342	8.438	0.342	8.432
12	0.358	8.835	0.358	8.829
13	0.374	9.238	0.374	9.234
14	0.390	9.635	0.390	9.634
15	0.406	10.031	0.406	10.026
16	0.416	10.285	0.416	10.284
17	0.427	10.570	0.427	10.567
18	0.436	10.787	0.436	10.785
19	0.446	11.042	0.446	11.045
20	0.456	11.284	0.456	11.282
21	0.466	11.546	0.466	11.535
22	0.474	11.742	0.474	11.737
23	0.486	12.034	0.486	12.034
24	0.271	6.686	0.271	6.684
25	0.271	6.686	0.271	6.684
26	0.271	6.686	0.271	6.684
27	0.271	6.686	0.271	6.681
28	0.358	8.836	0.358	8.835
29	0.358	8.837	0.358	8.834
30	0.358	8.839	0.358	8.834
31	0.231	5.695	0.231	5.696

32	0.231	5.697	0.231	5.689
33	0.358	8.838	0.358	8.834
34	0.231	5.695	0.231	5.694
35	0.312	7.697	0.312	7.699
36	0.312	7.697	0.312	7.698
37	0.312	7.694	0.312	7.694

Table 8-12 Voltage and current measured on the evaporator heaters on PHP1 and PHP2 at Tcond~77.4 K and the initial FR of 75% (3-turn PHP)

Run	I PHP1[A]	V PHP1[V]	I PHP2[A]	V PHP2[V]
1	0.166	4.092	0.166	4.092
2	0.200	4.931	0.200	4.931
3	0.215	5.298	0.215	5.298
4	0.231	5.703	0.231	5.703
5	0.253	6.242	0.253	6.242
6	0.271	6.679	0.271	6.679
7	0.285	7.031	0.285	7.031
8	0.298	7.356	0.298	7.356
9	0.312	7.704	0.312	7.704
10	0.327	8.071	0.327	8.071
11	0.342	8.447	0.342	8.447
12	0.358	8.837	0.358	8.837
13	0.374	9.232	0.374	9.232
14	0.374	9.241	0.374	9.241
15	0.390	9.644	0.390	9.644
16	0.406	10.042	0.406	10.042
17	0.416	10.292	0.416	10.292
18	0.427	10.560	0.427	10.560
19	0.436	10.798	0.436	10.798
20	0.446	11.039	0.446	11.039
21	0.456	11.289	0.456	11.289
22	0.466	11.540	0.466	11.540
23	0.474	11.740	0.474	11.740
24	0.486	12.059	0.486	12.059
25	0.496	12.311	0.496	12.311
26	0.271	6.682	0.271	6.682
27	0.271	6.682	0.271	6.682
28	0.271	6.684	0.271	6.684
29	0.200	4.927	0.200	4.927
30	0.271	6.680	0.271	6.680

Table 8-13 Voltage and current measured on the evaporator heaters on PHP1 and PHP2 at Tcond~84.5 K and the initial FR of 38% (5-turn PHP)

Run	I PHP1[A]	V PHP1[V]	I PHP2[A]	V PHP2[V]
1	0.231	5.705	0.231	5.706
2	0.253	6.240	0.253	6.243
3	0.271	6.683	0.271	6.680
4	0.285	7.032	0.285	7.031
5	0.298	7.352	0.298	7.349
6	0.312	7.700	0.312	7.696
7	0.327	8.076	0.327	8.076
8	0.342	8.443	0.342	8.439
9	0.358	8.838	0.358	8.836
10	0.374	9.234	0.374	9.235
11	0.390	9.634	0.390	9.638
12	0.406	10.035	0.406	10.037
13	0.416	10.282	0.416	10.284
14	0.427	10.553	0.427	10.549
15	0.436	10.782	0.436	10.782
16	0.446	11.030	0.446	11.029
17	0.456	11.278	0.456	11.280
18	0.466	11.527	0.466	11.526
19	0.474	11.741	0.474	11.725
20	0.312	7.699	0.312	7.695
21	0.312	7.699	0.312	7.695
22	0.312	7.703	0.312	7.696
23	0.312	7.703	0.312	7.696
24	0.327	8.081	0.327	8.070
25	0.327	8.081	0.327	8.070
26	0.327	8.081	0.327	8.070
27	0.327	8.082	0.327	8.070
28	0.456	11.280	0.456	11.278
29	0.390	9.640	0.390	9.636
30	0.201	4.956	0.201	4.955
31	0.201	4.956	0.201	4.955

Table 8-14 Voltage and current measured on the evaporator heaters on PHP1 and PHP2 at Tcond~84.5 K and the initial FR of 50% (5-turn PHP)

Run	I PHP1[A]	V PHP1[V]	I PHP2[A]	V PHP2[V]
1	0.231	5.703	0.231	5.693

2	0.253	6.246	0.253	6.250
3	0.271	6.692	0.271	6.687
4	0.285	7.037	0.285	7.038
5	0.298	7.358	0.298	7.362
6	0.312	7.702	0.312	7.704
7	0.327	8.076	0.327	8.079
8	0.342	8.448	0.342	8.454
9	0.358	8.850	0.358	8.848
10	0.374	9.242	0.374	9.247
11	0.390	9.640	0.390	9.636
12	0.406	10.047	0.406	10.045
13	0.416	10.286	0.416	10.288
14	0.327	8.080	0.327	8.078
15	0.416	10.276	0.416	10.277
16	0.427	10.559	0.427	10.789
17	0.436	10.788	0.436	10.789
18	0.446	11.036	0.446	11.029
19	0.456	11.284	0.456	11.280
20	0.466	11.527	0.466	11.526
21	0.474	11.732	0.474	11.726
22	0.486	12.025	0.486	12.038
23	0.496	12.277	0.496	12.272
24	0.507	12.566	0.507	12.547
25	0.327	8.081	0.327	8.072
26	0.327	8.081	0.327	8.072
27	0.327	8.081	0.327	8.072
28	0.466	11.527	0.466	11.525
29	0.466	11.528	0.466	11.526
30	0.466	11.528	0.466	11.526
31	0.466	11.538	0.466	11.528
32	0.312	7.704	0.312	7.701
33	0.298	7.360	0.298	7.354
34	0.285	7.035	0.285	7.032
35	0.271	6.691	0.271	6.684
36	0.253	6.247	0.253	6.243
37	0.231	5.702	0.231	5.701

Table 8-15 Voltage and current measured on the evaporator heaters on PHP1 and PHP2 at Tcond~84.5 K and the initial FR of 63% (5-turn PHP)

Run	I PHP1[A]	V PHP1[V]	I PHP2[A]	V PHP2[V]
1	0.231	5.702	0.231	5.702
2	0.253	6.245	0.253	6.243
3	0.271	6.691	0.271	6.690
4	0.285	7.032	0.285	7.032
5	0.298	7.351	0.298	7.351
6	0.312	7.700	0.312	7.702
7	0.327	8.076	0.327	8.077
8	0.342	8.448	0.342	8.447
9	0.358	8.844	0.358	8.846
10	0.374	9.240	0.374	9.240
11	0.390	9.639	0.390	9.634
12	0.406	10.034	0.406	10.037
13	0.416	10.287	0.416	10.288
14	0.427	10.562	0.427	10.562
15	0.446	11.034	0.446	11.027
16	0.456	11.288	0.456	11.283
17	0.466	11.537	0.466	11.535
18	0.486	12.046	0.486	12.024
19	0.496	12.285	0.496	12.280
20	0.507	12.557	0.507	12.551
21	0.519	12.857	0.519	12.854
22	0.530	13.129	0.530	13.125
23	0.540	13.380	0.540	13.374
24	0.550	13.632	0.550	13.625
25	0.561	13.906	0.561	13.904
26	0.572	14.177	0.572	14.175
27	0.285	7.033	0.285	7.032
28	0.285	7.034	0.285	7.035
29	0.285	7.034	0.285	7.035
30	0.285	7.034	0.285	7.035
31	0.466	11.534	0.466	11.531
32	0.466	11.534	0.466	11.531
33	0.466	11.535	0.466	11.531
34	0.446	11.032	0.446	11.033
35	0.446	11.032	0.446	11.033
36	0.466	11.534	0.466	11.536
37	0.358	8.848	0.358	8.845

38	0.358	8.848	0.358	8.845
39	0.358	8.848	0.358	8.845
40	0.358	8.848	0.358	8.845

Table 8-16 Voltage and current measured on the evaporator heaters on PHP1 and PHP2 at Tcond~77.4 K and the initial FR of 38% (5-turn PHP)

Run	I PHP1[A]	V PHP1[V]	I PHP2[A]	V PHP2[V]
1	0.201	4.956	0.201	4.955
2	0.231	5.691	0.231	5.691
3	0.253	6.236	0.253	6.238
4	0.271	6.675	0.271	6.680
5	0.285	7.024	0.285	7.026
6	0.298	7.353	0.298	7.349
7	0.285	7.030	0.285	7.027
8	0.298	7.346	0.298	7.349
9	0.312	7.696	0.312	7.696
10	0.327	8.061	0.327	8.066
11	0.342	8.433	0.342	8.432
12	0.358	8.834	0.358	8.835
13	0.374	9.230	0.374	9.234
14	0.390	9.631	0.390	9.632
15	0.406	10.024	0.406	10.026
16	0.416	10.272	0.416	10.273
17	0.427	10.554	0.427	10.553
18	0.342	8.433	0.342	8.431
19	0.342	8.434	0.342	8.431
20	0.342	8.433	0.342	8.431
21	0.342	8.433	0.342	8.431
22	0.342	8.433	0.342	8.431

Table 8-17 Voltage and current measured on the evaporator heaters on PHP1 and PHP2 at Tcond~77.4 K and the initial FR of 44% (5-turn PHP)

Run	I PHP1[A]	V PHP1[V]	I PHP2[A]	V PHP2[V]
1	0.253	6.234	0.253	6.238
2	0.271	6.675	0.271	6.680
3	0.285	7.022	0.285	7.022
4	0.298	7.347	0.298	7.349

5	0.312	7.691	0.312	7.696
6	0.327	8.068	0.327	8.071
7	0.342	8.439	0.342	8.441
8	0.358	8.842	0.358	8.845
9	0.374	9.231	0.374	9.235
10	0.390	9.630	0.390	9.633
11	0.406	10.028	0.406	10.032
12	0.416	10.280	0.416	10.283
13	0.427	10.551	0.427	10.554
14	0.436	10.784	0.436	10.781
15	0.374	9.237	0.374	9.240
16	0.374	9.236	0.374	9.238
17	0.374	9.237	0.374	9.240
18	0.374	9.236	0.374	9.240
19	0.374	9.237	0.374	9.240
20	0.374	9.235	0.374	9.239
21	0.374	9.235	0.374	9.239
22	0.342	8.441	0.342	8.441
23	0.327	8.068	0.327	8.071
24	0.312	7.692	0.312	7.697

Table 8-18 Voltage and current measured on the evaporator heaters on PHP1 and PHP2 at Tcond~77.4 K and the initial FR of 50% (5-turn PHP)

Run	I PHP1[A]	V PHP1[V]	I PHP2[A]	V PHP2[V]
1	0.231	5.675	0.231	5.693
2	0.253	6.238	0.253	6.239
3	0.271	6.681	0.271	6.682
4	0.285	7.025	0.285	7.027
5	0.298	7.349	0.298	7.350
6	0.312	7.693	0.312	7.697
7	0.327	8.047	0.327	8.067
8	0.342	8.437	0.342	8.438
9	0.358	8.832	0.358	8.836
10	0.374	9.231	0.374	9.235
11	0.390	9.631	0.390	9.633
12	0.406	10.027	0.406	10.027
13	0.416	10.270	0.416	10.274
14	0.427	10.551	0.427	10.554
15	0.436	10.776	0.436	10.778
16	0.446	11.027	0.446	11.028
17	0.455	11.279	0.455	11.275
18	0.466	11.546	0.466	11.536

19	0.391	9.660	0.391	9.663
20	0.391	9.660	0.391	9.663
21	0.391	9.631	0.391	9.634
22	0.390	9.627	0.390	9.634
23	0.390	9.627	0.390	9.634
24	0.390	9.628	0.390	9.634
25	0.390	9.628	0.390	9.634

Table 8-19 Voltage and current measured on the evaporator heaters on PHP1 and PHP2 at Tcond~77.4 K and the initial FR of 56.5% (5-turn PHP)

Run	I PHP1[A]	V PHP1[V]	I PHP2[A]	V PHP2[V]
1	0.406	10.028	0.406	10.032
2	0.253	6.233	0.253	6.234
3	0.271	6.679	0.271	6.681
4	0.298	7.345	0.298	7.345
5	0.312	7.692	0.312	7.697
6	0.327	8.067	0.327	8.072
7	0.342	8.445	0.342	8.447
8	0.358	8.836	0.358	8.837
9	0.374	9.231	0.374	9.236
10	0.390	9.629	0.390	9.634
11	0.406	10.033	0.406	10.033
12	0.416	10.284	0.416	10.284
13	0.436	10.778	0.436	10.782
14	0.455	11.256	0.455	11.252
15	0.474	11.731	0.474	11.726
16	0.496	12.282	0.496	12.277
17	0.519	12.854	0.519	12.856
18	0.374	9.235	0.374	9.236
19	0.374	9.236	0.374	9.236
20	0.374	9.237	0.374	9.237
21	0.374	9.237	0.374	9.237
22	0.374	9.237	0.374	9.237
23	0.271	6.685	0.271	6.686
24	0.507	12.562	0.507	12.562
25	0.416	10.289	0.416	10.284
26	0.416	10.289	0.416	10.285
27	0.416	10.289	0.416	10.285
28	0.416	10.288	0.416	10.284

Table 8-20 Voltage and current measured on the evaporator heaters on PHP1 and PHP2 at Tcond~77.4 K and the initial FR of 63% (5-turn PHP)

Run	I PHP1[A]	V PHP1[V]	I PHP2[A]	V PHP2[V]
1	0.231	5.690	0.231	5.693
2	0.253	6.233	0.253	6.235
3	0.271	6.674	0.271	6.676
4	0.285	7.028	0.285	7.028
5	0.298	7.352	0.298	7.350
6	0.312	7.699	0.312	7.697
7	0.327	8.065	0.327	8.067
8	0.342	8.436	0.342	8.438
9	0.358	8.835	0.358	8.836
10	0.374	9.230	0.374	9.235
11	0.390	9.629	0.390	9.629
12	0.406	10.028	0.406	10.028
13	0.416	10.290	0.416	10.284
14	0.427	10.556	0.427	10.559
15	0.436	10.780	0.436	10.782
16	0.446	11.031	0.446	11.034
17	0.455	11.259	0.455	11.261
18	0.466	11.534	0.466	11.536
19	0.474	11.734	0.474	11.735
20	0.486	12.033	0.486	12.034
21	0.496	12.284	0.496	12.282
22	0.507	12.564	0.507	12.562
23	0.519	12.853	0.519	12.856
24	0.530	13.131	0.530	13.136
25	0.540	13.386	0.540	13.379
26	0.550	13.633	0.550	13.630
27	0.561	13.908	0.561	13.906
28	0.572	14.185	0.572	14.181
29	0.586	14.536	0.586	14.528
30	0.597	14.819	0.597	14.798
31	0.342	8.439	0.342	8.442
32	0.374	9.231	0.374	9.235
33	0.312	7.693	0.312	7.701
34	0.312	7.693	0.312	7.701

Table 8-21Voltage and current measured on the evaporator heaters on PHP1 and PHP2 at Tcond~84.5 K and the initial FR of 50% (7-turn PHP)

Run	I PHP1[A]	V PHP1[V]	I PHP2[A]	V PHP2[V]
1	0.327	8.065	0.327	8.067
2	0.342	8.447	0.342	8.445

3	0.358	8.839	0.358	8.839
4	0.374	9.241	0.374	9.243
5	0.390	9.634	0.390	9.632
6	0.406	10.036	0.406	10.031
7	0.416	10.280	0.416	10.282
8	0.436	10.773	0.436	10.771
9	0.455	11.246	0.455	11.240
10	0.474	11.729	0.474	11.724
11	0.496	12.270	0.496	12.270
12	0.519	12.840	0.519	12.840
13	0.530	13.122	0.530	13.119
14	0.550	13.614	0.550	13.609
15	0.572	14.164	0.572	14.168
16	0.586	14.512	0.586	14.510
17	0.600	14.866	0.600	14.865
18	0.406	10.031	0.406	10.030
19	0.406	10.031	0.406	10.030
20	0.406	10.031	0.406	10.030
21	0.406	10.031	0.406	10.030
22	0.374	9.247	0.374	9.243
23	0.374	9.247	0.374	9.243
24	0.374	9.247	0.374	9.243
25	0.436	10.773	0.436	10.770
26	0.436	10.773	0.436	10.770
27	0.436	10.773	0.436	10.770
28	0.436	10.773	0.436	10.770
29	0.474	11.715	0.474	11.714
30	0.474	11.715	0.474	11.714

Table 8-22 Voltage and current measured on the evaporator heaters on PHP1 and PHP2 at Tcond~77.4 K and the initial FR of 30% (7-turn PHP)

Run	I PHP1[A]	V PHP1[V]	I PHP2[A]	V PHP2[V]
1	0.271	6.682	0.271	6.681
2	0.285	7.031	0.285	7.030
3	0.298	7.352	0.298	7.348
4	0.327	8.066	0.327	8.062
5	0.342	8.429	0.342	8.431
6	0.358	8.831	0.358	8.829
7	0.374	9.228	0.374	9.229
8	0.390	9.625	0.390	9.627
9	0.406	10.017	0.406	10.016
10	0.416	10.277	0.416	10.278

11	0.436	10.763	0.436	10.757
12	0.455	11.239	0.455	11.244
13	0.231	5.698	0.231	5.696
14	0.253	6.225	0.253	6.228
15	0.271	6.675	0.271	6.674
16	0.271	6.676	0.271	6.675
17	0.271	6.676	0.271	6.675
18	0.298	7.350	0.298	7.348
19	0.374	9.231	0.374	9.229
20	0.327	8.064	0.327	8.061
21	0.327	8.064	0.327	8.061
22	0.327	8.064	0.327	8.061
23	0.342	8.443	0.342	8.441
24	0.342	8.443	0.342	8.441
25	0.416	10.266	0.416	10.269

Table 8-23 Voltage and current measured on the evaporator heaters on PHP1 and PHP2 at Tcond~77.4 K and the initial FR of 38% (7-turn PHP)

Run	I PHP1[A]	V PHP1[V]	I PHP2[A]	V PHP2[V]
1	0.271	6.682	0.271	6.681
2	0.285	7.031	0.285	7.028
3	0.298	7.348	0.298	7.345
4	0.327	8.061	0.327	8.062
5	0.342	8.440	0.342	8.433
6	0.358	8.837	0.358	8.836
7	0.374	9.239	0.374	9.235
8	0.390	9.638	0.390	9.633
9	0.406	10.024	0.406	10.027
10	0.416	10.273	0.416	10.269
11	0.436	10.775	0.436	10.776
12	0.455	11.254	0.455	11.250
13	0.474	11.718	0.474	11.715
14	0.496	12.278	0.496	12.270
15	0.519	12.848	0.519	12.845
16	0.416	10.263	0.416	10.264
17	0.416	10.263	0.416	10.264
18	0.416	10.263	0.416	10.264
19	0.358	8.841	0.358	8.840
20	0.358	8.841	0.358	8.840
21	0.358	8.841	0.358	8.840

22	0.455	11.249	0.455	11.251
23	0.390	9.627	0.390	9.627
24	0.390	9.627	0.390	9.626
25	0.390	9.627	0.390	9.626

Table 8-24 Voltage and current measured on the evaporator heaters on PHP1 and PHP2 at Tcond~77.4 K and the initial FR of 50% (7-turn PHP)

Run	I PHP1[A]	V PHP1[V]	I PHP2[A]	V PHP2[V]
1	0.285	7.030	0.285	7.031
2	0.298	7.352	0.298	7.349
3	0.327	8.065	0.327	8.066
4	0.358	8.832	0.358	8.831
5	0.374	9.239	0.374	9.235
6	0.390	9.636	0.390	9.633
7	0.416	10.273	0.416	10.269
8	0.436	10.776	0.436	10.776
9	0.455	11.254	0.455	11.251
10	0.476	11.776	0.476	11.773
11	0.496	12.270	0.496	12.266
12	0.519	12.835	0.519	12.841
13	0.530	13.112	0.530	13.107
14	0.550	13.620	0.550	13.610
15	0.572	14.165	0.572	14.161
16	0.586	14.522	0.586	14.521
17	0.476	11.760	0.476	11.755
18	0.476	11.760	0.476	11.755
19	0.416	10.286	0.416	10.284
20	0.416	10.286	0.416	10.284
21	0.416	10.286	0.416	10.284
22	0.476	11.765	0.476	11.763
23	0.391	9.646	0.391	9.640
24	0.390	9.637	0.390	9.633
25	0.390	9.637	0.390	9.633
26	0.496	12.270	0.496	12.265
27	0.496	12.270	0.496	12.265

Table 8-25 Voltage and current measured on the evaporator heaters on PHP1 and PHP2 at Tcond~77.4 K and the initial FR of 63% (7-turn PHP)

Run	I PHP1[A]	V PHP1[V]	I PHP2[A]	V PHP2[V]
1	0.327	8.068	0.327	8.065

2	0.390	9.628	0.390	9.625
3	0.416	10.280	0.416	10.277
4	0.455	11.256	0.455	11.253
5	0.496	12.261	0.496	12.259
6	0.519	12.851	0.519	12.853
7	0.530	13.129	0.530	13.128
8	0.550	13.626	0.550	13.626
9	0.572	14.167	0.572	14.162
10	0.586	14.526	0.586	14.523
11	0.597	14.808	0.597	14.798
12	0.572	14.168	0.572	14.163
13	0.572	14.168	0.572	14.163
14	0.572	14.167	0.572	14.163
15	0.496	12.272	0.496	12.268
16	0.496	12.273	0.496	12.269
17	0.416	10.277	0.416	10.273
18	0.416	10.277	0.416	10.273
19	0.416	10.277	0.416	10.273
20	0.390	9.637	0.390	9.627
21	0.416	10.282	0.416	10.277
22	0.455	11.244	0.455	11.245
23	0.496	12.273	0.496	12.270

8.2 EES Script for estimating the initial fill ratio of each PHP subsection

File:Fill Ratio Estimation for Varied PHP 7-turn.EES 2024/8/19 10:35:53 Page 1
EES Ver. 11.733: #100: For use only by Students and Faculty, College of Engineering University of Wisconsin - Madison

```
"Fill Ratio Estimation"
$UnitSystem SI K kPa kJ masSs
 "Inputs"
F$='Nitrogen'
R=R#/MW                          "gas constant"
MW=molarmass(F$)                 "molar mass of nitrogen"
//Dimension of tubings
ID_cap=0.02[in]*convert(in,m)    "internal diameter of the capillary tubing"
A_cap=(pi#*id_cap^2/4)
OD_cap=0.032[in]*convert(in,m)   "outer diameter of the capillary tubing"
OD_ss=0.0625[in]*convert(in,m)   "outer diameter of the ss tubing"
ID_ss=0.032[in]*convert(in,m)    "inner diameter of the ss tubing"
//V_G1,
"Dimensions"
V_tank=3.607e-3[m^3]             "reservoir, same as Helium PHP System"
L_G1_Table=(23.6+19.2-0.6+2.15+0.6+6+22.8+2.8)[cm]*convert(cm,m)   "!(Need Revise)The Dimension of the Tubing and
 Swagelok T and cross of the pipelines on the table"
V_G1_Table=L_G1_table*pi#*((.18[in]*convert(in,m))^2)/4            "The Volume of the Tubing and Swagelok T and cross of
 the pipelines on the table"
V_G1_old1=V_G1_Table+V_PHP1_cu_fill+V_PHP2_cu_fill                 "Total Volume of Gasline 1"
V_G1_old2=0.00001589[m^3]+V_PHP1_cu_fill+V_PHP2_cu_fill            "tubings are updated, and dimension is from Fill Ratio
 V1.EES"
V_G1=V_NPT+V_PHP1_cu_fill+V_PHP2_cu_fill
V_NPT=37832[mm^3]*convert(mm^3,m^3)
"PHP1 and PHP2 Fill"
{L_PHP1_cu_fill_single_turn=(17*10[cm]+3[cm])*convert(cm,m)        "To fit new Swagelok fitting, the tube is cut by 3.2cm"
L_PHP1_cu_fill=170[cm]*convert(cm,m)+(23-2*3.3)[mm]*convert(mm,m)   "! Update Again due to Swagelok cutting"
V_PHP1_cu_fill=L_PHP1_cu_fill*(pi#*(.18[in]*convert(in,m))^2/4)}
"! 5-turn PHP, PHP1 new fill line length"
L_PHP1_cu_fill=(23*100+2.8-37)[mm]*convert(mm,m)                    "check, 37mm of the tube is cut to fit new swagelok for 7
-turn PHP "
V_PHP1_cu_fill=L_PHP1_cu_fill*(pi#*(.18[in]*convert(in,m))^2/4)
{"!1-turn PHP fill line length"
L_PHP2_cu_fill_single_turn=(240.2[cm]-3.25[cm])*convert(cm,m)
"!after replacing three Swagelok, this is what left"
L_PHP2_cu_fill=230[cm]*convert(cm,m)+(60.91-2*3.3)[mm]*convert(mm,m)
V_PHP2_cu_fill=L_PHP2_cu_fill*(pi#*(.18[in]*convert(in,m))^2/4)     "To fit new Swagelok fitting, the tube is cut by 3.25cm"}
"!after replacing three Swagelok,5-turn PHP, PHP2 new fill line length"
L_PHP2_cu_fill=(9*100+59.9)[mm]*convert(mm,m)
V_PHP2_cu_fill=L_PHP2_cu_fill*(pi#*(.18[in]*convert(in,m))^2/4)     "To fit new Swagelok fitting, the tube is cut by 3.25cm"
"After PHP valves but before the PHP core"
//V_feed_ambient includes the pipeline next to the PHP valve and stainless steel tubing (includes the portion within KF40 line) and
pressure relief valve sections//
V_feed_PHP1_amb=7405[mm^3]*convert(mm^3,m^3)
V_feed_PHP2_amb=7628[mm^3]*convert(mm^3,m^3)
///this is the gas-line G2 from Diego's experiment, Fill Line of PHP2 is defined from the top surface of the VCR to the top surface of the
VCR, THIS IS WITHIN THE DEWAR
V_G2_PHP1=913[mm^3]*convert(mm^3,m^3)+V_10                          "INclude V10!!"
V_G2_PHP2=857.8[mm^3]*convert(mm^3,m^3)+V_16                        "include V16"
// Misc Items of PHP1, NOT on PHP CORE
"condenser side"
V_10=48.63[mm^3]*convert(mm^3,m^3)                                  "from the tip of VCR3 to the top of copper T, fill side,
 include VCR"
V_3=3.142[mm^3]*convert(mm^3,m^3)                                   "! cold top of inside of T"
V_5=19.79[mm^3]*convert(mm^3,m^3)                                   "!cold, the center of T-block"
V_2=2.538[mm^3]*convert(mm^3,m^3)                                   "! cold left side inside of T"
V_1=49.74[mm^3]*convert(mm^3,m^3)                                   "From the left side of the T, to the VCR lip of the P_cond
```

```
 sensor, include VCR"
V_19=93.52[mm^3]*convert(mm^3,m^3)                    "from VCR gland to Copper Sleeve of Condenser Pressure
 Transducer, include VCR"
V_20=103.8[mm^3]*convert(mm^3,m^3)                    "Copper Sleeve to the End of Condenser Transducer"
V_4=6.496[mm^3]*convert(mm^3,m^3)                     "! cold, the bridge between two T blocks"
"evaporator side"
V_11=47.72[mm^3]*convert(mm^3,m^3)                    "from top of T to the lip of VCR, include VCR"
V_12=3.04[mm^3]*convert(mm^3,m^3)                     "!top of T, should be cold"
V_14=250.4[mm^3]*convert(mm^3,m^3)                    "from VCR to Copper Sleeve of Transducer, include VCR"
V_15=80.42[mm^3]*convert(mm^3,m^3)                    "copper sleeve on pressure transducer, same spec as ss
 sleeve"

// Misc Items of PHP2, NOT on PHP CORE
V_16=76.5[mm^3]*convert(mm^3,m^3)                     "from the tip of VCR3 to the top of copper T, fill side,
 include VCR"
V_17=3.04[mm^3]*convert(mm^3,m^3)                     "top of T"

//PHP Core Dimension
{N_turn=2}                          "!check"
{N_turn=6                           "!total number of tubes, three turn PHP, TOP3 and BOTTOM 3"}
{N_turn=10                          "!total number of tubes, 5-turn PHP"}
N_turn=14                           "!total number of tubes, 7-turn PHP"
L_cond=90[mm]*convert(mm,m)
L_evap=60[mm]*convert(mm,m)
L_adiabatic=1[m]
//PHP1 Core//
N=N_turn-1                          "the number of tube excluded the one with fill line, transducers tapping"
L_cap_6=10[mm]*convert(mm,m)        "within T with OD of ss sleeve"
L_cap_13=9.4[mm]*convert(mm,m)      "within T with OD of ss sleeve"
"!7-turn PHP"
L_PHP1_top_turn_78=((2*12.51+7.75)*2+(12+12.65+11.65)+(11.96+11+11.56)+(11+11+12)+(12+8+12)+(68+29))[mm]*convert(mm,m)
"the length of the U-SHAPE capillary tube for PHP1, the first two u-turn is the original u-turn, second two are built during 5-turn PHP
 and last two are from 7-turn PHP, 6 U-turn with a U-bend"
L_PHP1_bottom_turn_78=(7*3)[mm]*convert(mm,m)                    "5 u-turn at the bottom"
{"!5-turn PHP"
L_PHP1_top_turn_78_5TURN=((2*12.51+7.75)*2+(12+12.65+11.65)+(11.96+11+11.56)+(32+10+40))[mm]*convert(mm,m)"the length
of the U-SHAPE capillary tube for PHP1, the first two u-turn is the original u-turn, four U-turn with a U-bend"
L_PHP1_bottom_turn_78=(5*3)[mm]*convert(mm,m)                   "5 u-turn at the bottom"}
{"!3-turn PHP"
L_PHP1_top_turn_78=((2*12.51+7.75)*2+62.9)[mm]*convert(mm,m)"the length of the U-SHAPE capillary tube for PHP1, TWO U-turn
with a U-bend"
L_PHP1_bottom_turn_78=(3*3)[mm]*convert(mm,m)                   "3 u-turn at the bottom"}
"! 1-turn"
{L_PHP1_top_turn_78=33[mm]*convert(mm,m)                        "the length of the U-SHAPE capillary tube for PHP1"
L_PHP1_bottom_turn_78=3[mm]*convert(mm,m)}                      "!check"
L_PHP1_turn=L_PHP1_top_turn_78+L_PHP1_bottom_turn_78            "the U shape portion of capillary tubing"
//Total Length of the capillary portion
L_PHP1_cap_total=(L_cond+L_evap+L_adiabatic)*N+((L_cond+L_evap+L_adiabatic)-L_cap_6-L_cap_13)+L_PHP1_turn
V_PHP1_cap_core=L_PHP1_cap_total*A_cap
V_PHP1_ss_core=(L_cap_6+L_cap_13)*(pi#*od_ss^2/4)+V_2+V_3+V_4+V_5+V_12
V_PHP1_core=V_PHP1_cap_core+V_PHP1_ss_core                      "include the capillary tubing sections and some part of the
 T block"
//PHP1 Pressure Transducer
V_PHP1_cond_cold=V_1+V_19
V_PHP1_cond_amb=V_20
V_PHP1_evap_cold=V_11+V_14
```

```
V_PHP1_evap_amb=V_15
V_PHP1_transducer=V_PHP1_cond_cold+V_PHP1_cond_amb+V_PHP1_evap_cold+V_PHP1_evap_amb
V_PHP1_P_cold=V_PHP1_cond_cold+V_PHP1_evap_cold
RATIO_P_PHP=V_PHP1_P_cold/V_PHP1_core
//! PHP2 Core//
L_cap_18=10[mm]*convert(mm,m)     "within T with OD of ss sleeve"
"!7-turn PHP"
L_PHP2_top_turn_78=((2*12.51+7.75)*2+(9.83+13+9.95)+(10.32+11.5+10.51)+(11.8+11+11.5)+(12+9.5+11.5)+(72.5+23))[mm]
*convert(mm,m)"the length of the U-SHAPE capillary tube for PHP1,the first two are the originals, 4 U-turn with a U-bend"
L_PHP2_bottom_turn_78=(7*3)[mm]*convert(mm,m)                    "5 u-turn at the bottom"
{"!5-turn PHP"
L_PHP2_top_turn_78_5TURN=((2*12.51+7.75)*2+(9.83+13+9.95)+(10.32+11.5+10.51)+(37+41.5))[mm]*convert(mm,m)"the length of
the U-SHAPE capillary tube for PHP1,the first two are the originals, 4 U-turn with a U-bend"
L_PHP2_bottom_turn_78=(5*3)[mm]*convert(mm,m)                    "5 u-turn at the bottom"}
{"!3-turn PHP"
L_PHP2_top_turn_78=((2*12.51+7.75)*2+62.9)[mm]*convert(mm,m)"the length of the U-SHAPE capillary tube for PHP1, TWO U-turn
with a U-bend"
L_PHP2_bottom_turn_78=(3*3)[mm]*convert(mm,m)                    "3 u-turn at the bottom"}
{L_PHP2_top_turn_78=33[mm]*convert(mm,m)                         "the length of the U-SHAPE capillary tube for PHP1"
L_PHP2_bottom_turn_78=3[mm]*convert(mm,m)}                                                    "!check"
L_PHP2_turn=L_PHP2_top_turn_78+L_PHP2_bottom_turn_78
L_PHP2_cap_total=(L_cond+L_evap+L_adiabatic)*N+((L_cond+L_evap+L_adiabatic)-L_cap_18)+L_PHP2_turn
// Volume Capillary
V_PHP2_cap_core=L_PHP2_cap_total*A_cap                           "total volume of the capillary tube"
V_PHP2_ss_core=(L_cap_18)*(pi#*od_ss^2/4)+V_17
V_PHP2_core=V_PHP2_cap_core+V_PHP2_ss_core                       "include the capillary tubing sections and some part of the
 T block"
DeltaV=V_PHP2_core/V_PHP1_core

"Fill Ratio Estimation"
"PHP1"
"1st step is to evacuate the entire system"
T_o=converttemp('C','K',20.2[C])      "ambient temperature"
T_1=84.5[K]                           "cold end temperature"
T_ave=(T_o+T_1)/2                     "average temperature between top flange and aluminum flange"
"2nd step is to fill the tank "
P_o=46.90283[psi]*convert(psi,kPa)    "charge pressure"
m_o=(P_o*V_tank)/(R*T_o)              "Idea Gas Law for calculating the initial mass of gas within the tank"
"3rd, once the supply valve is opened, mass is conserved. The tank pressure is reduced to P_supply"
P_supply=41.36554[psi]*convert(psi,kPa)                          "charge pressure reduced to supply pressure"
"!! Portion needs to be commented on when did FR for PHP2"
"mass balance"
m_supply=m_G1+m_feed_PHP1_amb+m_G2_PHP1+m_PHP1_cold              "mass supplied from the gas tank"
//Room Temperature Side
m_supply=((P_o-P_supply)*V_tank)/(R*T_o)                         "so this mass is the pressure drop of the tank based on IG
 LAW"
m_tank=(P_supply*V_tank)/(R*T_o)      "the gas left in the tank"
P_gauge={P_PHP}217.953[kPa]           "the gauge pressure mounted on the G1"
m_G1=(P_gauge*V_G1)/(R*T_o)           "mass of the N2 in G1(between gas tank and PHP valve)"
m_feed_PHP1_amb=(P_PHP*(V_feed_PHP1_amb+V_PHP1_cond_amb+V_PHP1_evap_amb))/(R*T_o)"!Include the ambient
 section of both sensors"

V_PHP_AMB_PHP1=V_feed_PHP1_amb+V_PHP1_cond_amb+V_PHP1_evap_amb                "!Include the ambient
 section of both sensors"
"Between ambient and cold"
m_G2_PHP1=(P_PHP*(V_G2_PHP1+V_PHP1_cond_cold+V_PHP1_evap_cold))/(R*T_ave)
```

```
V_PHP_AMB_cold_PHP1=V_G2_PHP1+V_PHP1_cond_cold+V_PHP1_evap_cold
"Cold end"
V_PHP1_cold=V_PHP1_core
P_PHP=p_sat(F$,T=T_1)              "saturation temperature of the fluids at cold end temperature"
rho_l_sat=density(F$,x=0,T=T_1)    "density of saturated liquid"
rho_v_sat=density(F$,x=1,T=T_1)    "density of saturated vapor"
m_PHP1_cold=rho_l_sat*V_PHP1_l+rho_v_sat*(V_PHP1_cold-V_PHP1_l)                    "mass of fluid within
 cold end part"
"!Fill Ratio of PHP1"
FR_PHP1=V_PHP1_l/V_PHP1_cold
"!! Portion needs to be commented on when did FR for PHP2"
T_SAT_DEMO=t_sat(Nitrogen,P=P_GAUGE)
V_PHP1=V_feed_PHP1_amb+V_G2_PHP1+V_PHP1_CORE
v_t_PHP1=V_PHP1_cold/m_PHP1_cold

{"!When WORK ON FR for PHP2, COULD comment PHP1 section above"
"2nd step is to fill the tank "
T_o=converttemp('C','K',20.2[C])
T_1=84.5[K]                        "cold end temperature"
T_ave=(T_o+T_1)/2                  "average temperature between top flange and aluminum flange"
P_o_2=41.35614[psi]*convert(psi,kPa)                    "charge pressure, after filling PHP1"
m_o_2=(P_o_2*V_tank)/(R*T_o)       "Idea Gas Law for calculating the mass of gas AFTER FILL PHP1 within the tank"
"3rd, once the supply valve is opened, mass is conserved. The tank pressure is reduced to P_supply_2"
P_supply_2=35.89757[psi]*convert(psi,kPa)               "charge pressure reduced to supply pressure, when filling PHP2 is ov
"mass balance"
m_supply_2=m_G1_2+m_feed_PHP2_amb+m_G2_PHP2+m_PHP2_cold "mass supplied from the gas tank, for conservation of
filling PHP2"
//Room Temperature Side
m_supply_2=((P_o_2-P_supply_2)*V_tank)/(R*T_o)          "so this mass is the pressure drop of the tank based on IG LAW"
m_tank_2=(P_supply_2*V_tank)/(R*T_o)                    "the gas left in the tank"
V_PHP2=V_feed_PHP2_amb+V_G2_PHP2+V_PHP2_CORE
"! Gauge Pressure might need to be updated"
P_gauge_2={P_PHP}217.8106[kPa]   "!the gauge pressure mounted on the G1. updated when fill PHP2!!!!!"
m_G1_2=(P_gauge_2*V_G1)/(R*T_o) "mass of the N2 in G1(between gas tank and PHP valve)"
m_feed_PHP2_amb=(P_PHP*V_feed_PHP2_amb)/(R*T_o)         "No sensors on PHP2"
"Between ambient and cold"
m_G2_PHP2=(P_PHP*V_G2_PHP2)/(R*T_ave)                   "No pressure Transducer"
"Cold end"
V_PHP2_cold=V_PHP2_core
P_PHP=p_sat(F$,T=T_1)              "saturation temperature of the fluids at cold end temperature"
rho_l_sat=density(F$,x=0,T=T_1)    "density of saturated liquid"
rho_v_sat=density(F$,x=1,T=T_1)    "density of saturated vapor"
m_PHP2_cold=rho_l_sat*V_PHP2_l+rho_v_sat*(V_PHP2_cold-V_PHP2_l)                    "mass of fluid within cold end par
"!Fill Ratio of PHP1"
FR_PHP2=V_PHP2_l/V_PHP2_cold
{v_t_PHP2=V_PHP2_cold/m_PHP2_cold}
P_sat_demo=P_gauge_2
T_sat_demo=t_sat(Nitrogen,P=44.865[psi]*convert(psi,kPa))}
```

8.3 MATLAB script for plotting the temperature and pressure profiles of the PHP

8/19/24 10:02 AM E:\VARIED-PHP\5-t...\PHP_run_update_kPa.m 1 of 4

```
close all
clear
clc
%inititliaze matrix
% THIS IS FOR 5-turn PHP
%% Read Power
xls_name = 'Power Range 77-38.xlsx'; % File that contains the parameters
xls_data = xlsread(xls_name);
prompt = "Power Step? ";
power_step = input(prompt);
%% Read Labview File
file_name = (['run',num2str(power_step),'.LVM']);
% file_name = horzcat('run13.LVM');
data_0 = load(file_name);
data = data_0(:,2:17);
% file_name2 = 'Thermal EMF.xlsx';
% data_EMF = xlsread(file_name2);
[data_row, data_column] = size(data);
%% Geometry configurations
% Two PHP Sections in Parallel
% 5-turn PHP
N = 10;    % 10 loops on each PHP section, 2Sections
d_in = 0.0005;   %inner diameter, .5mm
L_adiabatic = 1;
L_cond = .09;   L_evap = .06;   % length of evap and condenser section
A_c = pi*d_in^2/4; %the cross section area of each capillary tubing
% L_eff = L_adiabatic +(L_cond +L_evap)/2;
L_eff = L_adiabatic;
%  k_effective estimation
%% Heat Input
V_PHP1 = xls_data(power_step,1);I_PHP1 = xls_data(power_step,2);
V_PHP2 = xls_data(power_step,3);I_PHP2 = xls_data(power_step,4);
% V_PHP1 = 7.7077;   I_PHP1 = .312;
% V_PHP2 = 7.7083;   I_PHP2 = I_PHP1;
Q_PHP1_prime = V_PHP1 * I_PHP1;Q_PHP1 = round(Q_PHP1_prime,3);
Q_PHP2_prime = V_PHP2 * I_PHP2;Q_PHP2 = round(Q_PHP2_prime,3);
% Q_PHP1_prime = 2.0945;
Q_PHP1 = round(Q_PHP1_prime,3);Q_PHP2 = round(Q_PHP1_prime,3);
Q1 = num2str(Q_PHP1);
% % T11 = data(:,3);T12 = data(:,12);
% % T4 = data(:,9);T5 = data(:,4);T9 = data(:,11);
% % T10 = data(:,2);T6 = data(:,1);T7 = data(:,10);
% % T8 = data(:,6);T2 = data(:,8);T3 = data(:,5);
% % T1 = data(:,7);
% Retrive Data from the matrix
%%
d_time =1201;
% start = 1200; finish = (start + d_time);
start = 1; finish = data_row;
T11 = data(start:finish,3);T12 = data(start:finish,12);
T4 = data(start:finish,9);T5 = data(start:finish,4);T9 = data(start:finish,11);
```

```
T10 = data(start:finish,2);T6 = data(start:finish,1);T7 = data(start:finish,10);
T8 = data(start:finish,6);T2 = data(start:finish,8);T3 = data(start:finish,5);
T1 = data(start:finish,7);
% Pressure
P_tank = data(start:finish,13)*6.89476;P_evap = data(start:finish,14)*6.89476;
P_cond = data(start:finish,15)*6.89476;
% NumCols_data is the number of data points, or aka seconds
[NumRows_data, NumCols_data]=size(T11);
time = NumRows_data;
% %% Thermal EMF Update
% T1 = T1+ .22; T2 = T2+.065; T3 = T3+.195; T4=T4+.11; T5= T5+.17;
% T6= T6+.21; T7=T7+.205; T8= T8+.175; T9= T9+.085; T10 =T10+.15;
% T11 = T11+ 0.12;T12=T12+.085;
%% End of Themral EMF
T_total = [T1, T2, T3, T4, T5, T6, T7, T8, T9, T10, T11, T12];
P_total = [P_tank, P_evap, P_cond];
for K = 1:12;

    T_ave(:,K) = sum(T_total(:,K))/time;

end
for K = 1:3;

    P_ave(:,K) = sum(P_total(:,K))/time;

end
T12_ave = T_ave(12); T11_ave = T_ave(11);
T5_ave = T_ave(5);T4_ave = T_ave(4);T7_ave=T_ave(7);
T3_ave = T_ave(3); T1_ave = T_ave(1);T6_ave = T_ave(6);
T_cond_diff = T12_ave- T11_ave;
delta_time = finish - start;
%% Pressure Oscillation Analysis
% P_evap_osc =  data(start-1:finish,14);
% Delta_Pevap_tot(1)= 0;
% P_cond_osc =  data(start-1:finish,15);
% Delta_Pcond_tot(1)= 0;
% P_evap_osc_ave = sum(P_evap_osc)/(finish-start+2)
% peak = 0;
% for i = 1:delta_time+1
%     Delta_Pevap(i)= abs(P_evap_osc(i+1)-P_evap_osc(i));
%     Delta_Pevap_tot(i+1) = Delta_Pevap_tot(i) + Delta_Pevap(i);
%     Delta_Pcond(i)= abs(P_cond_osc(i+1)-P_cond_osc(i));
%     Delta_Pcond_tot(i+1) = Delta_Pcond_tot(i) + Delta_Pcond(i);
%     T12_CORRECT(i)=T11(i)+T_cond_diff;
%     if P_evap_osc(i) > P_evap_osc_ave
%         peak = peak +1;
%     else
%         peak = peak +0;
% %     end
% end
```

```
% Delta_P_evap_total = Delta_Pevap_tot(delta_time+2)
% T12_ave_correct = sum(T12_CORRECT)/i;
% T12 = T12_CORRECT;
%% Effective Thermal Cond
k_eff_PHP1_prime = (Q_PHP1* L_eff)/(N*A_c*(T3_ave - T12_ave));
k_eff_PHP2_prime = (Q_PHP2* L_eff)/(N*A_c*(T1_ave - T11_ave));
% Round Significant Numbers
k_eff_PHP1 = round(k_eff_PHP1_prime,-3);
k_eff_PHP2 = round(k_eff_PHP2_prime,-3);
% folder_dir = 'E:\VARIED-PHP\run 03-01-23\';
%% Create Time Figure%%
% figure(1)
% t = 0:1:time - 1;
% plot(t, T1, t, T2, t, T3, t, T4, t, T5, t, T6, t, T7, t, T8, t, T9, ...
% t, T10, t, T11, t, T12)
% xlabel('time[sec]'); ylabel('T[K]');
% legend('Location','best')
% legend('T1', 'T2','T3','T4','T5','T6', 'T7', 'T8', 'T9','T10', 'T11', 'T12');
% title('Temperature vs Time ')
figure(2)
t = 0:1:time - 1;
% plot(t, T12, t, T4, t, T5, t, T6, t, T7, t, T3)
plot(t, T12,'b', t, T4,'g', t, T5, t, T6,'c', t, T7,'m', t, T3,'r')
title({['Temperature vs Time for PHP1 at ', num2str(Q_PHP1),'[W]'];...
    ['Keff=',num2str(k_eff_PHP1),'[W/m-K]']})
% title(['Temperature vs Time for PHP1 at ', num2str(Q_PHP1),'[W]'])
% title({['Temperature vs Time for PHP1 at ', num2str(Q_PHP1),'[W]'];...
%     ['repeat test and heat load is increased from 0[W]']})
% title('Temperature Profile before Filling Nitrogen into PHP1')
xlabel('time[sec]'); ylabel('T[K]');
% ylim([84 87]);    %limit of y-axis
legend('Location','best')
legend({'T12', 'T4', 'T5', 'T6', 'T7', 'T3'}, 'NumColumns',2);

figure(3)
t = 0:1:time - 1;
plot(t, T11,'b', t, T9,'g', t, T10, t, T8,'c', t, T2,'m', t, T1,'r')
xlabel('time[sec]'); ylabel('T[K]');
% ylim([77 80.75]);
legend('Location','best')
legend({'T11', 'T9', 'T10', 'T8', 'T2', 'T1'}, 'NumColumns', 2);
title({['Temperature vs Time for PHP2 at ', num2str(Q_PHP2),'[W]'];...
    ['Keff=',num2str(k_eff_PHP2),'[W/m-K]']})
% title(['Temperature vs Time for PHP2 at ', num2str(Q_PHP2),'[W]'])
figure(4)
plot(t, P_evap, t, P_cond)
xlabel('time[sec]'); ylabel('P[kPa]');
legend('Location','best')
legend('Pevap', 'Pcond');
title(['Pressure vs Time of PHP1 at ',num2str(Q_PHP1),'[W]'])
%
```

```
% figure(5)
% t = 0:1:time - 1;
% plot(t, T11, t, T12, t, T3, t, T1)
% xlabel('time[sec]'); ylabel('T[K]'); %ylim([77 103]);
% legend('Location','best')
% legend('T11', 'T12', 'T3 (PHP1)','T1(PHP2)');
% title({['Temperature Profile of Evaporator and Condenser on PHP1 and PHP2'];...
%     ['from 0W to 1.24W on each PHP']})

% figure(5)
% plot(t,P_tank)
% xlabel('time[sec]'); ylabel('P[psi]');
% legend('Location','best')

% Summary
run_number = 1;
Summary(run_number,1:12) = T_ave;
Summary(run_number, 13:15) = P_ave;
Summary(run_number, 16:19) = [Q_PHP1, Q_PHP2, k_eff_PHP1, k_eff_PHP2];
Summary(run_number, 20:21) = [start, finish];
```

8.4 MATLAB script for calculating the effective thermal conductivity of the PHP


```
close all
clear
clc
%inititliaze matrix
%%Read Excel
number_test = 23;
xls_name = 'Power Range 7-TURN 77-63.xlsx'; % File that contains the parameters
xls_data = xlsread(xls_name);
Summary = zeros(number_test,28);
%% Geometry configurations
% Two PHP Sections in Parallel
N = 14;    % 2 loops on each PHP section, 2Sections
d_in = 0.5/1000;   %inner diameter, .5mm
L_adiabatic = 1;
L_cond = .09;   L_evap = .06;   % length of evap and condenser section
A_c = pi*d_in^2/4; %the cross section area of each capillary tubing
% L_eff = L_adiabatic +(L_cond +L_evap)/2;
L_eff = L_adiabatic;
% %  k_effective estimation
I_PHP1_sum = xls_data(:,2);I_PHP2_sum = xls_data(:,4);
V_PHP1_sum = xls_data(:,1);V_PHP2_sum = xls_data(:,3);
Q_PHP1_sum = xls_data(:,5);Q_PHP2_sum = xls_data(:,6);
%{The start and end point for each run %}
start_sum = xls_data(:,7);finish_sum = xls_data(:,8);
accuracy_I = 0.5/100; accuracy_V = 0.0035/100;
u_Te = 250/1000; u_Tc = 250/1000;
for j = 1:number_test
   % read each raw txt file
   run = j;
   run_name = num2str(run);
   name = horzcat('run',run_name,'.LVM');
   data_0 = load(name);
   data = data_0(:,2:19);
   %% Load the steady state
   start =start_sum(run); finish = finish_sum(run);
   Q_PHP1 = round(Q_PHP1_sum(run),3);Q_PHP2 = round(Q_PHP2_sum(run),3);
   V_PHP1 = V_PHP1_sum(run);V_PHP2 = V_PHP2_sum(run);
   I_PHP1 = I_PHP1_sum(run);I_PHP2 = I_PHP2_sum(run);
   T11 = data(start:finish,3);T12 = data(start:finish,12);
   T4 = data(start:finish,9);T9 = data(start:finish,11);
   T10 = data(start:finish,2);T6 = data(start:finish,1);
   T8 = data(start:finish,6);T2 = data(start:finish,8);T3 = data(start:finish,5);
   T1 = data(start:finish,7); R5 = data(start:finish,18);
   T7 = data(start:finish,10);T5 = data(start:finish,4);


% Pressure
   P_tank = data(start:finish,13);P_evap = data(start:finish,14);
   P_cond = data(start:finish,15);
   P_evap_max = round(max(P_evap),3);P_evap_min = round(min(P_evap),3);
   P_cond_max = round(max(P_cond),3);P_cond_min = round(min(P_cond),3);
```

```
% NumCols_data is the number of data points, or aka seconds
   [NumRows_data, NumCols_data]=size(T11);
   time = NumRows_data;

   T_total = [T1, T2, T3, T4, T5, T6, T7, T8, T9, T10, T11, T12];
   P_total = [P_tank, P_evap, P_cond];
   for K = 1:12;

    T_ave(:,K) = round(sum(T_total(:,K))/time, 3);

    end
    for K = 1:3;

    P_ave(:,K) = round(sum(P_total(:,K))/time,3);

    end
    T12_ave = T_ave(12); T11_ave = T_ave(11);
    T5_ave = T_ave(5);T4_ave = T_ave(4);T7_ave=T_ave(7);
    T3_ave = T_ave(3); T1_ave = T_ave(1);T6_ave = T_ave(6);
    R5_ave = sum(R5)/time;
% T12 = T12_CORRECT;
%% Effective Thermal Cond
k_eff_PHP1_prime = (Q_PHP1* L_eff)/(N*A_c*(T3_ave - T12_ave));
k_eff_PHP2_prime = (Q_PHP2* L_eff)/(N*A_c*(T1_ave - T11_ave));
%% Uncertainty Analysis
%% PHP1
dkdQ_PHP1 = L_eff/(N*A_c*(T3_ave-T12_ave));
dkdTe_PHP1 = -Q_PHP1*L_eff/(N*A_c*(T3_ave-T12_ave)^2);
dkdTc_PHP1 = Q_PHP1*L_eff/(N*A_c*(T3_ave-T12_ave)^2);
dQdI_PHP1 = V_PHP1; dQdV_PHP1 = I_PHP1;
uI_PHP1= accuracy_I * I_PHP1;uV_PHP1= accuracy_V * V_PHP1;
uQ_PHP1=sqrt((dQdI_PHP1*uI_PHP1)^2+(dQdV_PHP1*uV_PHP1)^2);
uKeff_PHP1 = sqrt((dkdQ_PHP1*uQ_PHP1)^2+(dkdTe_PHP1*u_Te)^2+(dkdTc_PHP1*u_Tc)^2);
%% PHP2
dkdQ_PHP2 = L_eff/(N*A_c*(T1_ave-T11_ave));
dkdTe_PHP2 = -Q_PHP2*L_eff/(N*A_c*(T1_ave-T11_ave)^2);
dkdTc_PHP2 = Q_PHP2*L_eff/(N*A_c*(T1_ave-T11_ave)^2);
dQdI_PHP2 = V_PHP2; dQdV_PHP2 = I_PHP2;
uI_PHP2= accuracy_I * I_PHP1;uV_PHP2= accuracy_V * V_PHP2;
uQ_PHP2=sqrt((dQdI_PHP2*uI_PHP2)^2+(dQdV_PHP2*uV_PHP2)^2);
uKeff_PHP2 = sqrt((dkdQ_PHP2*uQ_PHP2)^2+(dkdTe_PHP2*u_Te)^2+(dkdTc_PHP2*u_Tc)^2);
% Round Significant Numbers
k_eff_PHP1 = round(k_eff_PHP1_prime,-3);
k_eff_PHP2 = round(k_eff_PHP2_prime,-3);
Summary(run,:) = [T_ave, P_ave, P_cond_max, P_cond_min, P_evap_max, P_evap_min, ...
     Q_PHP1, Q_PHP2, k_eff_PHP1, k_eff_PHP2, uKeff_PHP1, uKeff_PHP2, uQ_PHP1, uQ_PHP2,↙
R5_ave];
end
Excel_output(1,:) = ["T1" "T2" "T3" "T4" "T5" "T6" "T7" "T8" "T9" "T10" "T11" "T12"...
    "P_tank" "P_evap" "P_cond" "P_cond_max" "P_cond_min" "P_evap_max" "P_evap_min" ...
    "Q_PHP1" "Q_PHP2" "k_eff_PHP1" "k_eff_PHP2" "u_keff_PHP1" "u_keff_PHP2" "uQ_PHP1"↙
```

```
"uQ_PHP2" "R5"];
Excel_output(2:number_test+1,:) = Summary;
output_file = '7-turn PHP 77-63result_uncertainty V2 No Correction.xlsx';
xlswrite(output_file, Excel_output)
```

8.5 Calibration curve of the pressure transducers

All three calibration curves presented in this chapter are plotted and calculated in EES [25].

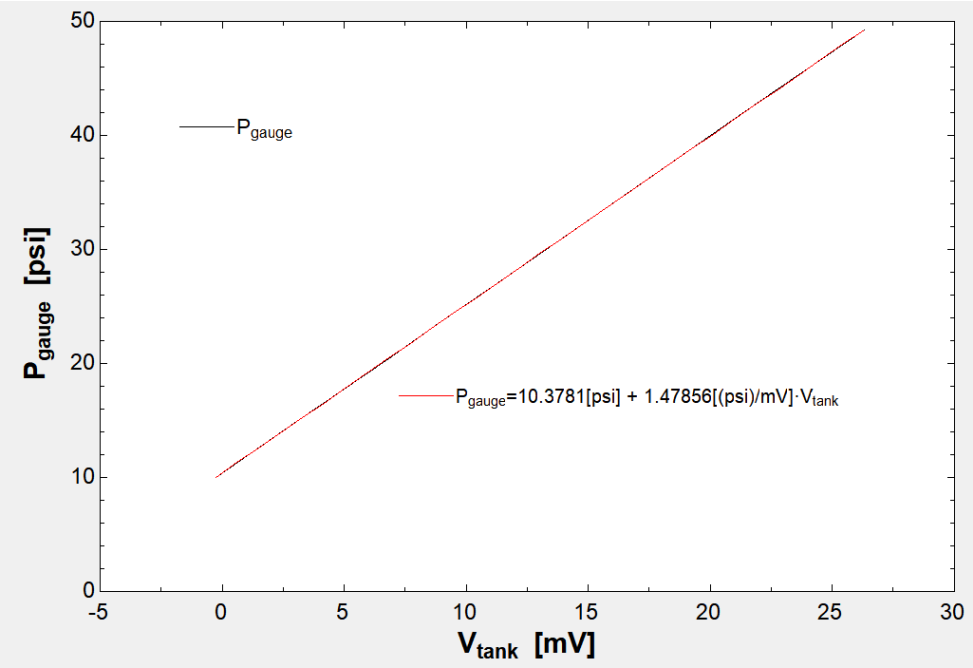

Figure 8-1 Calibration for the pressure transducer mounted on the buffer tank.

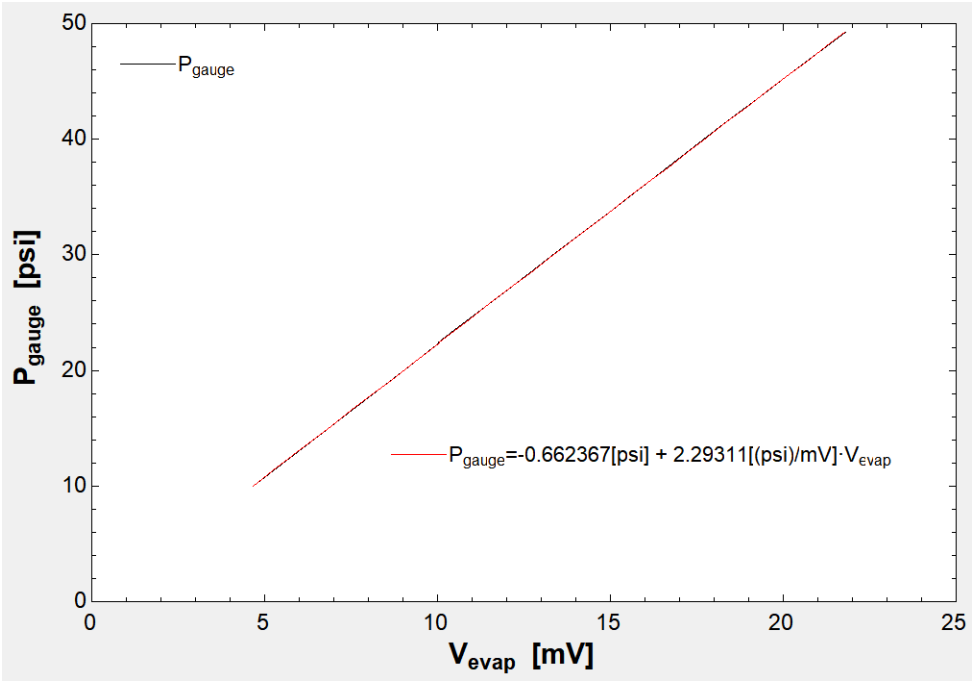

Figure 8-2 Calibration for the pressure transducer tapped near the evaporator.

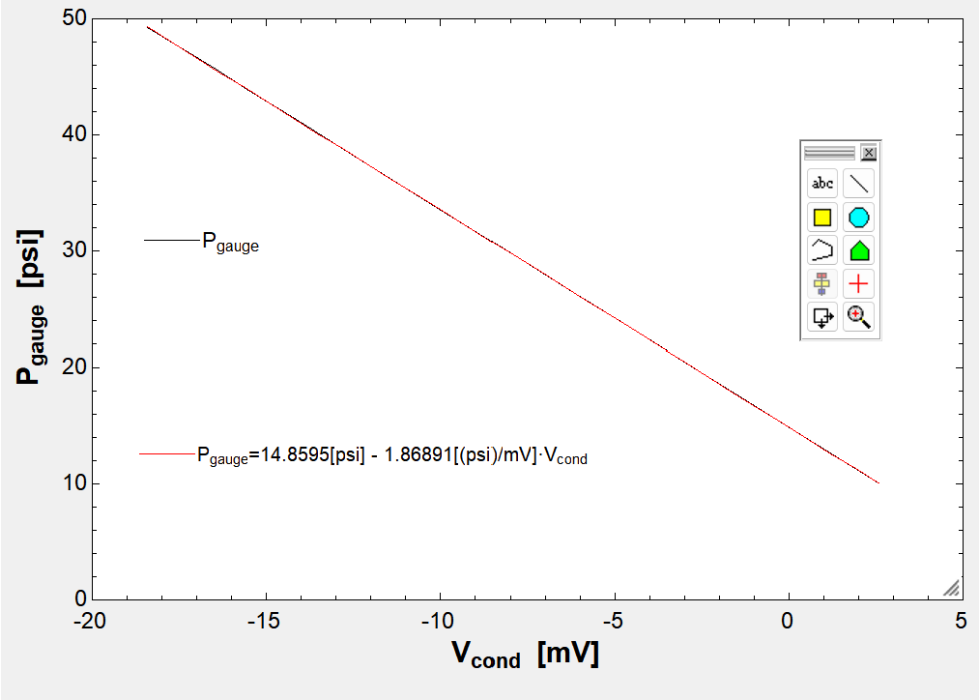

Figure 8-3 Calibration for the pressure transducer tapped near the condenser.

References

[1] K. Natsume, T. Mito, N. Yanagi, and H. Tamura, “Development of a flat-plate cryogenic oscillating heat pipe for improving HTS magnet cooling,” *Phys. Procedia*, vol. 45, pp. 233–236.

[2] T. Dixit, G. Authelet, C. Mailleret, F. Gouit, V. Stepanov, and B. Baudouy, “Neon pulsating heat pipe with innovative flexible evaporator to facilitate cryocooling of superconducting devices,” *IOP Conf. Ser. Mater. Sci. Eng.*, vol. 1301, no. 1, p. 012040, May 2024, doi: 10.1088/1757-899X/1301/1/012040.

[3] H. Akachi, “Structure of heat pipe,” No. 4921041, 1990

[4] S. K. Gandla and R. C. Longsworth, “Mobile refrigeration system for precool and warm up of superconducting magnets,” *IOP Conf. Ser. Mater. Sci. Eng.*, vol. 278, p. 012179, Dec. 2017, doi: 10.1088/1757-899X/278/1/012179.

[5] B. Mueller, J. Pfotenhauer, and F. Miller, “Performance of nitrogen pulsating heat pipes as passive thermal switches in a redundant cryocooler application,” *Appl. Therm. Eng.*, vol. 196, p. 117213, Sep. 2021, doi: 10.1016/j.applthermaleng.2021.117213.

[6] H. Akachi, F. Polasek, and P. Stulc, “Pulsating Heat Pipes,” *Proc 5th Int. Heat Pipe Symp*, pp. 208–217, 1996.

[7] S. Khandekar, C. Piyanun, G. Manfred, and T. Pradit, “Closed loop pulsating heat pipes Part B: visualization and semi-empirical modeling,” *Appl. Therm. Eng.*, vol. 23, no. 16, pp. 2021–2033.

[8] S. Khandekar, “Thermo-hydrodynamics of closed loop pulsating heat pipes,” Universität Stuttgart, 2004.

[9] P. Charoensawan, S. Khandekar, M. Groll, and P. Terdtoon, “Closed loop pulsating heat pipes: Part A: parametric experimental investigations,” *Appl. Therm. Eng.*, vol. 23, no. 16.

[10] S. Khandekar, N. Dollinger, and G. Manfred, “Understanding operational regimes of closed loop pulsating heat pipes: an experimental study,” *Appl. Therm. Eng.*, vol. 23, no. 6.

[11] M. Barba, R. Bruce, A. Bonelli, and B. Baudouy, “Experimental study of Large-scale cryogenic Pulsating Heat Pipe,” *IOP Conf. Ser. Mater. Sci. Eng.*, vol. 278, no. 1, p. 012156, Dec. 2017, doi: 10.1088/1757-899X/278/1/012156.

[12] R. Bruce, M. Barba, A. Bonelli, and B. Baudouy, “Thermal performance of a meter-scale horizontal nitrogen Pulsating Heat Pipe,” *Cryogenics*, vol. 93, pp. 66–74, Jul. 2018, doi: 10.1016/j.cryogenics.2018.05.007.

[13] M. Li, L. Li, and D. Xu, “Effect of filling ratio and orientation on the performance of a multiple turns helium pulsating heat pipe,” *Cryogenics*, vol. 100, pp. 62–68, Jun. 2019, doi: 10.1016/j.cryogenics.2019.04.006.

[14] N. Saha, P. K. Das, and P. K. Sharma, “Influence of process variables on the hydrodynamics and performance of a single loop pulsating heat pipe,” *Int. J. Heat Mass Transf.*, vol. 74, pp. 238–250, Jul. 2014, doi: 10.1016/j.ijheatmasstransfer.2014.02.067.

[15] X. Sun, J. Pfotenhauer, B. Jiao, L. D. Fonseca, D. Han, and Z. Gan, “Investigation on the temperature dependence of filling ratio in cryogenic pulsating heat pipes,” *Int. J. Heat Mass Transf.*, vol. 126, pp. 237–244, Nov. 2018, doi: 10.1016/j.ijheatmasstransfer.2018.05.147.

[16] K. R. Sagar, H. B. Naik, and H. B. Mehta, “Novel condenser based cryogenic pulsating heat Pipe: Investigations on influence of geometrical parameters,” *Cryogenics*, vol. 126, p. 103543, Sep. 2022, doi: 10.1016/j.cryogenics.2022.103543.

[17] J. L. Xu, Y. X. Li, and T. N. Wong, “High speed flow visualization of a closed loop pulsating heat pipe,” *Int. J. Heat Mass Transf.*, vol. 48, no. 16, pp. 3338–3351, Jul. 2005, doi: 10.1016/j.ijheatmasstransfer.2005.02.034.
[18] S. Li, H. Pei, D. Liu, Y. Shen, X. Tao, and Z. Gan, “Visualization study on the flow characteristics of a nitrogen pulsating heat pipe,” *Int. Commun. Heat Mass Transf.*, vol. 143, p. 106722, Apr. 2023, doi: 10.1016/j.icheatmasstransfer.2023.106722.
[19] S. Khandekar and G. Manfred, “On the definition of pulsating heat pipes: an overview,” *Proc. 5th Minsk Int. Conf.*, 2003.
[20] B. P. Singh and M. D. Atrey, “Numerical investigation of a nitrogen based cryogenic pulsating heat pipe,” *Cryogenics*, vol. 115, p. 103246, Apr. 2021, doi: 10.1016/j.cryogenics.2021.103246.
[21] L. D. Fonseca, F. Miller, and J. Pfotenhauer, “Experimental heat transfer analysis of a cryogenic nitrogen pulsating heat Pipe at various liquid fill ratios,” *Appl. Therm. Eng.*, vol. 130, pp. 343–353, Feb. 2018, doi: 10.1016/j.applthermaleng.2017.11.029.
[22] M. Li, L. Li, and D. Xu, “Effect of number of turns and configurations on the heat transfer performance of helium cryogenic pulsating heat pipe,” *Cryogenics*, vol. 96, pp. 159–165, Dec. 2018, doi: 10.1016/j.cryogenics.2018.09.005.
[23] B. Y. Tong, T. N. Wong, and K. T. Ooi, “Closed-loop pulsating heat pipe,” *Appl. Therm. Eng.*, vol. 21, no. 18, pp. 1845–1862, Dec. 2001, doi: 10.1016/S1359-4311(01)00063-1.
[24] “Platinum,” Default. Accessed: Jul. 07, 2024. [Online]. Available: https://www.lakeshore.com/products/categories/overview/temperature-products/cryogenic-temperature-sensors/platinum
[25] Engineering Equation Solver. Available: https://www.fchartsoftware.com/ees/